Shanghai HIgh repetitioN rate XFEL and Extreme light facility (SHINE)

Technical Design Report of FEL-I beamline

September 2025

1. Directory

1. Beamline introduction

The FEL-I beamline has a total length of about 1200 meters. It provides FEL for the Hard x-ray Scattering and Spectroscopy endstation (HSS) in the near experimental hall, as well as Coherent Diffraction Endstation for Single Molecules and Particles (CDS) and Station of Extreme Light (SEL) in the far experimental hall. SEL instrument belongs to the Shanghai Institute of Optics and Fine Mechanics, Chinese Academy of Sciences, while the FEL-I beamline supplies a direct beam after the offset mirrors, with focusing tasks handled by the SEL team.

The scientific goal of the CDS instrument is to achieve atomic-level structural imaging of single molecules and single particles, as well as femtosecond time-resolved imaging of chemical reaction processes through coherent diffraction imaging techniques. This provides high spatial resolution and high temporal resolution analytical methods for life sciences, materials science, and other fields. The CDS requires the beamline to transport and focus the free electron laser to achieve a focused beam below one hundred nanometers while ensuring the integrity of the wavefront and high spatial coherence.

The scientific goal of the HSS instrument is to study the electronic structure and electronic excitations in quantum correlated materials using inelastic resonant scattering experimental methods. This provides powerful tools for deepening the understanding of correlated electron physics and developing new quantum control methods. The HSS requires the beamline to have high energy resolution and high average flux.

The FEL-I beamline consists of offset mirrors, crystal monochromator, HSS focusing system, CDS focusing system, and related diagnostic systems. Figure 1-1 illustrates the schematic diagram of the FEL-I beamline system. The task of this beamline is to transport the beam while maintaining the wavefront as much as possible to the instruments, enabling high-resolution and high signal-to-noise ratio coherent diffraction experiments.

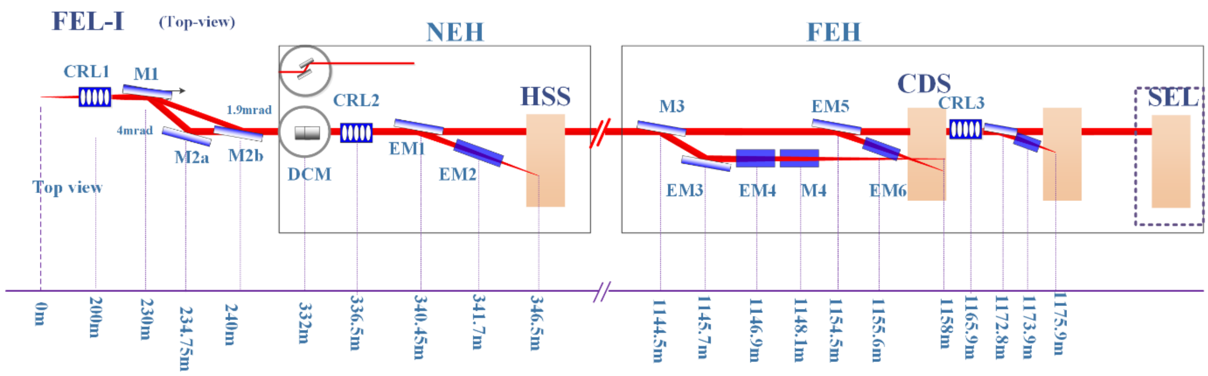

Figure 1-1 Layout of beamlines

2. Requirements and SASE properties

2.1 Beamline Parameters

Table 2.1-1 Parameters of FEL-I

Parameters	Objective	Nominal
Energy range	3.0 – 15.0 keV	5.0 – 13.0 keV
Energy resolution (△E/E)	2.0×10^{-4}@8.9 keV	2.0×10^{-4}@8.9 keV
Transmission efficiency	30%@7keV (no monochromator)	15%@7keV (no monochromator)
spot size	10 μm @HSS 0.1 μm&1 μm @CDS	15 μm @HSS

2.2 Endstation Requirements

Table 2.2-1 Parameters of the CDS/HSS

Endstation	Parameter	Objective	Nominal
CDS	Spatial resolution	0.5nm@>5×10^{13} photons/μm2@ 5 keV, 100 nm focus	≤5 nm
	Spot size	100 nm	≤300 nm

	Experiment techniques	(Time-resolved) Forward Scattering/SAXS/WAXS	
HSS	Spectrometer resolution	4×10^{-5}	4×10^{-5}
	Experiment techniques	Hard X-ray RIXS	

Table 2.2-2 Requirements of the CDS/HSS

	Parameter		CDS	HSS
1	Energy range		3~15 keV	3~15 keV
2	Energy resolution		/	Si(111): 2×10^{-4} @ 3~15 keV Si(311): 5×10^{-5} @ 5.6~15 keV
3	Efficiency of beamline		≥50% @ 7 keV	≥60%@7 keV[1]
4	Percent of harmonics		≤0.05%	≤0.01%
5	Spot size (FWHM)(H×V)		Objective：300 nm × 100 nm @ 7keV Nominal：600 nm × 300 nm @ 7keV	Objective：(10 μm ~ 200 μm) × (6 μm~200 μm) Nominal：10 μm × 10 μm
6	Working distance		>0.2 m @ 100 nm spot size	
7	Beam stability（RMS）		/	≤3 um[2]
8	Focusing		/	CRL and K-B
9	Attenuator		6 orders	4 orders
10	Diagnostics	Pulse Energy	≤ 10%	≤10%
		Single shot spectra	Single shot	Single shot
		Timing diagnostics(RMS)	Arriving time diagnostics accuracy ≤ 10 fs	Arriving time diagnostics accuracy ≤ 10 fs
		Wavefront diagnostics repeatability（RMS）	λ/50 @ λ=0.177 nm	/

(1) No monochromator.

(2) Calculate with the mirror stability of 50nrad.

2.3 Source Properties

FEL-I uses 42 segments of a 4 m long plane undulator with a 26 mm period. The space between segments is 1 m, and the total length is 209 m. It can offer SASE and self-seeding. Table 2.4 shows the SASE properties of FEL-I. The spot size is between 30-50 µm, and the divergence is between 1.3-5.5 µrad. 3-6 keV is generated by a 5 GeV electron beam, and 7-15 keV is generated by an 8 GeV electron beam. All these beam properties are from the simulation. From the reports[1, 2] of the LCLS and SACA, the divergences are uncertain, the difference between theory and measurements is a factor of 1.5~3, and it depends on the actual operation condition of the machine.

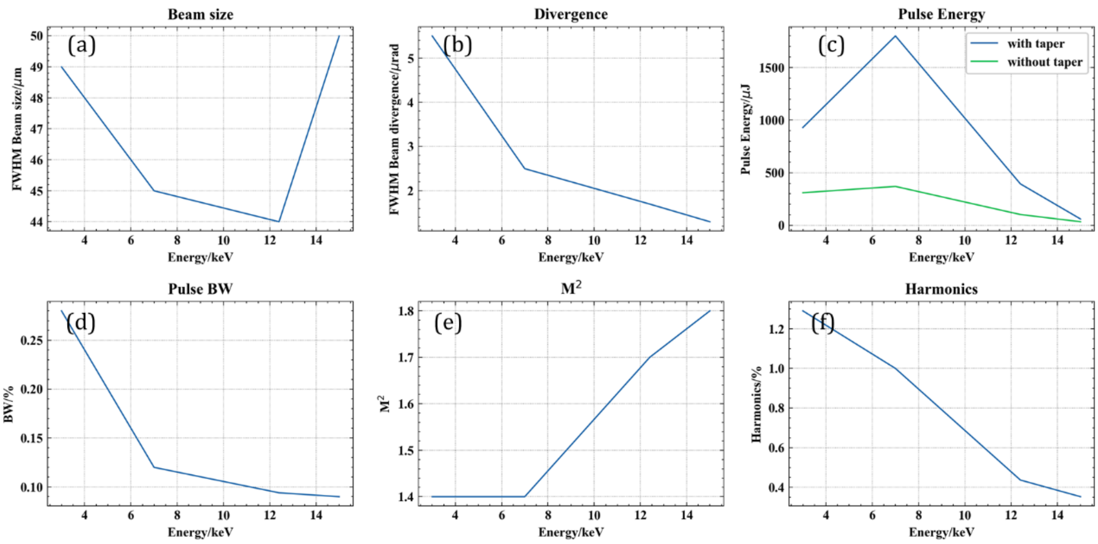

Figure 2.3-1 Source properties: (a) source size, (b) divergence, (c) pulse energy, (d) bandwidth, (e) M squared factor, and (f) content of high harmonics

Table 2.3-1 Source properties of FEL-I

	Low charge	High charge	Low charge	High charge	Low charge	High charge	Low charge	High charge
Bunch charge (pC)	20	100	20	100	20	100	20	100
Energy (keV)	3	3	7	7	12.4	12.4	15	15
Electron energy (GeV)	5		8					
FWHM pulse length (μm)	7	16	6	14	5	11	4.2	8.9
FWHM bandwidth (%)	0.28	0.28	0.14	0.19	0.09	0.12	0.09	0.09
Pulse energy (μJ, max)	73	310	43	370	30	103	19	34
FWHM source size (μm) (exit)	500	480	330	160	75	100	72	72
FWHM source size (μm, sat)	51	49	33	48	46	50	49	50
FWHM source divergence (μrad)	5	5.5	3.3	2.7	1.3	1.7	1.3	1.3
Coherence degree	1.4	1.5	1.4	1.7	1.4	2	1.8	1.8
Peak power (GW)	8	15	6	28	4	11	2.5	3
High order harmonics								
3rd pulse energy (μJ)	0.6	4	0.3	3.2	0.1	0.48	0.05	0.12
5th pulse energy (μJ)	0.05	0.3	0.02	0.2	0.01	0.03	0.001	0.01

3. Schematic design

3.1 International facilities

Currently, there are three high-repetition rate hard X-ray free electron laser facilities that have been completed or are under construction internationally (including SHINE). One of them is the European Free Electron Laser (European-XFEL), which operates in a pulse train mode at 10 Hz, with each train containing 2700 pulses. Three beamlines and six experimental stations have already been in operation.

The LCLS-II operates at a repetition rate of 1 MHz and includes both a soft X-ray beamline and a hard X-ray beamline. It allows for the switching between low-repetition and high-repetition accelerator, achieving several mJ of single-pulse energy with low repetition rate accelerator. Additionally, there are other low-repetition rate hard X-ray free electron lasers such as SACLA, PAL-XFEL and Swiss-FEL.

Table 3.1-1 High-repetition rate Hard X-ray Free Electron Lasers

Facility	Electron Energy (GeV)	Photon Energy (keV)	Repetition Rate
LCLS-II (LCLS-II-HE)	4, 8, 2-15.4	0.2-25	1 MHz
European-XFEL	10.5-17.5	0.4-20	10 Hz train, 4.5 MHz
SHINE	5-8	0.4-25	1 MHz

3.2 Scheme layout

The FEL-I beamline mainly consists of offset mirrors, three compound refractive lens (CRL) focusing system, a crystal monochromator, KB focusing systems, and diagnostic systems, as shown in Figure 3.2-1. The first component after the beam exits the insertion device and passes through the radiation collimator, fixed aperture, and synchrotron radiation aperture (SRA) is the single pulse energy diagnostic device (GMD). The GMD is the most important diagnostic device in the operation of the beamline. Due to the unstable nature of single pulse energy in free electron lasers, the GMD provides key parameters for normalization and filtering in experimental methods and data processing at the instruments. Some experimental methods cannot process data without GMD data.

Next are the gas attenuator (GATT) and solid attenuator (SATT), which are used to reduce the single pulse energy of the FEL. The gas attenuator can achieve an attenuation of 4-6 orders of magnitude at 3-7 keV without damaging the wavefront, 3-4 orders of magnitude at 7-9 keV, and 1 order of magnitude at 7-15 keV. The working conditions of the solid attenuator must be strictly controlled to avoid damage from single and multiple pulses; it can operate only after the gas attenuator has attenuated the power by more than one order of magnitude, ensuring its safety at high repetition rate case. Solid attenuators are typically made from radiation-resistant materials such as diamond and silicon. During the commissioning of the beamline and experimental station, it is usually necessary to attenuate the single pulse energy by 3-6 orders of magnitude to prevent single pulse damage at the focal point.

At 200 m, a set of compound refractive lenses (CRL1) is installed to collimate the beam, working in conjunction with CRL2 and CRL3 in front of the instruments for focusing. The CRL uses beryllium (Be) as the lens material; while Be has strong thermal load and radiation resistance, its operating conditions must also be strictly controlled.

Subsequently, offset mirrors (M1, M2a, M2b) are placed between 230 m and 240 m to absorb high-energy radiation while creating an offset for radiation protection. The offset mirrors are necessary optical component for X-ray free electron lasers; otherwise, high-energy radiation would be transmitted to the instruments. Its stability is crucial for the performance of the beamline, as it is located far from the source point, where even a few tens of nanoradians of jitter can lead to significant positional variations at the focus.

At 332 m, a crystal monochromator is added to monochromate the beam, providing monochromatic light in the range of 1E-4 to 1E-5 for the HSS instrument. The design of the crystal monochromator in high-frequency free electron lasers is still immature. On one hand, maintaining the wavefront of coherent light requires very tight shape error tolerances for the crystals; on the other hand, the thermal load is substantial, so stringent operating conditions are necessary.

At a position 10 m in front of the HSS instrument, CRL2 is added to provide focused light in the range of 5-15 keV. CRL2 is optimized to ensure that a small movement in the optical path direction keeps the focus at the sample position. An KB mirror system is added for focusing at the HSS instrument. The CRL is very effective in absorbing in the 3-5 keV range, while the KB mirrors can focus to very small spot sizes. This KB mirror system also needs to be removable for switching between CRL2 and the CDS or SEL instruments. A direct optical path is reserved in the cavity to connect with the ultra-long beamline during switching.

At 1110 m, a GMD is set up to monitor the pulse energy reaching the CDS experimental station, along with a solid attenuator to protect the KB mirrors during debugging. The CDS experimental station is equipped with four focusing systems. First, a CRL3 is placed at 1168 m to focus at 1165.9 m, initially used to debug the experimental station equipment, and it may also be considered for shared use with the SEL station. A micro-focused KB system is installed between 1144.5 m and 1148.1 m, utilizing a four-reflector KB system to maintain the beam transmission direction while aiming to focus the beam to approximately 1-2 μm. At 1154.5-1155.6 m, a nano-KB focusing system is installed, targeting a focus of around 100-300 nm. Imagers will be added before and after each key component in the beamline to observe the beam position and shape. At 1172 m, a KB focusing system with a focal length of 2 m is set up to achieve focusing below 100 nm.

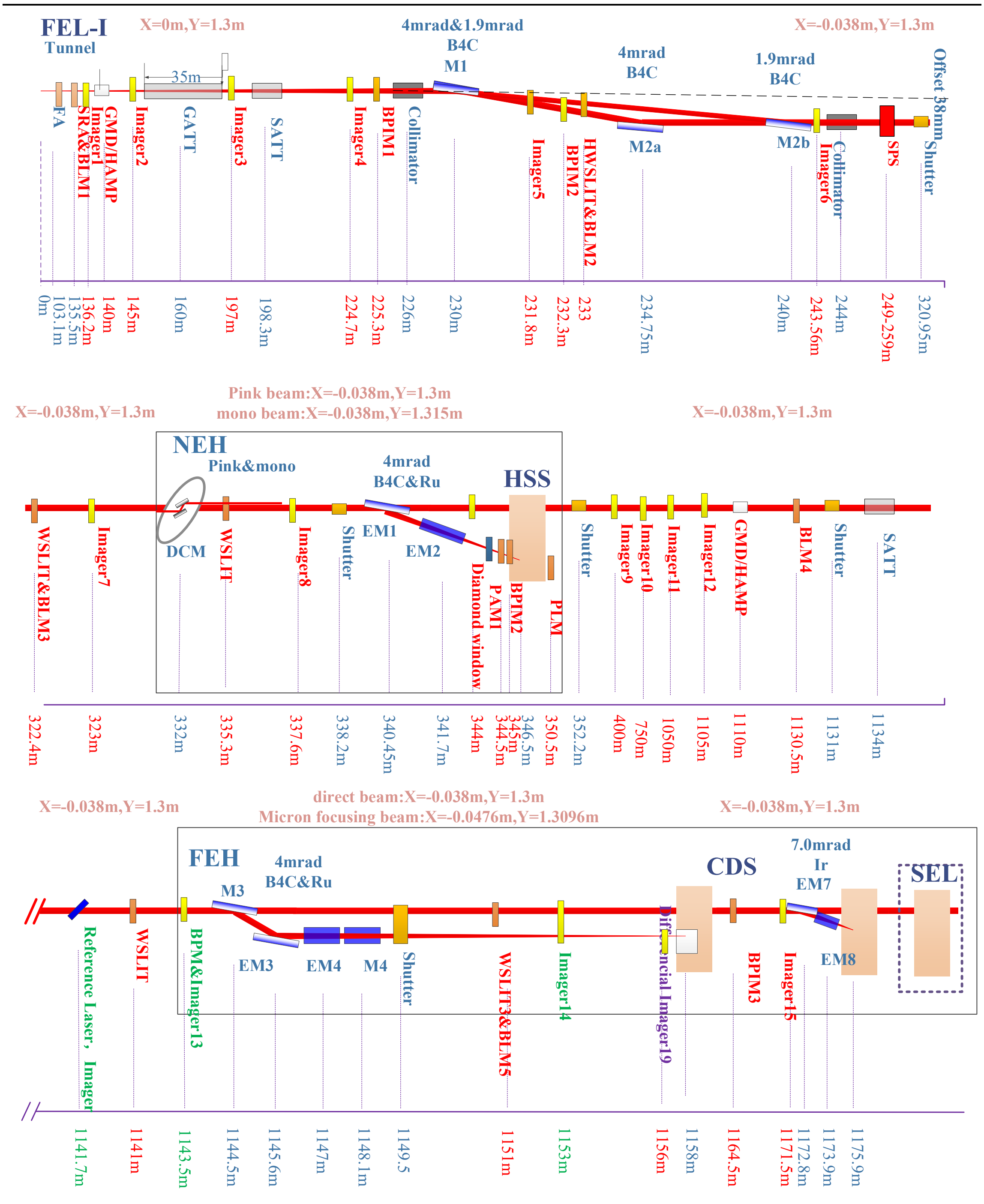

Figure 3.2-1 Layout of all devices in FEL-I beamline

3.3 Physical design

3.3.1 Offset Mirror Group

3.3.1.1 Specifications and Functions

Energy Range: 3-15 keV

Height Error Requirement: Maintain wavefront

Function: Block radiation, absorb thermal load

There are various types of radiation from the machine, including spontaneous radiation, high-energy radiation, and in special cases, high-energy electron beams. For radiation safety, a pair of parallel mirrors is needed to form the offset mirrors, which shifts the beam's position. Necessary radiation shielding must then be implemented in the original direction to ensure radiation safety for the beamline and instruments. Optically, the offset mirrors also absorb spontaneous radiation and cuts off higher harmonics. The requirement for beam offset is directly related to the divergence angle of the high-energy radiation, necessitating a beam offset of more than 20 mm.

While absorbing thermal loads, the wavefront must be maintained to fully utilize the brightness of the free electron laser.

3.3.1.2 Design Scheme

1. Optical Component Size and Position

For the FEL-I beamline, the source divergence angle varies from 5.5 μrad to 1.3 μrad in the 3-15 keV range. This means that at a fixed grazing incidence angle, a 1 m long mirror is required for 3 keV, while only 0.24 m is necessary for 15 keV. At high energies, power density is concentrated at the center of the optical component, making it very difficult to manage. We can refer to European designs, where two mirrors adjust their angles to accommodate different energies. However, this requires frequent adjustments of the M1 and M2 mirrors. Therefore, we consider using two M2 mirrors at different angles, corresponding to high-energy and low-energy regions. The divergence angle range is divided into 1.3-2.7 μrad and 2.6-5.5 μrad, with energy segments of 6-15 keV and 3-7 keV, respectively.

Regarding the coating of the offset mirrors, the reflectivity of B4C at densities of 2.34 g/cm³ for different grazing incidence angles at 7 keV and 15 keV was calculated, as shown in the figures. For angles in the range of 6-15 keV, a grazing angle of 1.9 mrad is used, while 4 mrad is suitable for 3-7 keV. This effectively matches the change in divergence angle at the low-energy position.

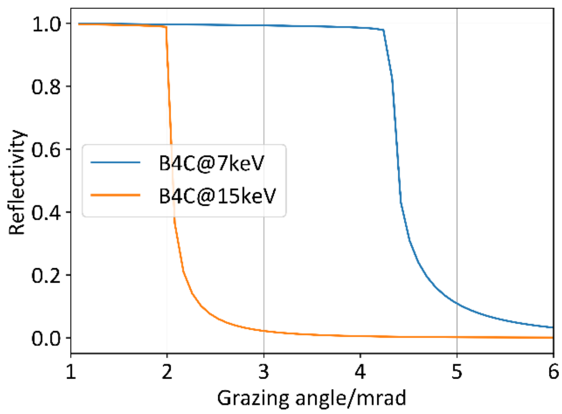

Figure 3.3-1 Reflectivity of B4C at 7 keV and 15 keV for different grazing angles.

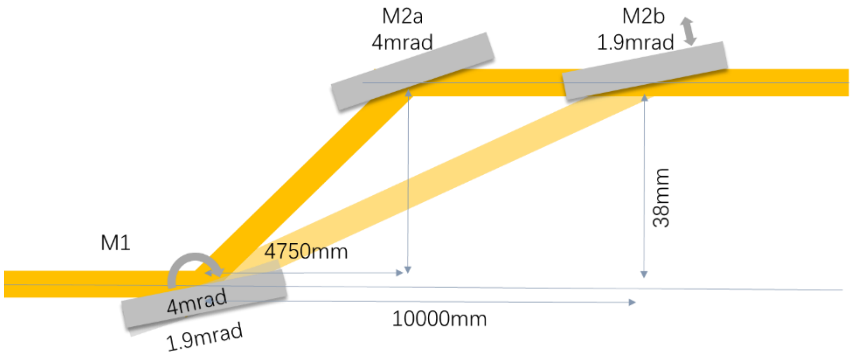

Figure 3.3-2 Geometric structure at two working angles.

The 38 mm offset is primarily for easier radiation protection. The M2b mirror is moved in the normal direction, theoretically requiring a 2 mm movement to be removed from the optical path.

The placement of the offset mirror group needs special consideration. The closer the offset mirror is to the source, the less it affects the stability of the source point, but the higher thermal power density. Considering the inherent instability of the free electron laser in terms of angle and position, the focus is on reducing power density while maximizing transmission repetition rate. Thus, the length of the optical components is designed based on the longest high-quality mirrors currently available worldwide. JTEC can provide 1 m long mirrors, with an effective size of 0.9 m for calculations. The effective size of 0.9 m corresponds to receiving sizes of 1.71 mm and 3.6 mm at 1.9 mrad and 4 mrad, respectively. Based on 2.7 μrad and 5.5 μrad, the calculations yield 6σ values of 6.9 μrad and 14 μrad. Therefore, the M1 mirror can be placed at 248 m, with M1 at 230 m, M2a at 234.75 m, and M2b at 240 m. When continuous operation across the entire energy range is required at the instruments, M2b can cover the full energy range. The horizontal receiving aperture and transmission efficiency are shown in Figures 3.3-3 and 3.3-4. With 1.9 mrad, the theoretical transmission efficiency exceeds 85%.

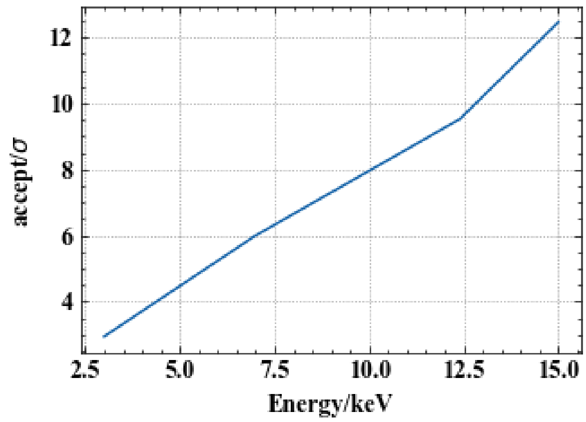

Figure 3.3-3 Horizontal receiving aperture variation for M2b operating at 3-15 keV.

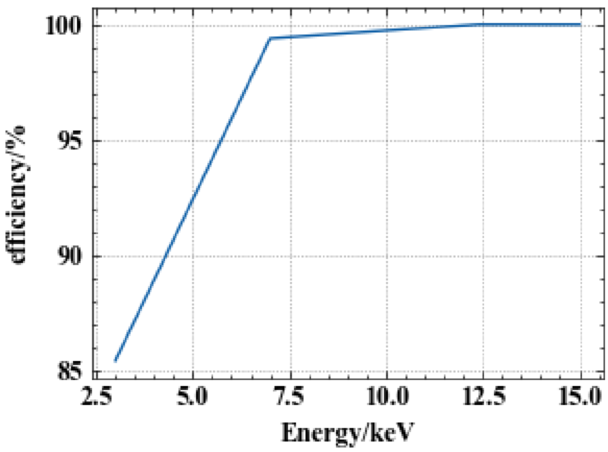

Figure 3.3-4 Transmission efficiency variation for M2b operating at 3-15 keV.

The M1 mirror primarily functions to absorb thermal loads; during this process, it will undergo thermal deformation. The M2a and M2b mirrors are designed to be flexibly bent to compensate for the thermal deformation caused by M1 and their own thermal deformation.

2. Optical Component Requirements

The surface shape accuracy of the optical components is required to meet a Strehl ratio of 0.82. For individual components, the height error can be calculated using the formula:

$$h_{rms} = \frac{\lambda}{14 \cdot \sqrt{N} \cdot 2\alpha}$$

Using this formula, the requirements for optical components at different energies can be calculated. The highest demand is for an RMS of 0.6 nm at 7 keV and 15 keV, while an RMS of 1.5 nm suffices at the low-energy end. The following figures show the 4σ footprint at different energies; as energy increases, the footprint decreases. For the M1 mirror, we can require that the center 450 mm length meets RMS 0.6 nm, the 550 mm length meets RMS 0.9 nm, and the entire length meets RMS 1.5 nm. This requirement is based on practical optical usage needs, including errors introduced by clamping and cooling, while the optical component should maintain an RMS of less than 0.5 nm across the entire mirror length.

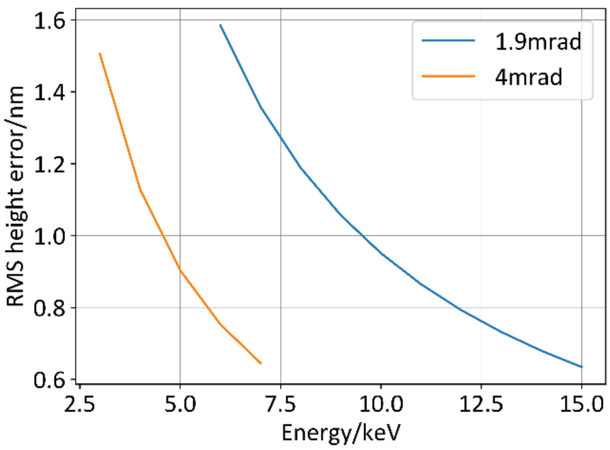

Figure 3.3-5 Height error requirements at different energies.

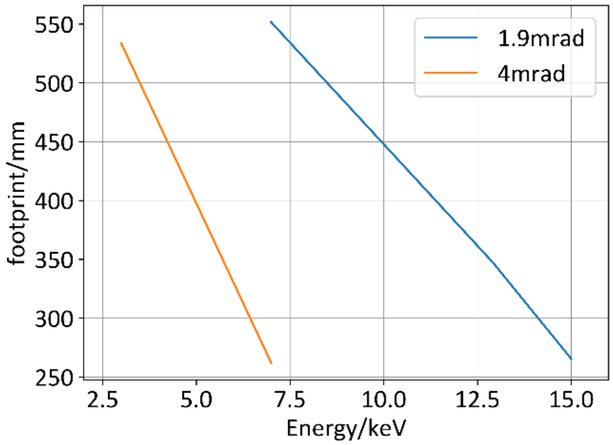

Figure 3.3-6 4σ footprint on the M1 mirror at different energies.

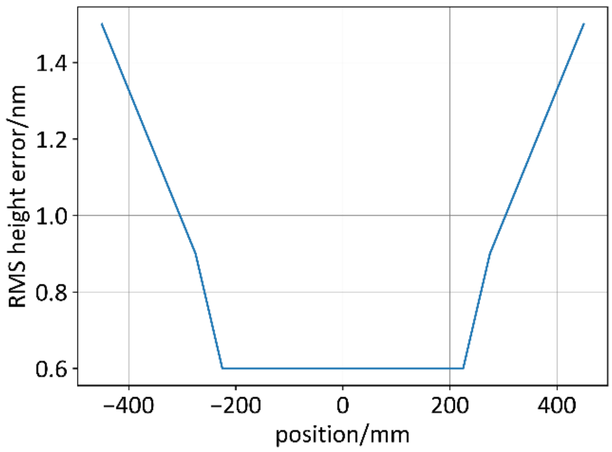

Figure 3.3-7 Height error requirements at different positions of the optical components.

3. Thermal Load on the Offset Mirror

As the first mirror, the heat load of M1 is the highest. Table 3.3-1 gives the parameters of the electron and undulator to calculate the spontaneous radiation. The FEL radiation is from simulations of tapered conditions.

Table 3.3-1 Accelerator parameters used to calculate the radiation power

Electron parameters		Undulator parameters	
Electron energy	8 GeV	Peak magnetic field	1 T
Bunch charge	100 pC	Period	26 mm

Average current	0.1 mA	Undulator length	4 m
Peak current	1000 A	Segments number	42
Pulse duration	100 fs	Distance between segments	1 m
Emittance	0.4 μm*rad		
Repetition rate	1 MHz		

The heat load of the offset mirror comes from three parts. The first part is the spontaneous radiation of the undulator. This part has a very large divergence, which can fill the entire mirror (limited by SRA) and is relatively uniform as a background. As shown in Figures 3.3-7~10, the total absorbed power of spontaneous radiation in the range of 1000 mm×4 mm is approximately 2.2 W, and the power density is 0.55 mW/mm^2. The second part is derived from the FEL. The FEL absorbs 1% (calculated B4C coating reflectivity>99%). According to the tapered undulator simulation, the maximum single pulse energy is 1.8 mJ at 7 keV, and the absorbed power is approximately 18 W. The third part comes from the higher harmonics of the FEL. The content of higher harmonics is between 0.1% and 1%, but the divergence angle of the third harmonics is one-third of the fundamental, which causes the power density of the harmonics to be higher than that of the fundamental and to be concentrated in the center of the fundamental, as shown in Figures 3.3-7~10. In the above estimation, the fundamental and the harmonics content both depend on the status of the electron beam. M2a and M2b are similar to M1, except for harmonics. It may be difficult for single pulse energy to reach the value of the tapered mode, and the heat load may be 1/3-1/5. Figure 3.3-11 shows the statistics of the absorbed power and power density.

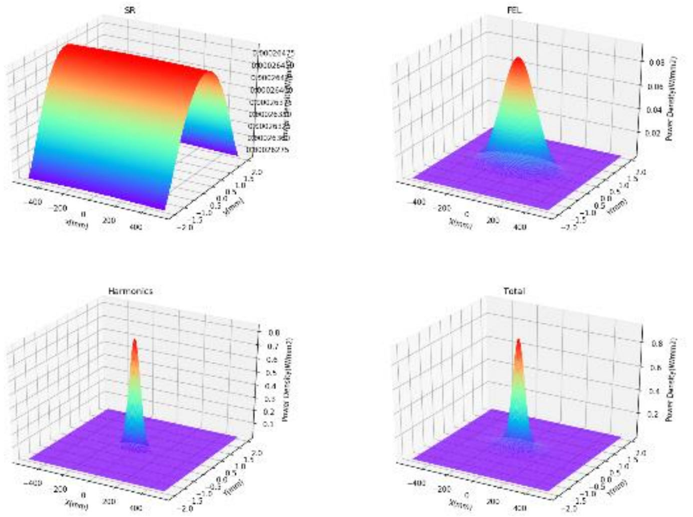

Figure 3.3-7 Power distribution at 1.9 mrad and 7 keV

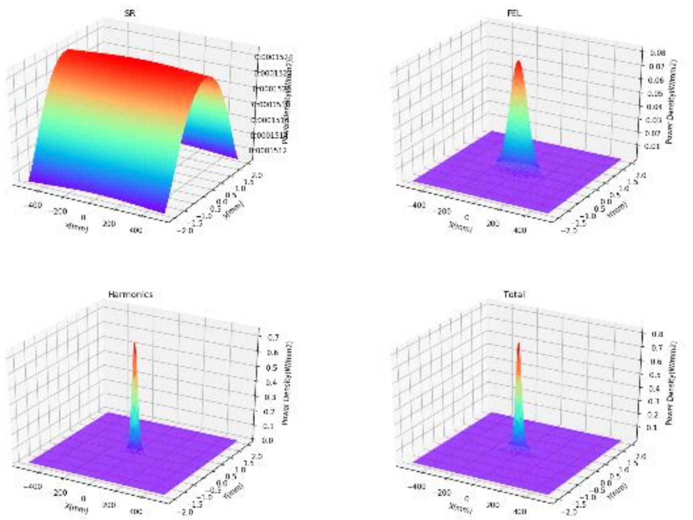

Figure 3.3-8 Power distribution at 1.9 mrad and 12.914 keV

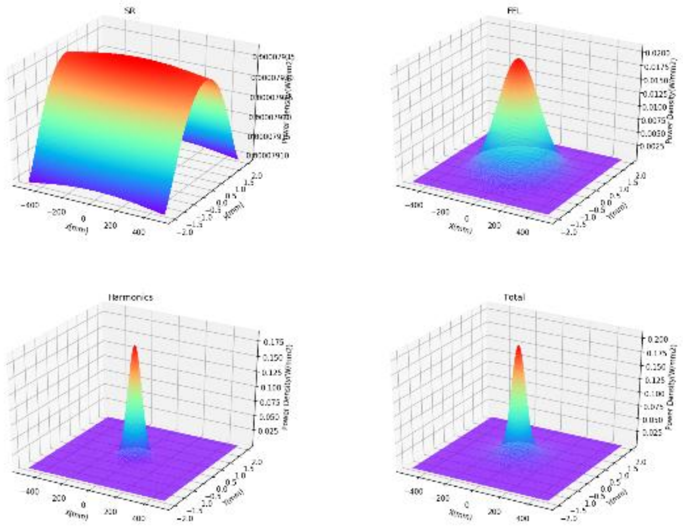

Figure 3.3-9 Power distribution at 4 mrad and 3 keV

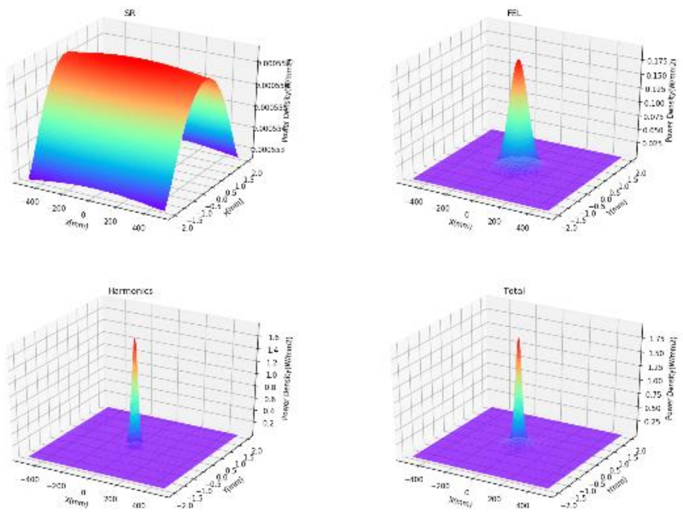

Figure 3.3-10 Power distribution at 4 mrad and 7 keV

Table 3.3-2 Calculation of M1 Mirror Absorbed Power

Photon energy (keV)	3	7	12.914	15
Electron energy (GeV)	5	8	8	8

Bunch charge (pC)	100	100	100	100
Single pulse energy (μJ)	930	1800	394	60
Source size FWHM (μm)	49	45	44	50
Source divergence FWHM (μrad)	5.5	2.7	1.7	1.3
Repetition rate (kHz)	1000	1000	1000	1000
Spontaneous radiation (2 mm*4 mm) (W)	0.3	2.2	0.6	0.2
Power of FEL (W)	930	1800	394	60
Absorbed power of FEL (1%)(W)	9.3	18	3.9	0.6
Power of harmonics (W)	9.3	18	3.9	0.6
Total absorbed power (W)	18.9	38.2	8.4	1.4

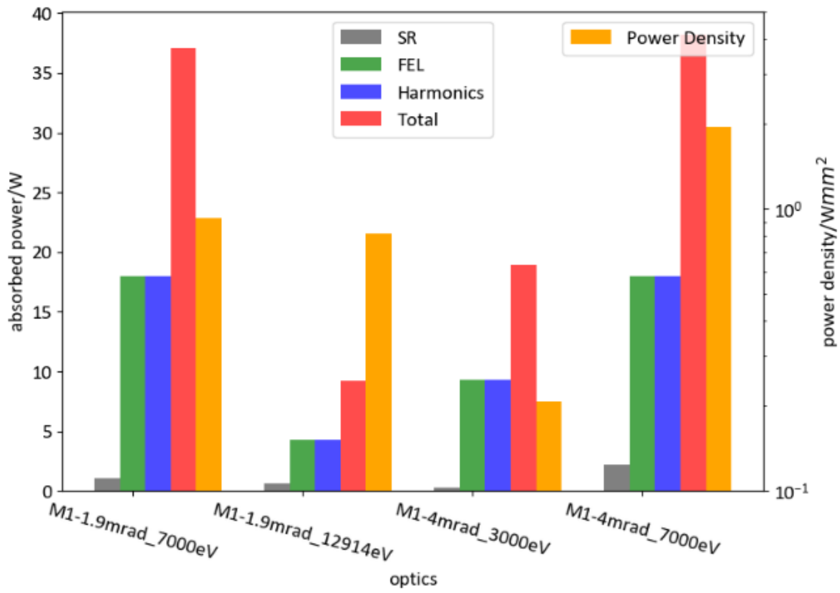

Figure 3.3-11 Absorbed power and power density of M1

4. M2a\M2b bending requirements

M1 and M2a\M2b can be bent independently to correct the deformation caused by heat, but this is complicated. It is also difficult to determine whether a single mirror has been fully compensated. Figures 3.3-12 and 3.3-13 show that bending two mirrors and bending only one mirror have almost the same focus spot size and peak intensity. Therefore, M2a\M2b is bent can meet the requirements.

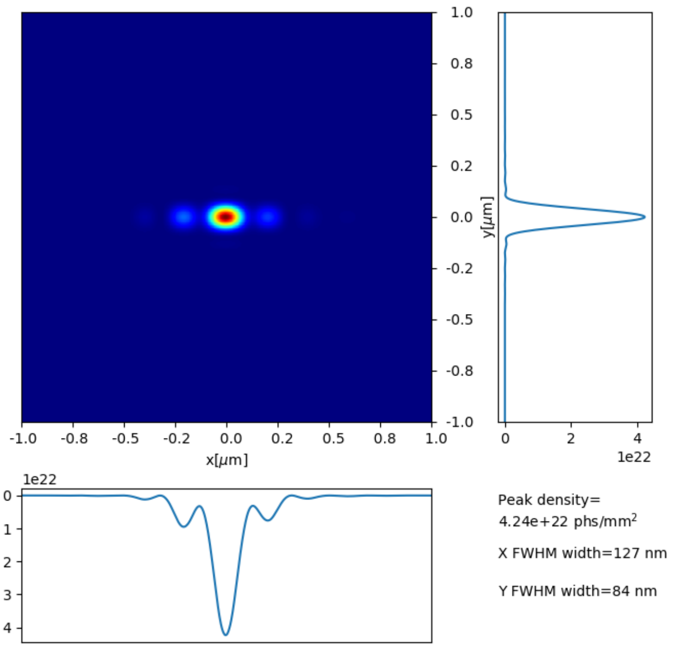

Figure 3.3-12 Simulation of bending M1 and M2 separately

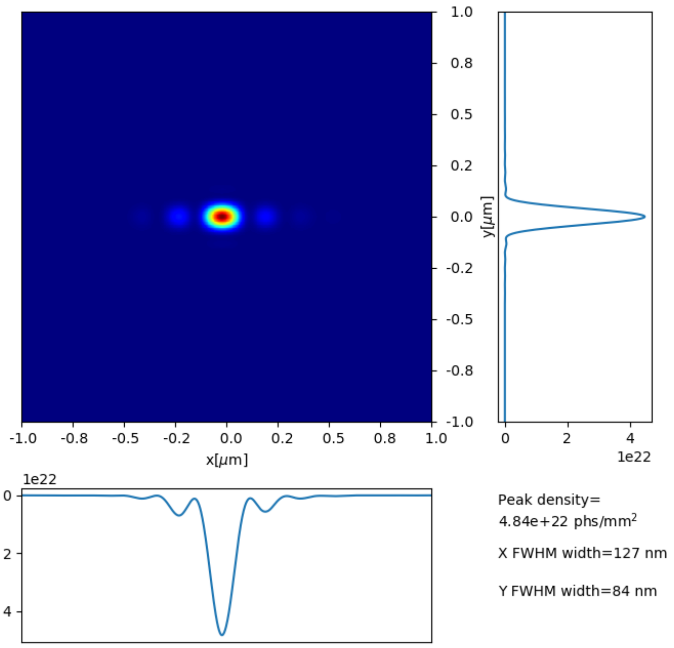

Figure 3.3-13 Simulation of bending M2

Since the divergence is very small and the beamline length is longer than 1100 m, the curvature of M1 and M2a\M2b can easily affect the beam size. For example, the divergence of the beam at 3 keV is 5.5 μrad FWHM. If the mirror has a curvature of 1000 km, it will produce an approximately 1 μrad divergence change within the FWHM. This is a 20% divergence. At the same time, such curvature will also affect the zoom ratio of the entire system. As shown in Figure 3.3-14 and Figure 3.3-15, in the case of 1.9 mrad, the residual curvature of 2000 km can produce a 10% change in the spot size; in the case of 4 mrad, the residual curvature of 1000 km can produce a 10% change in spot size.

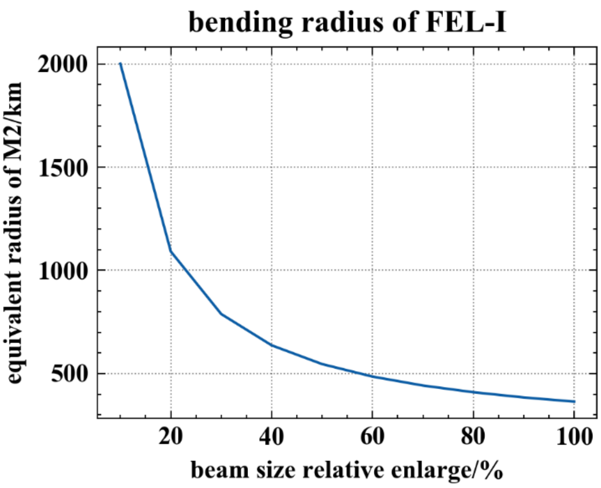

Figure 3.3-14 The relation of the residual curvature and spot size change of M2b at 1.9 mrad

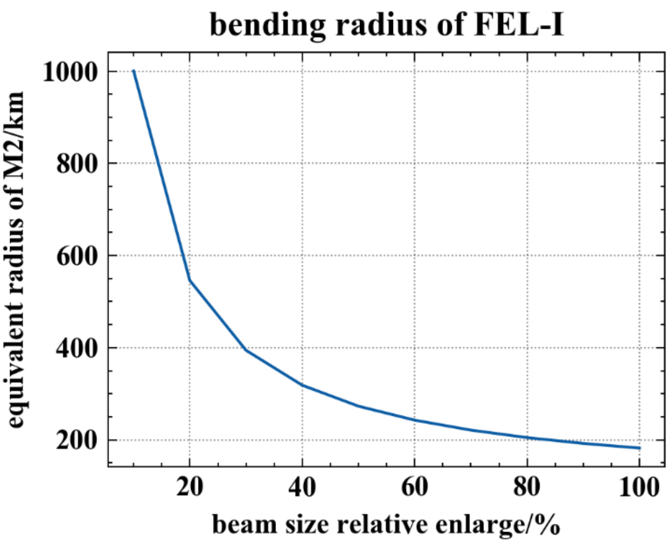

Figure 3.3-15 The relation of the residual curvature and spot size change of M2a at 4 mrad

3.3.2 Crystal Monochromator

3.3.2.1 Specifications and Functions

Energy Range: 3-15 keV

Monochromaticity Requirement: 2×10^{-4}@Si(111)，5×10^{-5}@Si(311)

Position Stability Requirement: The beam position should remain unchanged within a 50 eV range, with a maximum position variation of 10% over a 2 keV range.

The monochromator primarily monochromatizes the light generated by the FEL, requiring the handling of high thermal loads while maintaining beam stability.

3.3.2.2 Design Scheme

1. Crystal Selection

Based on the experimental station's requirements, crystal planes such as Si(111), Si(220), Si(311), and Si(333) can be selected. However, in the low-energy region, the Bragg angle of Si(311) increases sharply (see Figure 3.3-16), necessitating a larger angular range and greater crystal spacing in the mechanical design of the double-crystal monochromator. In this design, a maximum rotation angle of 45 degrees is considered; Si(311) can operate above 5.6 keV, while Si(111) can start from 3 keV. Diamond is also a good option, but current single-crystal diamond sizes present certain issues.

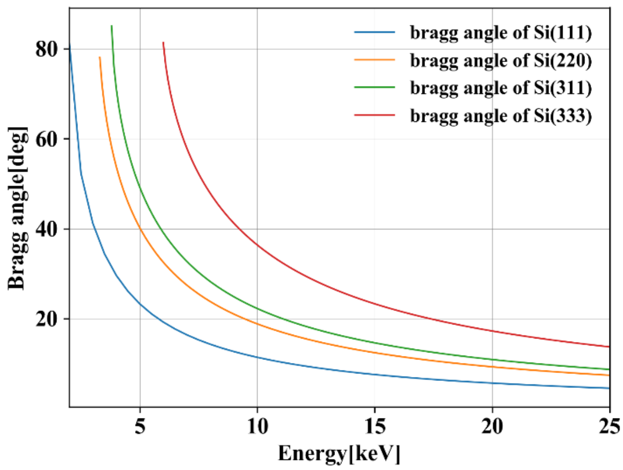

Figure 3.3-16 Bragg angles for different Si crystal planes.

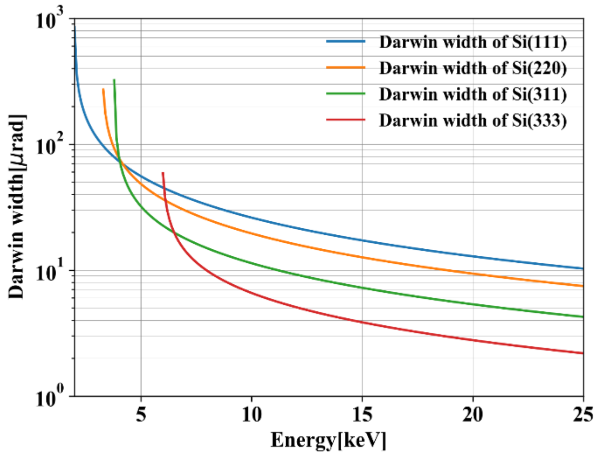

Figure 3.3-17 Darwin widths for different Si crystal planes.

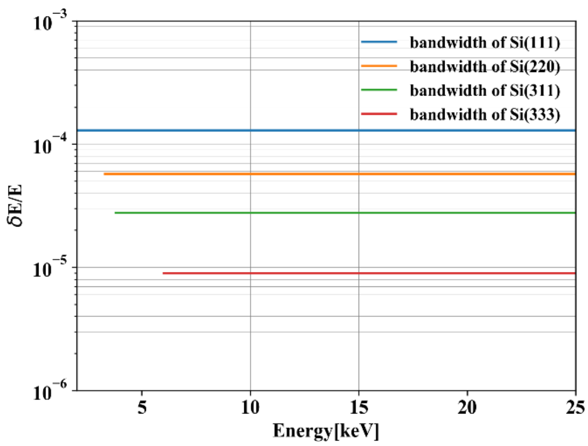

Figure 3.3-18 Energy resolution for different Si crystal planes.

2. Monochromator Geometric Parameters

According to the instrument's requirements, the beam position must remain unchanged during energy scanning. The optical path can vary during the transition from white light to monochromatic light, utilizing a low-temperature cooled double-crystal monochromator. The monochromator should be as close to the instrument as possible, located at 332 m in the near-end experimental hall, with the rotation axis set at the center of the first crystal surface. The Bragg axis rotation angle ranges from 7° to 45°. The rotation range of the Si(311) crystal does not cover the 3-5.6 keV range.

Figure 3.3-19 Schematic diagram of the monochromator at two extreme angles. The height difference H between the incident and outgoing light is fixed at 15 mm. To maintain this height difference, the distance between the crystals is adjusted by moving the second crystal along the normal direction. The distance h between the crystals can be expressed as:

$$h = \frac{H}{2\cos\theta}$$

Minimum length of the first crystal:

$$L_1 = \max\left(\frac{p \times \theta_{div1}}{\sin\theta_{B1}}, \frac{p \times \theta_{div2}}{\sin\theta_{B2}}\right)$$

Minimum length of the second crystal:

$$L_2 = \frac{p \times \theta_{div1}}{2 \times \sin\theta_{B1}} + \left(\frac{H}{2\sin\theta_{B2}} - \frac{H}{2\sin\theta_{B1}}\right) + \frac{p \times \theta_{div2}}{2 \times \sin\theta_{B2}}$$

Additionally, it must be ensured that the end of the first crystal does not block the diffraction light from the second crystal at large Bragg angles:

$$\frac{L_1}{2}\sin\theta_{B1} < H - \frac{p \times \theta_{div1}}{2}$$

Based on the above formulas, the calculated results are shown in Table 3.3-3. Considering the angle range of 5° to 45°, the crystal spacing is $7.53\text{mm} < \text{h} < 10.61\text{mm}$. To ensure the generality of the crystal holding mechanism, Si(111) and Si(311) will use the same dimensions, with the length of the first crystal set at 30 mm and the second crystal at 100 mm.

Table 3.3-3 Crystal monochromator parameter calculations.

crystal plane	angle range	H	h	L1	L2
Si(111)	7.58~41.3° （5-45°）	15mm	7.57~9.98mm （7.53~10.61mm）	10.9~40.3mm （16.5~37.6mm）	＞53.5mm （＞86.1mm）
Si(311)	14.62~42.5° （5-45°）	15mm	7.75~10.17mm （7.53~10.61mm）	6.9~37.5mm （16.53~35.8）	＞24.9mm （＞87mm）

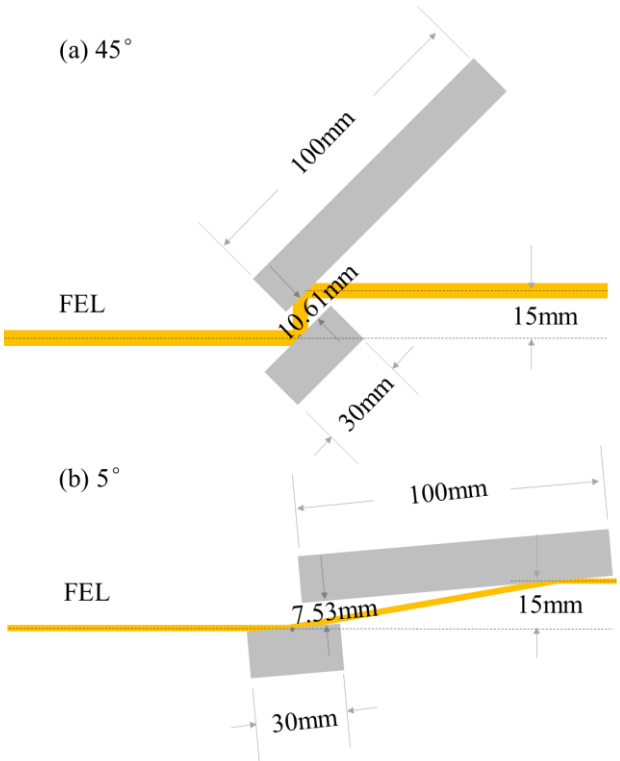

Figure 3.3-19 Schematic diagram of the crystal monochromator.

3. Energy resolution

Energy resolution is a crucial indicator for the crystal monochromator. Assuming no crystal deformation, the energy resolution of the double-crystal monochromator is determined by the divergence angle of the incoming light in the vertical direction and the Darwin width of the crystal.

$$\Delta E/E = \Delta\theta \cot\theta$$

$$\Delta\theta = \sqrt{\psi^2 + w^2}$$

Where ψ is the divergence angle of the light source and w is the Darwin width of the crystal. As shown in Figure 3.3-17, the Darwin width varies with energy for different crystal planes. The beam's vertical divergence angle ranges from 5.5 to 1.3 μrad. It is evident that for X-ray free electron lasers, the beam's divergence angle is much smaller than the Darwin width of Si(111); for Si(220), Si(311), and Si(333), there is a certain comparability at high energy positions.

4. Crystal Requirements

There is limited literature discussing the surface shape error requirements for crystal monochromators for coherent light. According to the wavefront protection requirements, the crystal deformation should satisfy:

$$\Delta\theta \ll \Delta\Psi$$

where $\Delta\Psi$ is the divergence angle σ of the incoming light, with the divergence angle of the free electron laser varying from 2.34 to 0.55 μrad. $\Delta\theta$ is the lattice deformation caused by crystal deformation, which must be less than one-tenth of the divergence angle σ, requiring less than 0.2-0.05 μrad for the 3-15 keV range. Additionally, considering the impact of residual height errors on focusing, the following formula must be satisfied to meet the Strehl ratio requirement:

$$\Delta h_i < \frac{\lambda}{14 \times 2 \times \sin\theta \times \sqrt{N}}$$

where Δh_i is the residual lattice surface distortion, and θ is the Bragg angle. When the crystal is clamped, cooled, and irradiated, the lattice may distort, causing bending and changes in lattice spacing. These can lead to wavefront distortion, reducing the efficiency of the crystal monochromator. The following figure shows the basic requirements for lattice distortion.

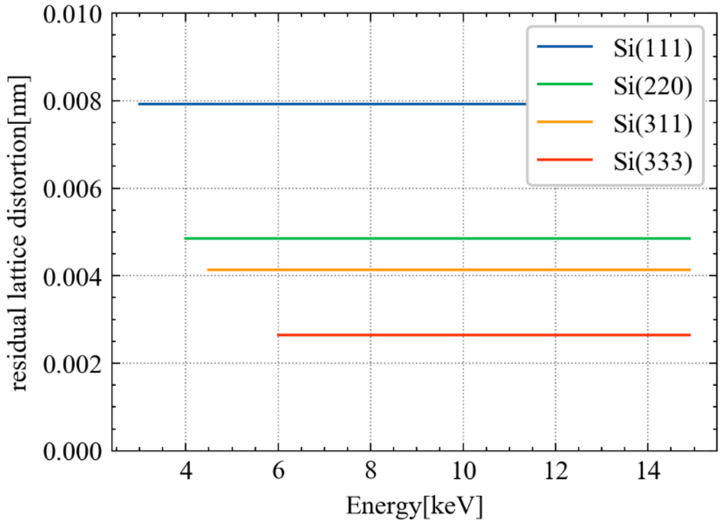

Figure 3.3-20 Requirements for residual lattice distortion.

The quality of the crystal surface processing also significantly affects the beam. There have been multiple reports from Japan's SACLA, primarily considering lattice damage, defects, and stress caused by processing, which can create speckles in coherent light. Using the calculation methods from SACLA articles, defects can be treated as phase objects, and as shown in Figure 3.3-21, under a Strehl ratio of 0.82, the defect error requirement for a single crystal is that the surface defect error should not exceed 65 nm RMS when accounting for six optical components.

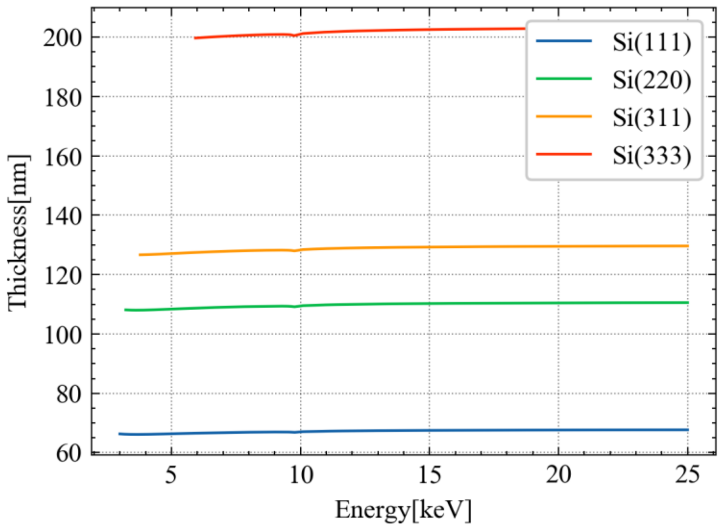

Figure 3.3-21 Surface defect error requirements for a single crystal calculated for SR=0.82.

Figures 3.3-22 and 3.3-23 show the curvature effects on the first crystal due to heating, simulated using Shadow. The results indicate that when the radius exceeds 500 m, the impact on flux and resolution is minimal.

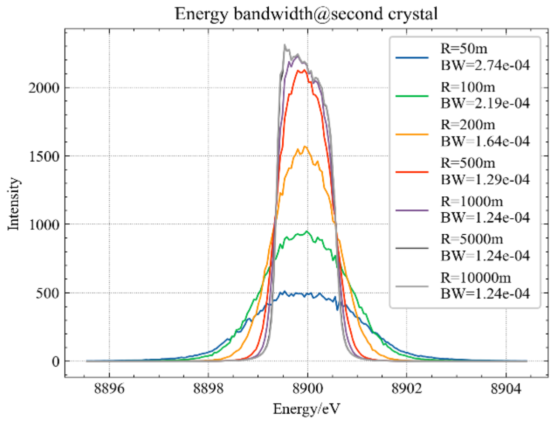

Figure 3.3-22 Resolution changes due to different curvatures of the Si(111) crystal at 8.9 keV.

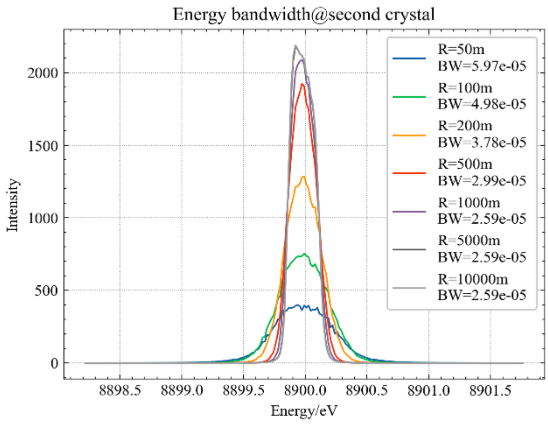

Figure 3.3-23 Resolution changes due to different curvatures of the Si(311) crystal at 8.9 keV.

5. Thermal Load on the Crystal Monochromator

Tables 3.3-4 and 3.3-5 provide the thermal load and power density for the monochromator at a repetition frequency of 1 MHz. The data indicate that for high-frequency FELs, the power density on the monochromator is extremely high. The crystal monochromator is not suitable for operation at high repetition frequencies; specific working conditions will require finite element analysis results. If limited to the order of watts per square millimeter, the repetition frequency should be restricted to 10 kHz or the single pulse energy reduced.

Table 3.3-4 Si(111) absorbed power and power density

Energy [keV]	Bragg angle [°]	Pulse energy (mJ)	Beam size (mm×mm)	power (W)	Power density (W/mm^2)
3	41.23	0.93	1.8×2.8	837	145
7	16.4	1.8	0.9×3.2	1620	583
12.4	8.8	0.4	0.57×3.7	387	280
15	7.57	0.06	0.43×3.3	54	33

Table 3.3-5 Si(311) power and power density

Energy [keV]	Bragg angle [°]	Pulse energy (mJ)	Beam size (mm×mm)	power (W)	Power density (W/mm^2)
5.5	43.4	0.93	1.3×1.9	1170	401
7	32.74	1.8	0.9×1.6	1620	1116
12.4	17.78	0.4	0.57×1.9	387	557
15	14.62	0.06	0.43×1.7	54	64

3.3.3 KB Focusing System

3.3.3.1 Requirements and Functions

Spot size: 5-200 µm @HSS, 1 µm @CDS, 100 nm @CDS

Energy range: 3-15 keV

FEL-I has four sets of KB systems: one is used for HSS, and the other three are used for CDS.

3.3.3.2 Scheme Design

1. HSS KB

The KB system can cover 3~15 keV, and give a smaller spot size. The spot size can be changed by bending the mirrors and working in an out-of-focus mode.

(1) Geometric parameters

The source size for FEL-I is approximately 50 μm. A 5 μm spot size requires a 10:1 zoom ratio. If the KB system is placed at 340 m, the image distance needs to be 34 m. A long image distance requires high stability of the KB system. The KB image distance needs to be set in an acceptable range. According to the working distance requirements of HSS, the minimum image distance is approximately 5 m. Thus, two mirrors are set at 340 m and 341.2 m. The theoretical spot size is less than 1 μm. And The KB system can work in an off-focus mode to fulfill the requirements of experiments.

The mirror length is 1 m long with a 0.9 m clear aperture and a 4 mrad grazing angle. It has two coatings, B_4C and Ru, for 3~7.5 keV and 7~15 keV, respectively (Figure 3.3-24). At 3 keV, the 4σ beam size is approximately 3.2 mm, and for 0.9 m, a clear aperture can accept 3.6 mm. The HSS requires that the spot size on the sample be varied from 5 μm to 200 μm. Therefore, the mirrors are bendable and have a pre-elliptical shape that can focus the beam to the smallest spot and then bend to a larger radius to defocus and realize a larger spot size.

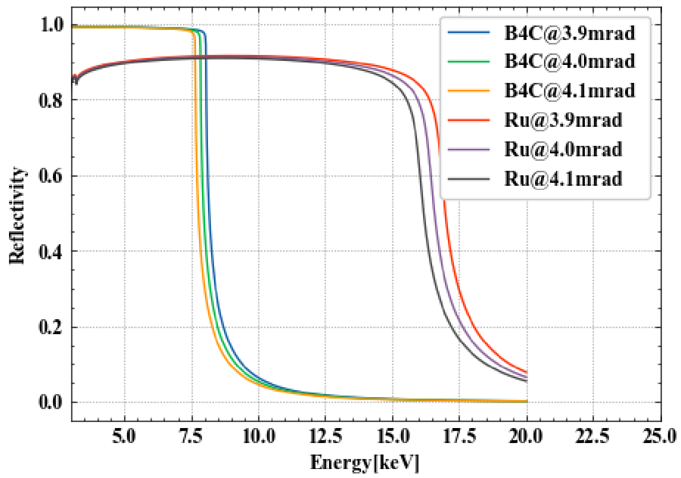

Figure 3.3-24 Reflectivity of B4C and Ru

(2) Figure error requirements

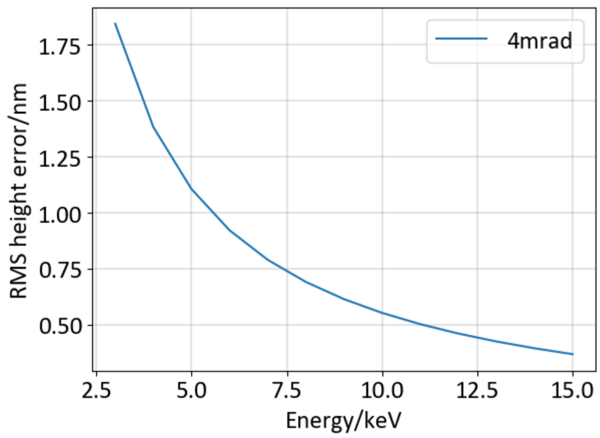

Figure 3.3-25 Height error requirement of the HSS KB system when SR=0.82

As shown in Figure 3.3-25, the height error requirement is less than 0.5 nm RMS at 15 keV, but the limit from the manufacturer is 0.5 nm RMS. In addition, this KB system works in the off-focus mode. This means that the uniformity of the spot is more sensitive to height error, but the requirement has reached the limit. When the endstation works in the accumulation mode, the spot will become more uniform and larger than that in the single pulse mode due to the instability of beam.

(3) Heat load

When the endstation works in monochromatic beam mode, most of the heat load is absorbed by the monochromator, and the monochromator limits the repetition rate. The incident power on KB mirrors does not exceed 1 W, and the absorption is on the order of mW. The cooling system is not needed.

In the non-monochromatic beam mode, the maximum absorption power is approximately 20 W at a 1 MHz repetition rate for B_4C coating. When using Ru as the coating, the reflectivity is only approximately 90%. In this case, although single pulse damage is not a problem, the heat load is very high. The power density distribution at 7 keV are shown in Figures 3.3-26 and 3.3-27 for different coatings.

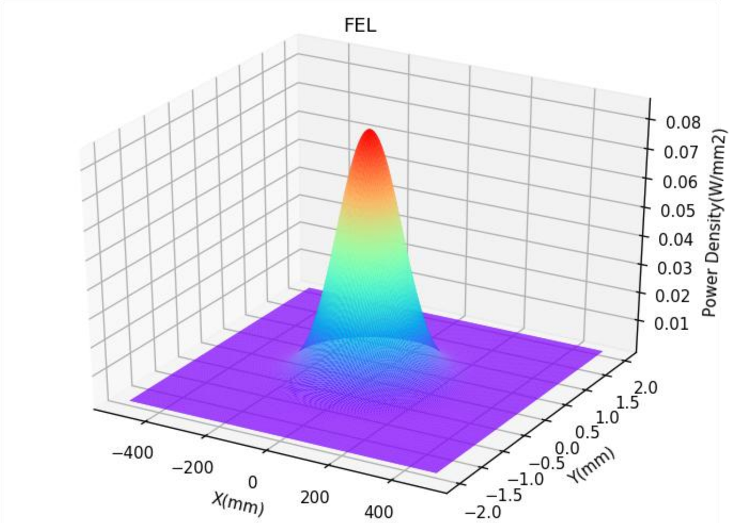

Figure 3.3-26 Power distribution on a HSS KB mirror with B_4C coating at 7 keV

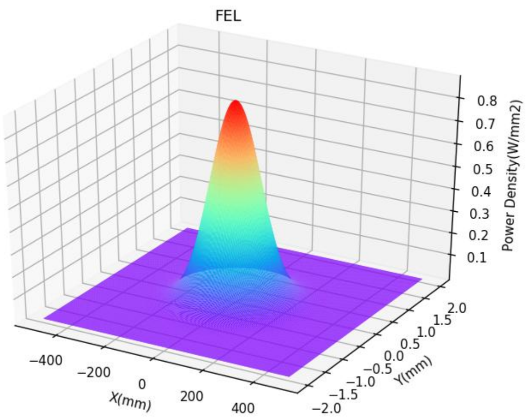

Figure 3.3-27 Power distribution on a HSS KB mirror with Ru coating at 7 keV

2. CDS KB

(1) Geometric parameters

There are three sets of KB systems: one micron-KB, and two nano-KBs. It requires a high peak intensity, which itself requires the wavefront preservation. It requires 100 nm and 1 μm focal spot sizes for different sample sizes.

Many factors affect the focal spot size:

i. Optical geometrical zoom ratio: This ratio is determined by the ratio of object distance p and image distance q, but the image distance is limited by the size of the optical element and the required working distance, and generally cannot be unlimitedly reduced $q > \frac{L_{chamber}}{2} + L_{wd}$.

ii. Source size: Under the zoom ratio defined in i, the focal spot size is affected by the source size. The source size is determined by the parameters of the accelerator and varies with the wavelength. Currently, the source size provided by the accelerator is approximately 30~50 μm.

iii. Numerical aperture (NA): NA limits the minimum spot size. The minimum spot size can be estimated with the Gaussian beam truncation theory.

iv. Wavefront distortion: This can be from the original figure error of optics, clamping, misalignment, and heat load.

Micron-focus KB layout: To focus the beam to 1 μm, the KB is set as p_h=1145.7, q_h=12.3 m, p_v=1146.9, and q_v=11.1 m. Since the beamline is very long and acceptance is limited by the mirror length, the focal spot size is mainly determined by the diffraction limit. Figure 3.3-28 shows the spot size, which is calculated with the Gaussian beam truncation theory. The focal spot size in the energy range above 7 keV can be less than 1 μm. The spot size will also be affected by the coherence, the source size, and the final figure error.

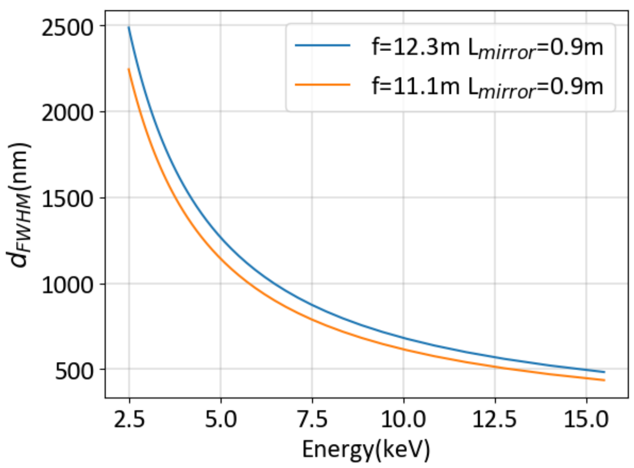

Figure 3.3-28 The focal spot size calculated with Gaussian beam truncation theory

In addition, to improve the stability of the beam and focus the beam to the nano focus as close as possible, a four-bounce KB system will be used, similar to SPB at European XFEL[3, 4]. Two flat mirrors are added. One is a horizontal deflection parallel to the horizontal focusing mirror; the other is a vertical deflection parallel to the vertical focusing mirror. Such a design can keep the beam direction unchanged but with horizontal and vertical offsets. At the same time, it can make the adjustment of the KB system more flexible and less sensitive to the stability. The arrangement of mirrors is M3, EM3, EM4 and M4. M3 and EM4 can be moved out of the optical path to let the beam pass to the nano-KB and SEL.

M3, EM3, EM4, and M4 have two coating strips, B_4C and Ru, used for 3~7.5 keV and 7.5~15 keV. On one hand, two coating strips can increase the clear aperture, and on the other hand, they can suppress harmonics in the low energy region.

The height error requirement is calculated, as shown in Figure 3.3-29. Six optical elements are considered, and the height error should be smaller than 0.5 nm RMS in the range of 8~15 keV, but the best mirror is 0.5 nm RMS.

To make the system as stable as possible, M3 and EM3 are in the same chamber and marble support, thereby reducing the effect of vibration. EM4 and M4 are the same.

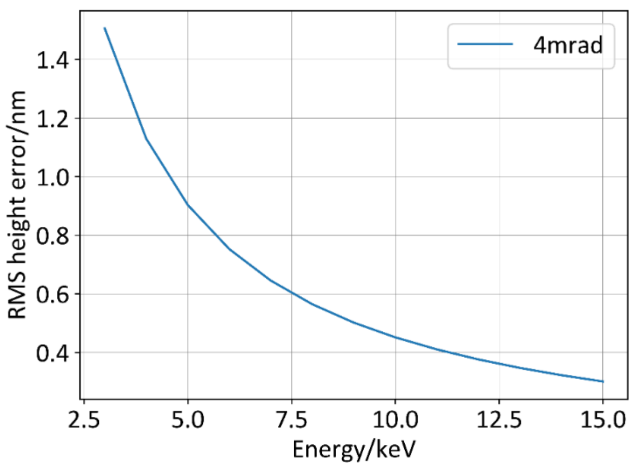

Figure 3.3-29 Height error requirements for micron-KB

Nano KB layout: According to the diffraction limit and working distance requirements, the KB is set as p_v=1155.6 m, q_v=2.4 m, p_h=1154.5 m, and q_h=3.5 m. Due to the large zoom ratio of the focus, the grazing incidence angle difference between the front and rear of the mirror will be approximately 1.1 mrad. To compensate for this difference, the grazing angle is set to 3.5 mrad, and the coatings are Ru and B_4C. The spot size is also determined by the diffraction limit. The theoretical spot sizes in the two directions are shown in Figure 3.3-30. The calculation includes the diffraction limit with truncation and the Gaussian beam without truncation. Due to the q difference, the horizontal focus size will be larger. The height error is better than 0.5 nm RMS.

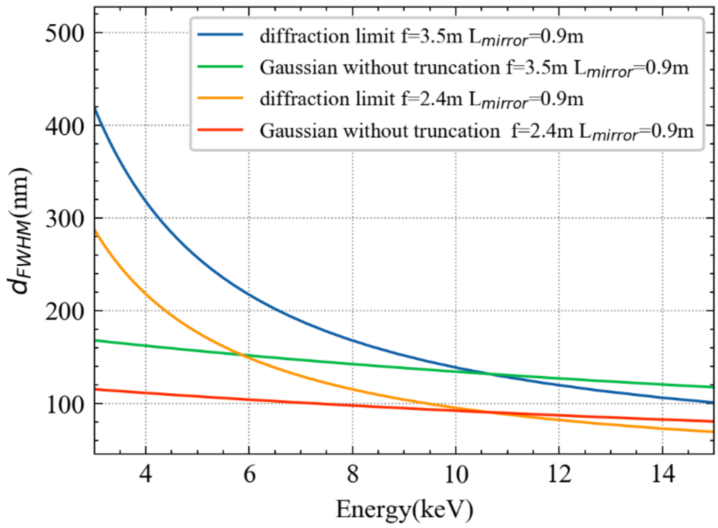

Figure 3.3-30 Spot size estimated with diffraction-limited and Gaussian beams without truncation of Nano KB

The second Nano KB layout: At the end of the experimental station, a KB system with a focal length of 1 m is set. After this KB, the differential pumping system cannot be installed and considered using a window and working with a low repetition rate. As shown in the Figure 3.3-31, focusing below 100 nm can be achieved. The grazing incidence angle is 7 mrad with Ir coatings. The energy range of this KB is 3-10 keV. The surface accuracy requirements are the same as above.

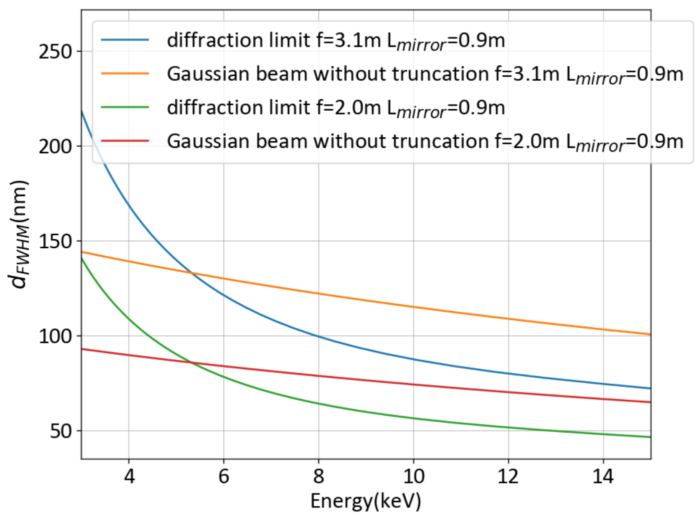

Figure 3.3-31 Spot size estimated with diffraction-limited with truncation and Gaussian beams without truncation of the second Nano KB

(2) Acceptance

The Acceptance of KB is a problem in the CDS. The micron KB and Nano KBs have 3.6mm and 3.15mm clear apertures. The acceptance is shown in Table 3.3-6. The acceptance is very small in the lower energy range. The M2a/M2b can slightly converge the beam by bending, but this only can converge in the horizontal. The CRL1 also can be used to weakly focus the beam for the high energy range weakly.

Table 3.3-6 Acceptance of KB at CDS

Energy[keV]	3.0	5.0	7.0	12.4	15.0
Divergence(FWHM)	5.5	4	2.5	1.7	1.3
Acceptance micron-	1.3	1.8	3.0	4.3	5.7
Acceptance first	1.2	1.6	2.6	3.8	5.0
Acceptance second	2.4	3.2	5.2	-	-

(3) Heat load

The same as HSS KB mirrors, the heat load of Ru coating is very high. And the footprint is big as it is more than 1100m far from the source. Figures 3.3-32 and 3.3-33 show the power distribution of CDS KB mirror with different coatings at 7keV.

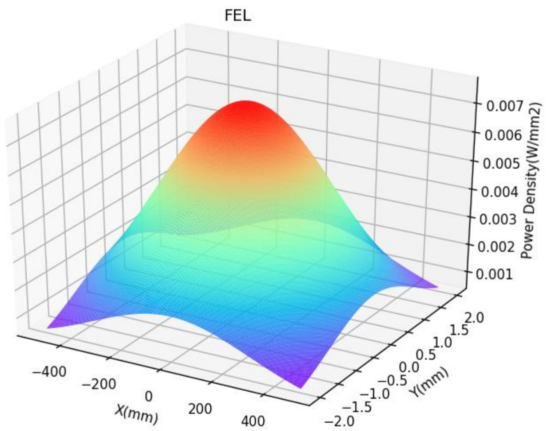

Figure 3.3-32 The power distribution on a CDS KB mirror with B_4C coating at 7 keV

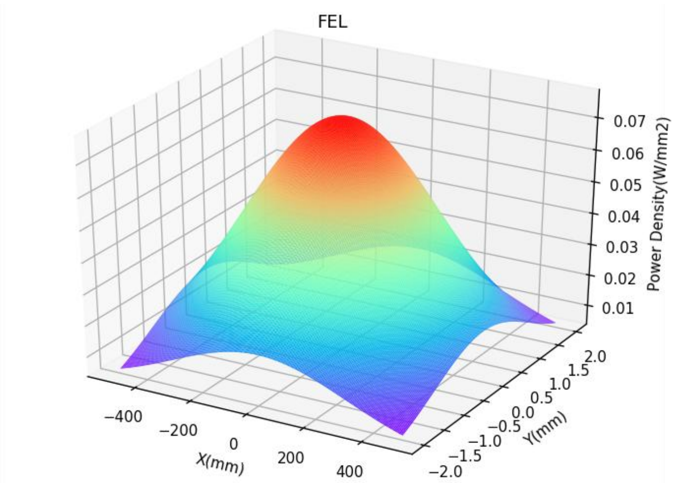

Figure 3.3-33 The power distribution on a CDS KB mirror with Ru coating at 7 keV

3.3.4 CRL system

3.3.4.1 Requirements and Functions

There are three sets of CRLs in the beamline, and the working energy ranges are from 5 keV to 15 keV. The first set serves as a collimated CRL. The second set provides a 5 μm focus for the HSS endstation. The third set provides a 5 μm focus for the CDS endstation.

3.3.4.2 Scheme Design

1. Principle of CRL

For X-rays, the complex refractive index of a material can be expressed as n=1-δ-iβ, where δ represents the correction of the real part of the refractive index and is a positive number much less than 1, and β is related to the absorption of the material. The refractive index of X-rays is very close to 1. The focusing of X-rays can be achieved by using concave lenses. Because δ is very small, a combination of multiple concave lenses is often required. Such a combination of concave lenses is called a compound refractive lens (CRL). Figure 3.3-34 shows the schematic diagram of the parabolic CRL, where R is the lens radius, d is the central thickness, Z_L is the lens thickness, $2R_0 = 2\sqrt{2R \cdot 0.5(Z_L - d)}$ is the geometric aperture.

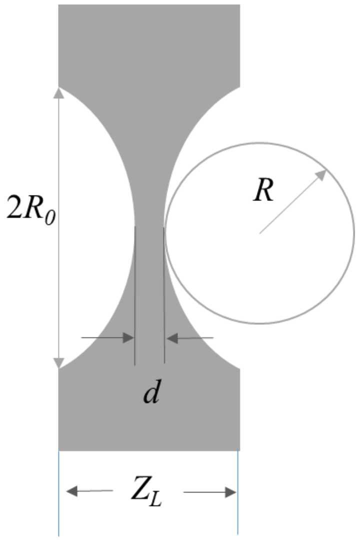

Figure 3.3-34 Schematic diagram of the parabolic CRL

(1) Focal length

The lens material is Be, which has good transmittance, high thermal conductivity, and high damage threshold. Different numbers of lenses are used to achieve different focal lengths for specific energy, and the same focal length needs different combinations of lenses for different energies. The principle diagram is shown in Figure 3.3-35. The focal length is determined by the following formula:

$$\frac{1}{2\delta f} = \sum_i \frac{N_i}{R_i}$$

where f is the focal length, N_i is the number of lenses, and R_i is the radius of the lenses, $\sum_i \frac{N_i}{R_i}$ is focusing power.

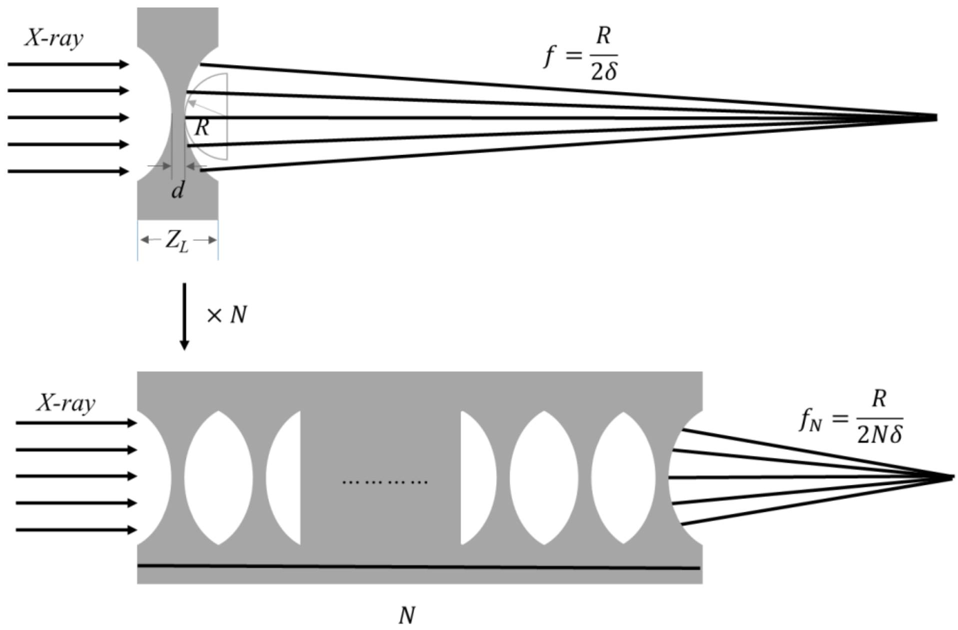

Figure 3.3-35 Schematic diagram of the CRL stack

(2) Effective aperture

Although the absorption of Be is small, tens of lens also cause changes in the effective aperture. The effective aperture can be expressed[5-7] as:

$$D_{eff} = \sqrt{\frac{4}{C_{N,R}}\left(1 - e^{-C_{N,R}R_{0,min}^2}\right)}$$

Where $C_{N,R} = \frac{\mu}{2}\sum_{in}\frac{N_i}{R_i}$ for the theoretical calculation without errors.

(3) Transmission

The optimation of CRL is to have the best transmission, and the transmission can be calculated by the following formula:

$$T = \frac{e^{-\mu N_{in} d}}{1 + 2\sigma^2\mu\sum_{in}\frac{N_i}{R_i}}\left(1 - e^{-(\frac{1}{2\sigma^2}+\mu\sum_{in}\frac{N_i}{R_i})R_{0,min}^2}\right)$$

where μ is the linear absorption coefficient, N_{in} is the lens number, σ is the standard deviation of the intensity distribution for Gaussian beam.

(4) Commercial lenses

The CRL design is based on the commercial Be lenses. The specifications provided by

RXOPTICS are shown in Table 3.3-7.

Table 3.3-7 Standard CRL parameters provided by RXOPTICS

Radius of curvature R(mm)	Beryllium 2D lenses	Beryllium 1D lenses
0.05	×	
0.1	×	
0.2	×	×
0.3	×	×
0.5	×	×
1.0	×	×
1.5	×	
2.0	×	
2.5	×	
3.0	×	
4.0	×	
5.0	×	

2. CRL1

The CRL1 is placed in front of the offset mirrors. This can be combined with other CRLs to focus the beam and weakly focus for increasing the KB acceptance.

The CRL1 is placed at 200 m away from the source. The requirements of the focusing power for different energies are shown in Figure 3.3-36. According to the focusing power, a group of lenses is selected, as shown in Table 3.3-8. There is a customized lens with 5.8 mm radius to avoid damage of instruments in the far experimental hall (FEH). The first optimation of transmission and the focal length was performed. Figure 3.3-37 shows (a) the focusing power, (b) the effective aperture and 6σ beam size, (c) the focal length differences ($\Delta f = f - f_{real}$), (d) the transmission of the optimized combinations. The effective aperture is much larger than the beam size. The focal differences are larger than 20m for some energies, and the image distances are calculated with the real focal length of CRL1, as shown in Figure 3.3-38. When the image distances are plus, the beam is converged and focused at these positions. It is dangerous and maybe damage the instruments. The minimum image distance is 1500 m, and the beam size at 340 m (in the NEH) is 3/4 of the beam size on CRL1, while the beam size at 1140 m (in the FEH) is 1/4 of beam size on CRL1. It can damage instruments, so the second optimation for FEH was performed. Figure 3.3-39 shows the image distance when optimized for FEH. Figure 3.3-40 shows the result of the second optimization. In addition, if the final divergence of FEL may be 1.5~3 times of the simulation result, CRL1 can be set to slightly converge the beam to keep the acceptance of the following optical elements.

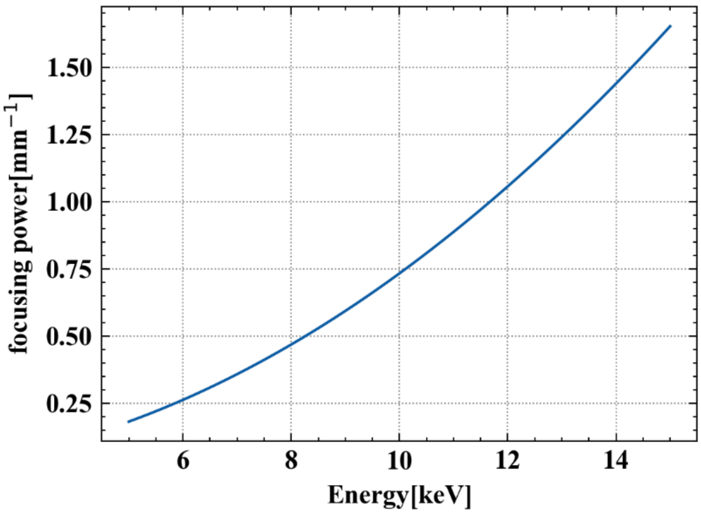

Figure 3.3-36 Focusing power requirements of CRL1 (f=200 m)

Table 3.3-8 CRL1 lenses

Actuator	1	2	3	4	5	6	7
Lenses N×R (mm)	1×5.8	1×5.0	1×4.0	1×3.0	1×2.5	2×4.0	2×3.0
N/R (mm-1)	0.17	0.2	0.25	0.33	0.4	0.5	0.67

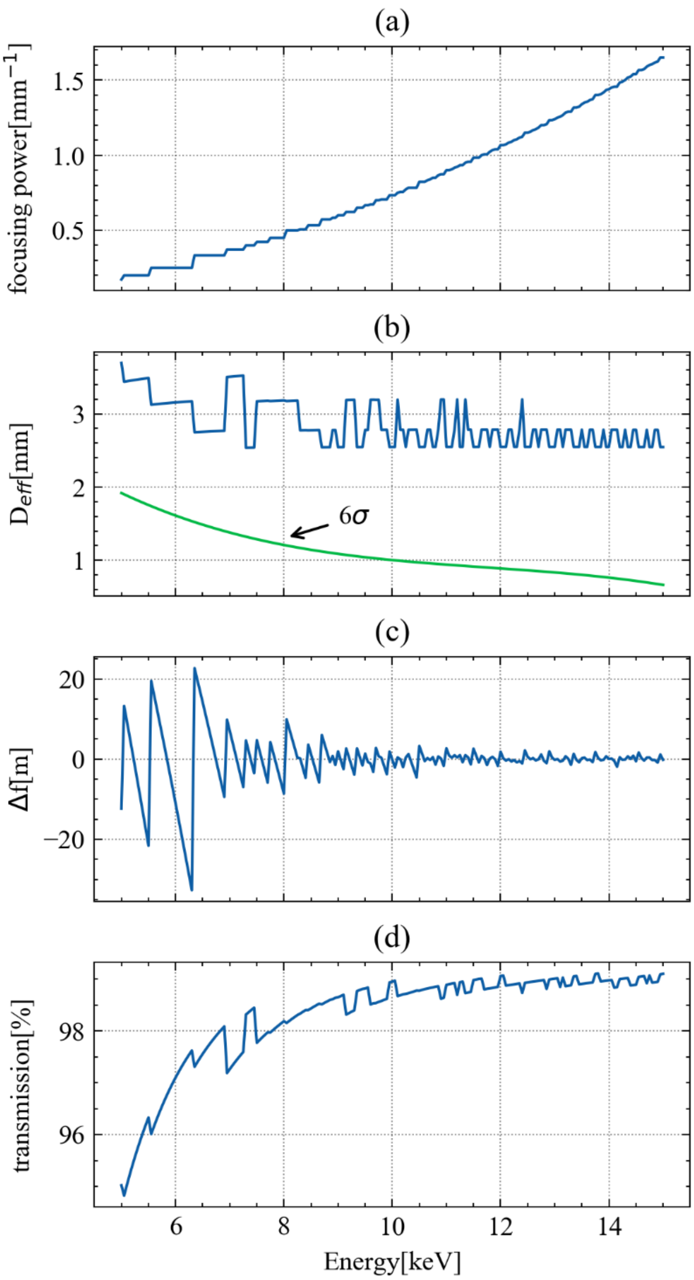

Figure 3.3-37 (a) the focusing power, (b) the effective aperture and 6σ beam size, (c) the focal length differences ($\Delta f = f - f_{real}$), (d) the transmission of the first optimization for CRL1 (f=200 m)

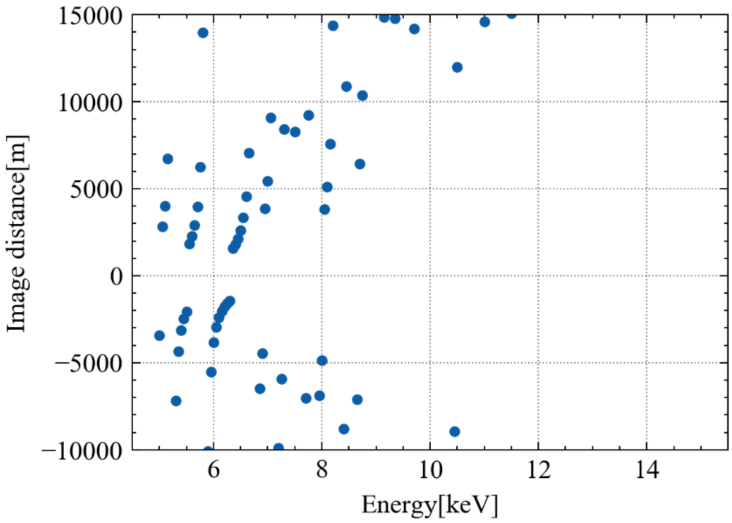

Figure 3.3-38 The image distance for the first optimization of CRL1 (f=200 m)

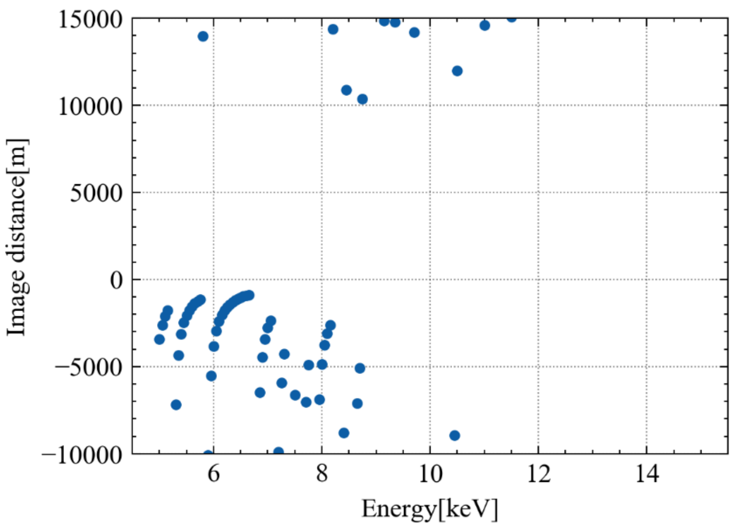

Figure 3.3-39 The image distance for the second optimization of CRL1 (f=200 m)

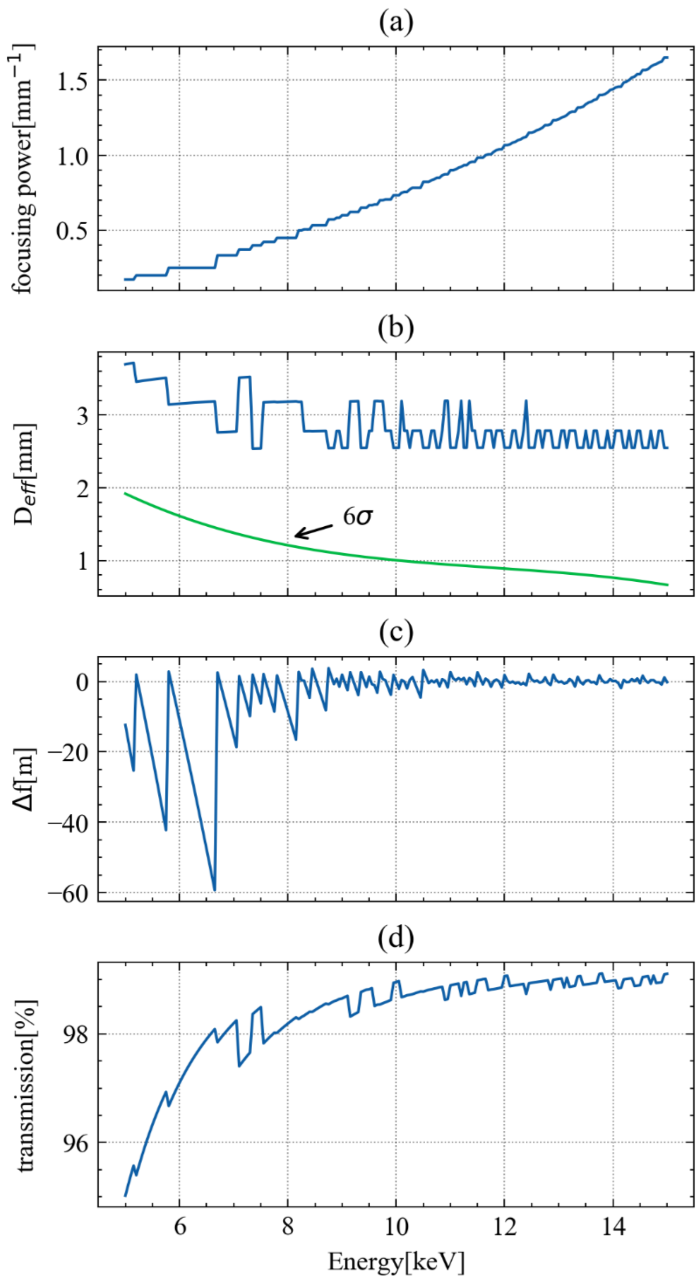

Figure 3.3-40 (a) the focusing power, (b) the effective aperture and 6σ beam size, (c) the focal length differences ($\Delta f = f - f_{real}$), (d) the transmission of the second optimization for CRL1 (f=200 m)

3. CRL2

CRL2 is placed at 10 m before the HSS sample position, and is combined with CRL1 to focus the beam to HSS. Figure 3.3-41 shows the focusing power requirement, and Figure 3.3-42 shows the Rayleigh length. The minimum Rayleigh length in the range of 5~15 keV is 60 mm. According to the focusing power, an optimization of transmission and cost is performed, finally, a group of lenses is selected, as shown in Table 3.3-9.

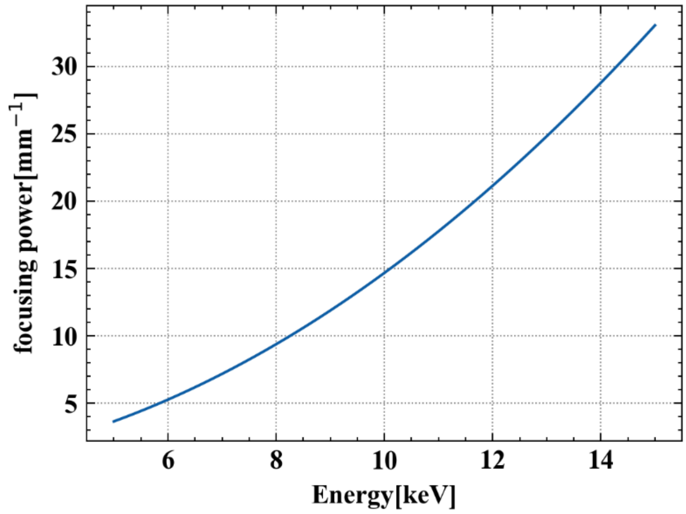

Figure 3.3-41 Focusing power requirements of CRL2 (f=10 m)

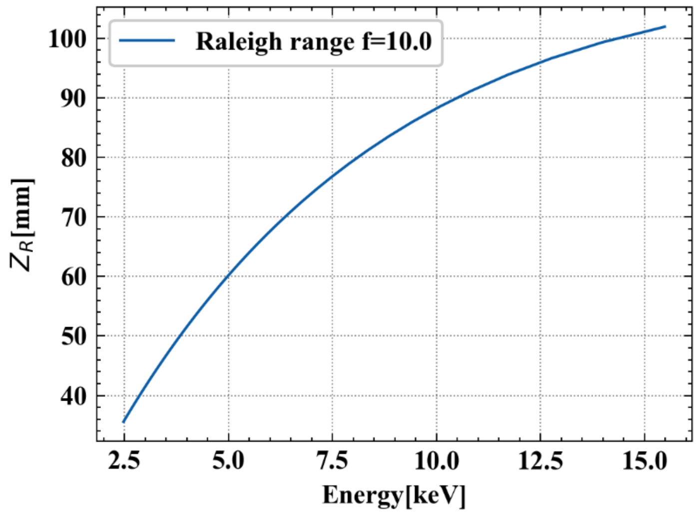

Figure 3.3-42 Rayleigh length of CRL2 (f=10 m)

Table 3.3-9 CRL2 lenses

Actuator	1	2	3	4	5	6	7	8	9	10
Lens N×R(mm)	1×5.0	1×4.0	1×2.5	1×2.0	2×2.5	2×2.0	3×1.5	4×1.0	4×0.5	5×0.3
N/R(mm^{-1})	0.2	0.25	0.4	0.5	0.8	1.0	2.0	4.0	8.0	16.67

The focusing power, effective aperture, focal length differences, and the transmission are shown in Figure 3.3-43. The maximum relative focal length error is 50mm, and the CRL1 focal length error also needs to be considered. Therefore, an adjustment along the optical path is set to compensate for the focal length error of CRL1 and CRL2. Figure 3.3-44 shows the spot size calculated with the Gaussian beam.

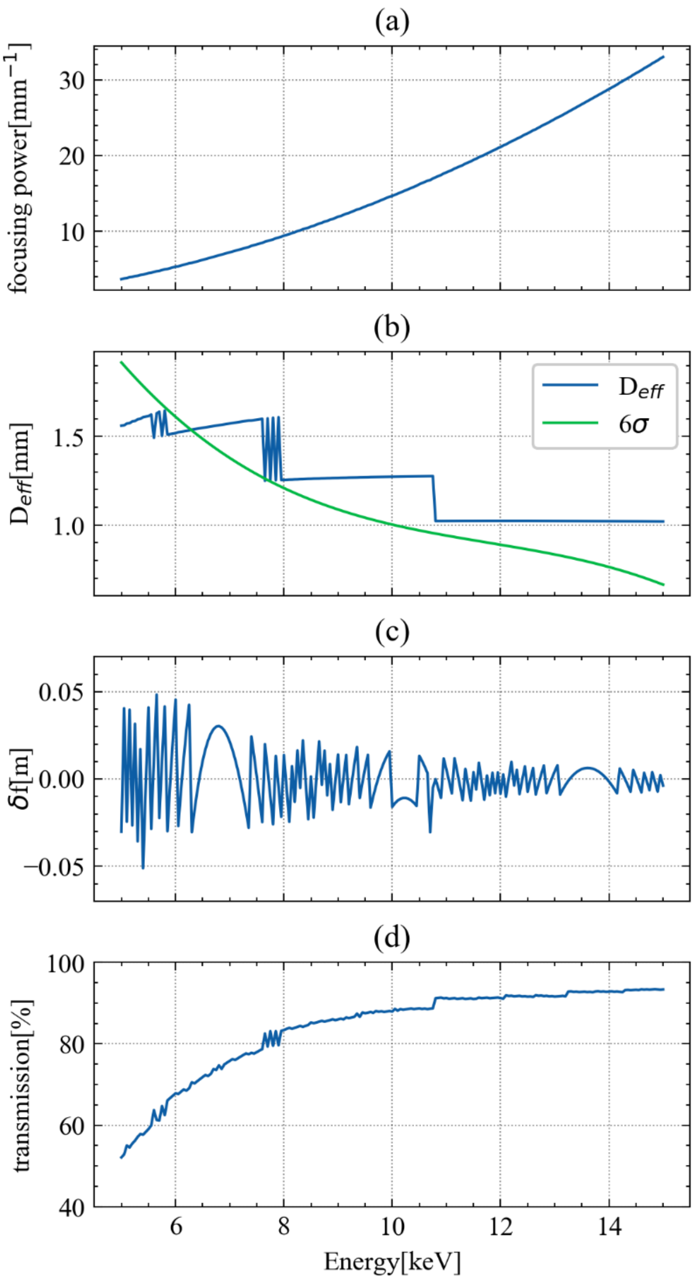

Figure 3.3-43 (a) the focusing power, (b) the effective aperture and 6σ beam size, (c) the focal length differences ($\Delta f = f - f_{real}$), (d) the transmission of CRL2 (f=10 m)

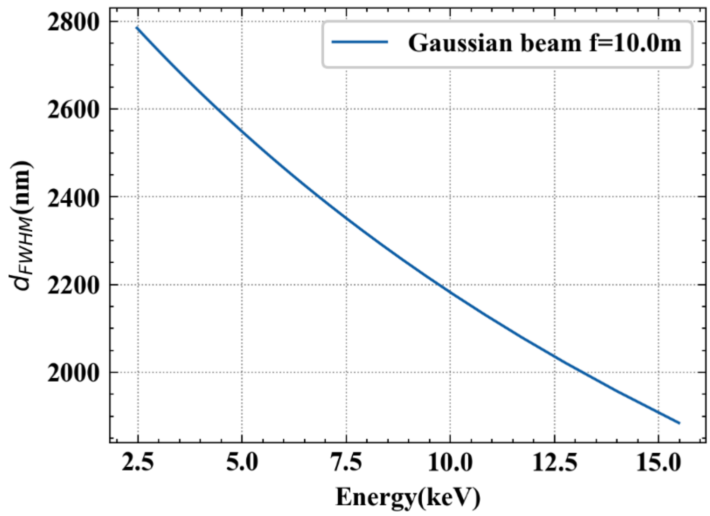

Figure 3.3-44 The focal spot size of CRL2 (f=10 m)

4. CRL3

CRL3 is set to focus the beam for the second chamber of the CDS. The parameters are the same as CRL2. But as described above, the CRL1 is needed to work at a optimized combination for collimating the beam near 5 keV. CRL3 can be used for experiments that do not require a small spot.

5. Requirements of CRL

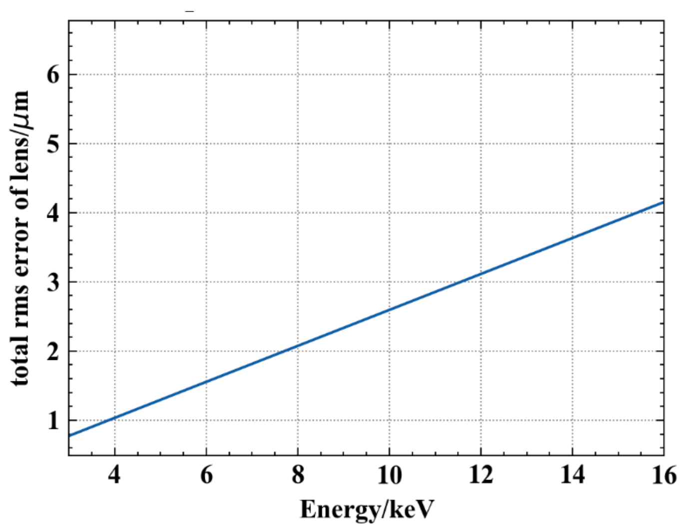

Figure 3.3-45 Figure error requirement of CRL when SR=0.82

The Be lens has some imperfections, and it will take the phase error into the wavefront. Figure 3.3-45 shows the total RMS figure error requirements when SR=0.82. The figure error of an individual lens is about 0.5~2 μm [8]. CRL1 and CRL2 are 32 pieces in total, which means the total figure error of convolution is about 2.8 μm to 11μm. So the better performance requires measurement and selection of CRL.

6. Heat load

From the above analysis, the absorption of CRL1 is 1%~5%. Figure 3.3-46 shows the absorbed power and power density for 1 MHz. The maximum heat load is less than 50W, but the power density is higher than 2000 W/mm^3.

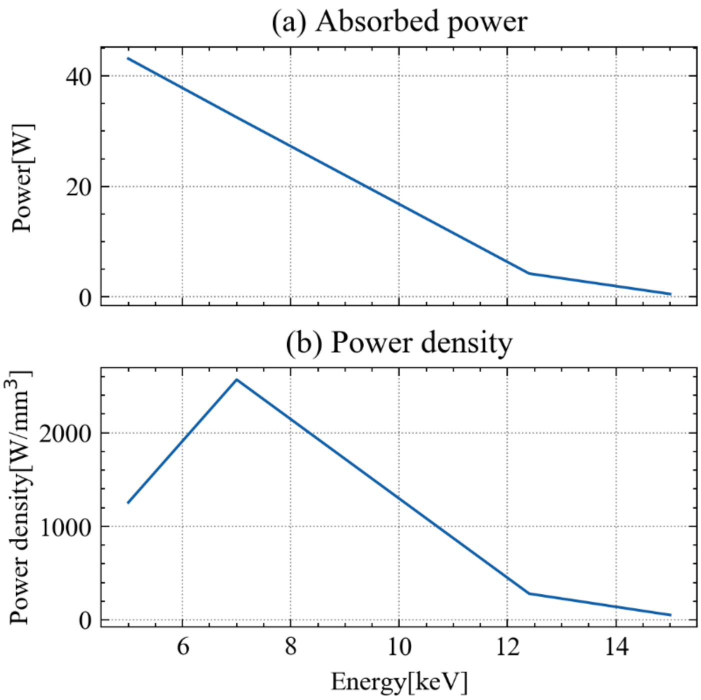

Figure 3.3-46 (a) Absorbed power and (b) power density on CRL1

CRL2 has two modes. One is the mono-beam mode, and its heat load is less than 22 W (see Figure 3.3-47), and it is absorbed by several pieces of lenses. The other is the pink-beam mode, and its heat load is more than 400W (see Figure 3.3-48), and the power density is similar to CRL1.

All of the above estimations is based on the tapered mode.

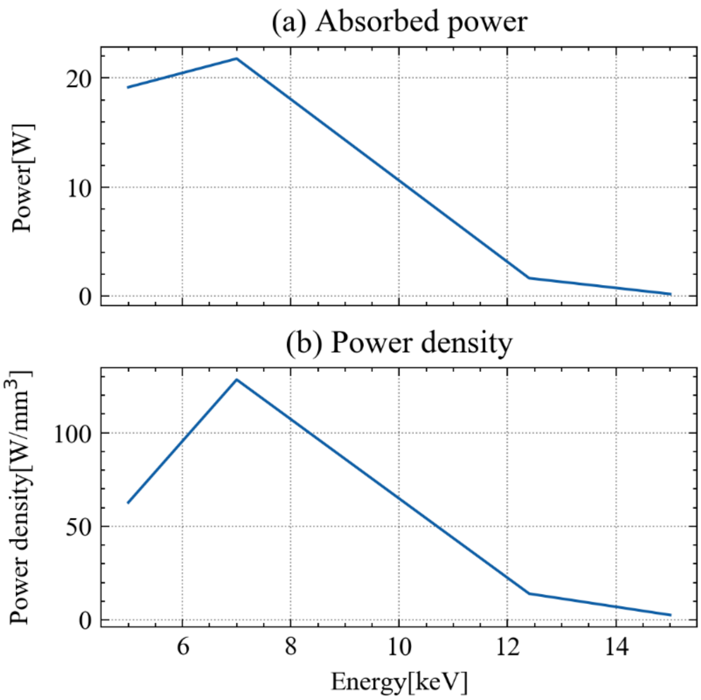

Figure 3.3-47 (a) Absorbed power and (b) power density on CRL2 for mono beam

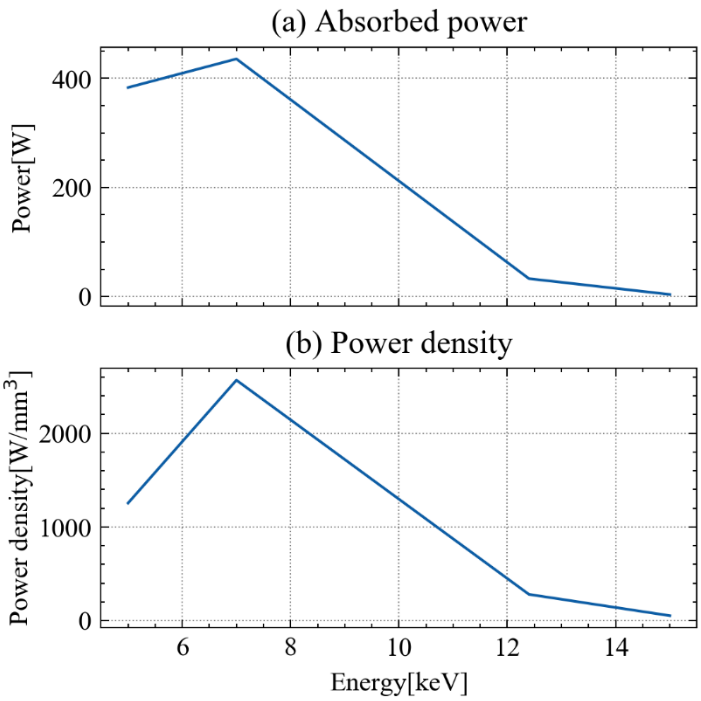

Figure 3.3-48 (a) Absorbed power and (b) power density on CRL2 for pink beam

3.3.5 Attenuator

3.3.5.1 Specifications and Functions

Since the pulse energy can reach hundreds of microjoules, single-pulse damage will occur when it is focused on any material. The high repetition rate will cause multipulse damage, even with no focus. Thus, extreme care should be used when operating the FEL. It is easy to destroy instruments and even the vacuum pip. During beamline commissioning and experiment preparation, the repetition rate should be set lower, and the beam should be attenuated to a non-damage level. In addition to ensuring the safety of the beamline and the endstations, the safety of the attenuator itself is also important.

Energy range: 3~15 keV

Attenuation coefficient: 1~10^{-6}

Clear aperture: ≥Φ10 mm

3.3.5.2 Physical Scheme

In the energy range of 3~15 keV, a gas attenuator can be considered. N2, Ar, Xe, and other high-Z gases can attenuate X-rays in the low-energy range. The advantage of gas is that it has little effect on the wavefront. In the high-energy range, the gas cell length and gas pressure requirements are high, so the solid attenuator has to be used. The solid attenuator should be uniform and radiation-resistant.

When a 15 m-long gas cell is filled with N2 and Ar gas, the pressure requirements for different energies are shown in Figures 3.3-49 and 3.3-50. With 30 Torr as the upper limit, the use of nitrogen is difficult to attenuate in the hard X-ray energy range, while Ar gas can attenuate at least one order of magnitude from 3~15 keV. Under a high repetition rate, the recovery of gas after ionization needs to be considered and further researched.

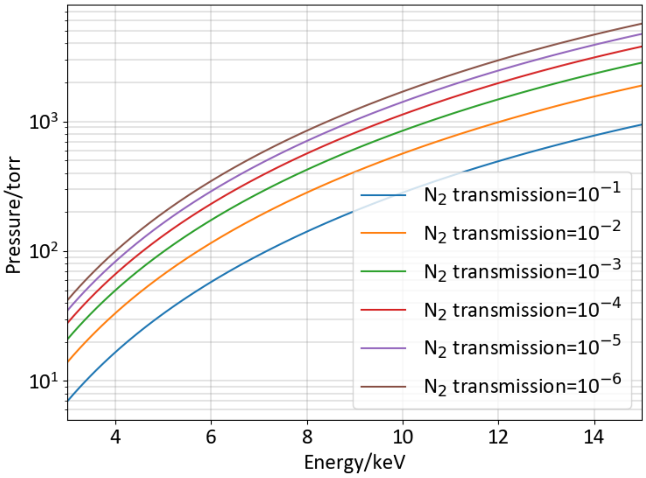

Figure 3.3-49 Pressure requirements of N2 for a 15 m long gas cell

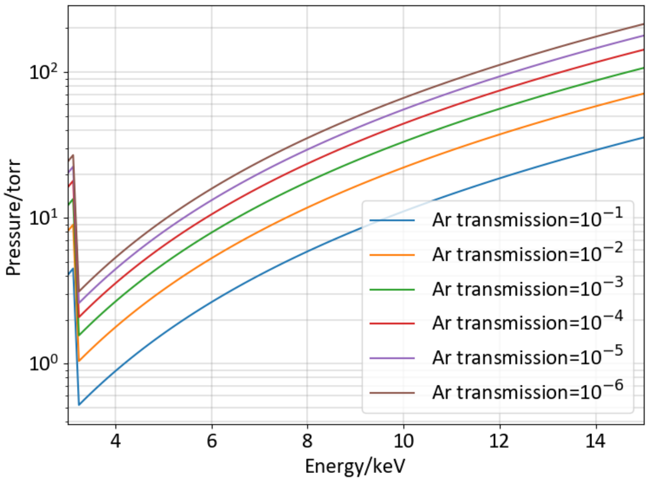

Figure 3.3-50 Pressure requirements of Ar for a 15 m long gas cell

The solid attenuator can be made of CVD, Si, graphite, and SiC. They have good uniformity and thermal conductivity. Figure 3.3-51~53 shows the material thickness requirements for different attenuation orders.

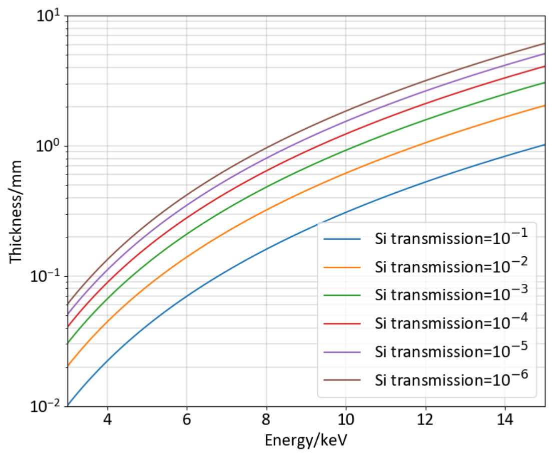

Figure 3.3-51 Requirements for the Si thickness for different attenuation orders

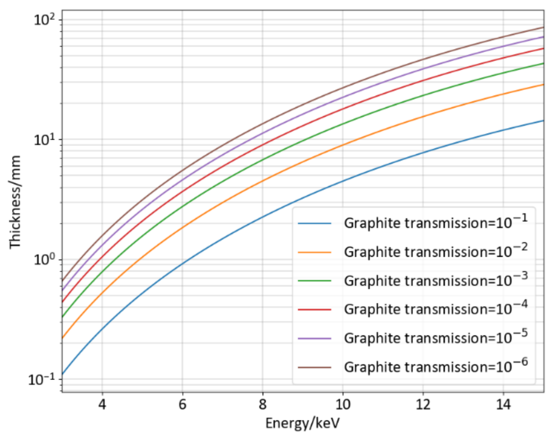

Figure 3.3-52 Requirements of graphite thickness for different attenuation orders

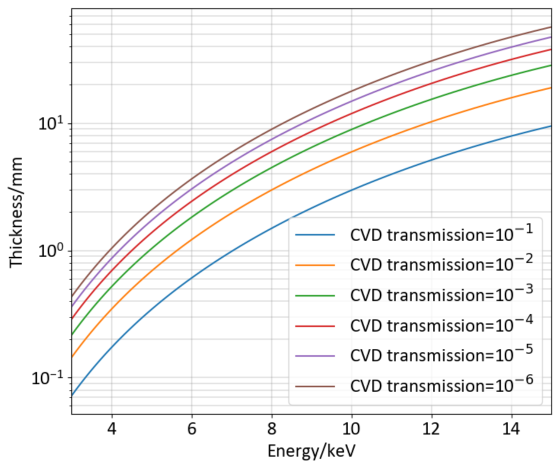

Figure 3.3-53 Requirements of CVD thickness for different attenuation orders

The optimal solution is to use Ar gas attenuator as pre-attenuator and a solid attenuator as post-attenuator when run at the high repetition rate. First, the beam is attenuated by at least one order of magnitude by Ar, and then it is attenuated downward with a solid attenuator. The Ar can give 6 orders attenuation in the lower energy range, and then the solid attenuator can be out of the beam. The solid attenuator configuration is given in Table 3.3-10. CVD must always be used to protect Si in the optical path. CVD is configured to up to 10 mm with a 40 μm step, and with graphite, 6 orders of attenuation can be achieved below 13 keV. Si is configured up to 5 mm with an 80 μm step, and 6 orders of attenuation can be achieved below 14 keV. For the high repetition rate, the CVD also has the risk of damage, so the gas attenuator should be used first.

Table 3.3-10 Solid attenuator configuration

Arm NO.		1	2	3	4	5	6	7	8
1	Material	CVD	CVD	CVD	CVD	CVD	CVD	CVD	CVD
	Thickness (μm)	40	80	160	320	640	1280	2560	5000
2	Material	Graphite	Graphite	Si	Si	Si	Si	Si	Si
	Thickness (μm)	10000	20000	80	160	320	640	1280	2560
3		empty	empty	empty	empty	empty	empty	empty	empty

3.3.5.3 Heat load

Figure 3.3-54 shows the attenuation length and power density of different materials at 1 MHz repetition rate and tapered mode. The power density is very high. There needs a power density threshold from FEA. When the power density is higher than the threshold, the gas attenuator should be working to absorb most of the heat load; otherwise, the solid attenuator can work independently. Even if the solid attenuator works independently, there should be rules to ensure the safety of Si.

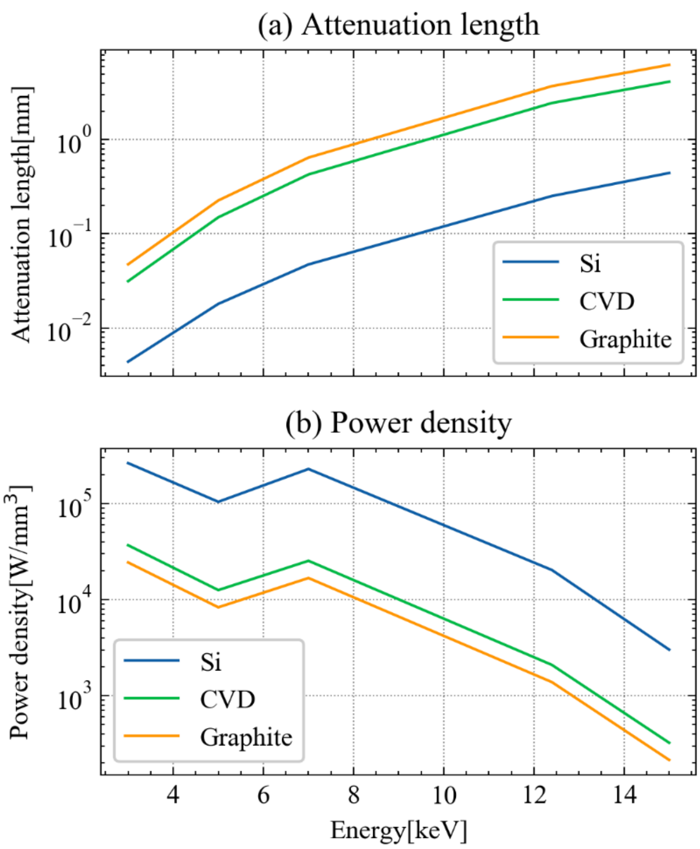

Figure 3.3-54 (a) Attenuation length and (b) power density on solid attenuator

3.4 Suppression of higher harmonics

The third-order harmonic content of the source is shown in Figure 3.3-1, and the third harmonic content is less than 2%. Figure 3.3-1 shows the high-order harmonic transmission efficiency of the optical system. When KB mirrors are used, at 3~7 keV, the high-order harmonic transmission efficiency is less than 2×10^{-4}. Taking the harmonic content of the source into account, it is less than 4×10^{-6}. When using CRL, at 5~7 keV only the offset mirror is considered, and the transmission efficiency of the higher harmonics is less than 4×10^{-5} (considering the harmonic content of the source, it is less than 8×10^{-6}). At 7~15 keV, only the offset mirror group is considered, and the transmission efficiency of high-order harmonics is less than 2×10^{-3}. Considering the harmonic content of the light source, it is less than 4×10^{-5}. In reality, there is also Ru coating KB, which makes the harmonic content much lower. CRL with an order selection aperture also makes harmonics content lower.

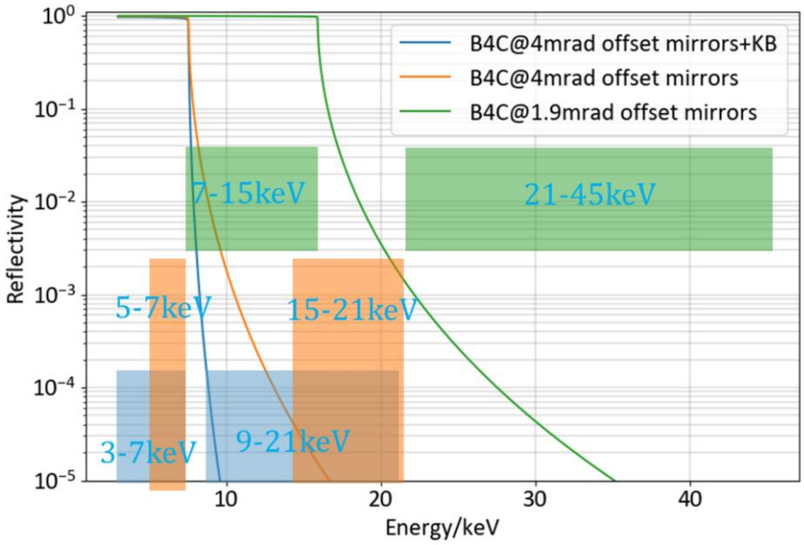

Figure 3.3-1 Transmission efficiency

3.5 Damage calculations

For single pulse damage, according to the existing results and experience[9-12], material melting or ablation can be estimated by the energy absorbed by each atom within each pulse. If the instantaneous lattice temperature rises above the melting temperature of the material, or above the phase-transition temperature (such as carbon), significant damage will occur due to the absorbed energy. The single pulse damage thresholds of typical coating materials, such as SiC, B4C, Ru, Pt, and Rh, have been reported. According to the Dulong-Petit law,the single pulse damage threshold can be calculated using the following formula:

$$D_{th} \approx 3k_B T_{melt}$$

Figure 3.5-1 shows the single-pulse damage threshold of some materials frequently used in FELs.

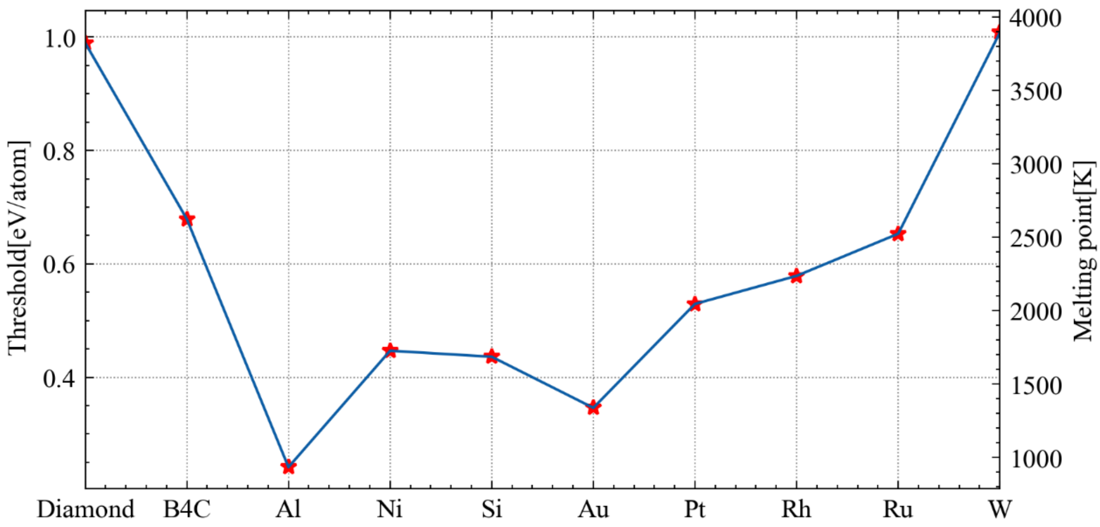

Figure 3.5-1 Damage threshold of different materials

For total reflection coatings, the following formula can be used to estimate the absorbed dose:

$$D_{ab} = \frac{4ln2(1-R)PAsin\theta}{\pi b^2 N_A d\rho}$$

$$d = \sqrt{{d_x}^2 + {d_e}^2}$$

where R is the reflectivity, P is the incident energy, ρ is the material density, θ is the grazing incidence angle, N_A is the Avogadro constant, A is the atomic mass, d_x is the penetration depth of X-rays during total reflection, and it is determined by the following formula:

$$\frac{1}{d_x} = \frac{2\sqrt{2}\pi}{\lambda}\sqrt{\sqrt{(2\delta-\theta^2)^2+4\beta^2}+2\delta-\theta^2}$$

d_e is the collision length of the electron related to the energy of the electron and the nature of the material. There are many related studies, but they mainly use measured data, and there are no formulas for calculating the collision length. However, it is very important, especially when the coating is working in the total reflection.

In the case of a transmissive device, in the above formula, R=0, and d is calculated with the absorption length.

According to the above formula, the absorbed dose is calculated for the offset mirrors, the monochromator, the KB mirror system, the solid attenuator, and the CRL. The calculation process uses a single pulse energy of 2 mJ, and the beam divergence angle is based on the source parameters. The calculation results are shown in Figure 3.5-2~7. It can be seen that neither the offset mirrors nor the monochromator exceed 0.1 eV/atom. When Ru is at 340 m, the absorbed dose in the high-energy range is greater than 0.1 eV/atom. However, because the pulse energy at the high-energy position is much smaller than 2 mJ, the final absorbed dose is low. The CRL and solid absorber are also far less than 0.1 eV/atom. Therefore, the materials currently used will not suffer single pulse damage.

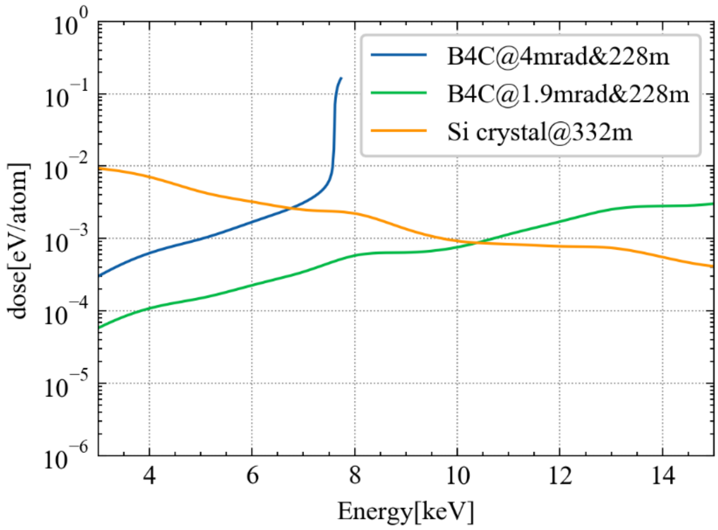

Figure 3.5-2 The absorbed dose of B4C coating and Si crystal when the pulse energy is 2 mJ

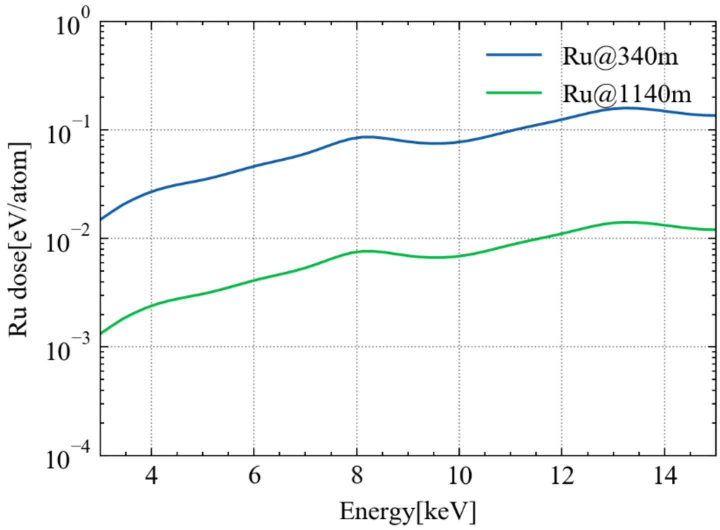

Figure 3.5-5 The absorbed dose Ru coating when the pulse energy is 2 mJ

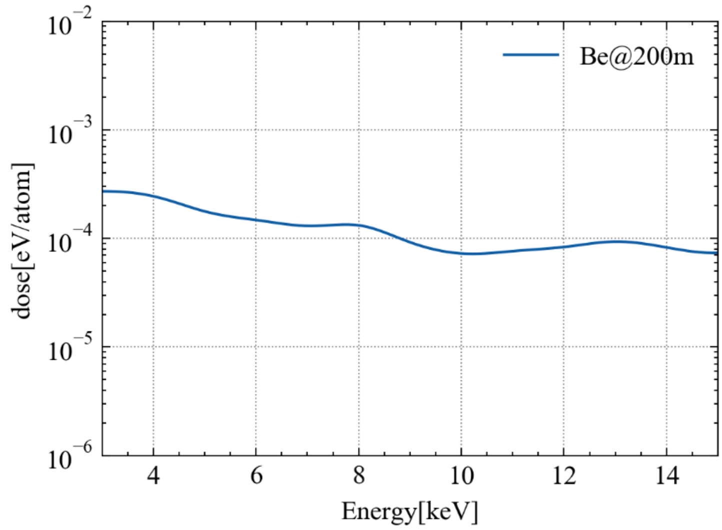

Figure 3.5-6 The absorbed dose of CRL when the pulse energy is 2 mJ

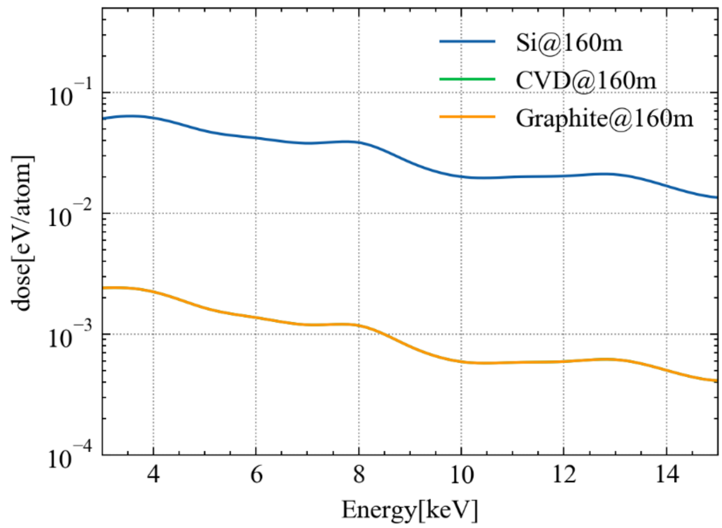

Figure 3.5-7 The absorbed dose of the solid attenuator when the pulse energy is 2 mJ

3.6 Vibrations

The stability of the source and the optical elements will affect the flux, spectral resolution, and spot position on the sample. The effects of different sources are expressed as follow:

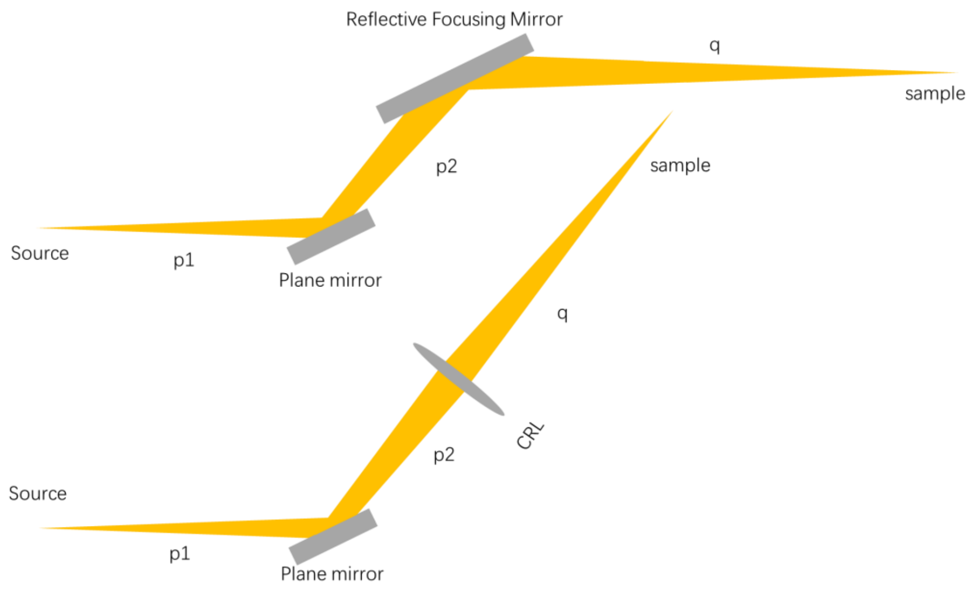

Figure 3.6-1 Schematic diagram of the vibration analysis

The source lateral position vibration:

$$V_{ss} = V_s \times \frac{q}{p_1 + p_2}$$

The vibration along the normal direction of the plane mirror:

$$V_{ps} = 2 \times V_p \times \frac{q}{p_1 + p_2}$$

The pitch vibration of the plane mirror:

$$V_{pas} = 2 \times V_{pa} \times \frac{p_1 \times q}{p_1 + p_2}$$

The vibration along the normal direction of the reflective focusing mirror:

$$V_{rs} = V_r \times \frac{p_1 + p_2 - q}{p_1 + p_2}$$

The pitch vibration of the reflective focusing mirror:

$$V_{ras} = 2 \times V_{ra} \times q$$

The CRL pitch vibration does not theoretically affect the spot position, and the effect of the lateral position vibration is expressed as follows:

$$V_{cs} = V_c \times \frac{p_1 + p_2 + q}{p_1 + p_2}$$

All of the above effects are convolved in directions according to the configuration of the beamline.

For the HSS endstation, the horizontal direction considers the offset mirrors and the horizontal focusing mirror, while the vertical direction considers the monochromator and the vertical focusing mirror, as well as the CRL. Figures 3.6-2~5 gives the effects of different cases in both directions.

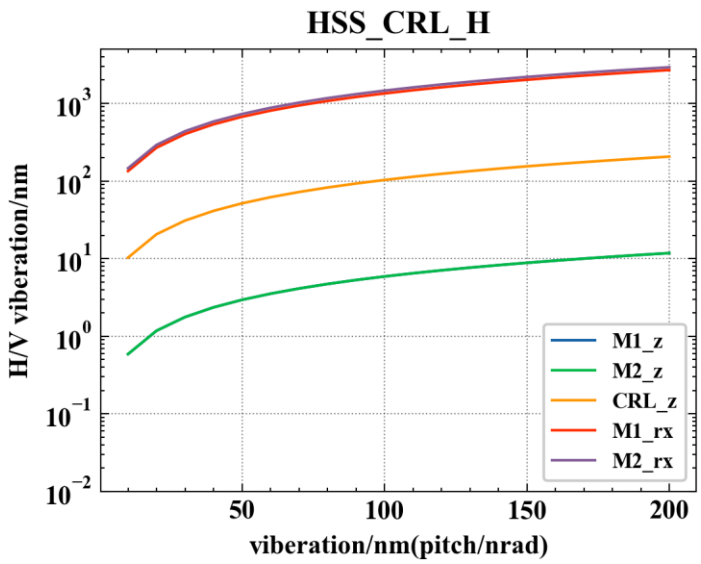

Figure 3.6-2 Comparison of the horizontal spot movement on the sample (HSS CRL case)

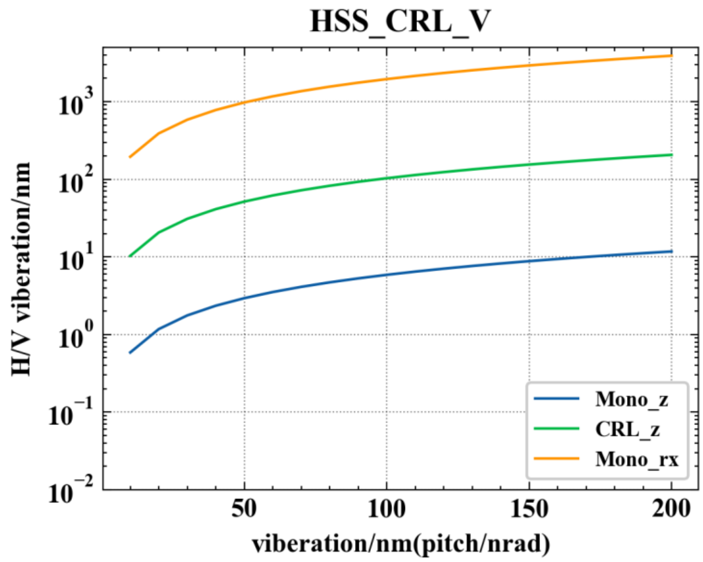

Figure 3.6-3 Comparison of the vertical spot movement on the sample (HSS CRL case)

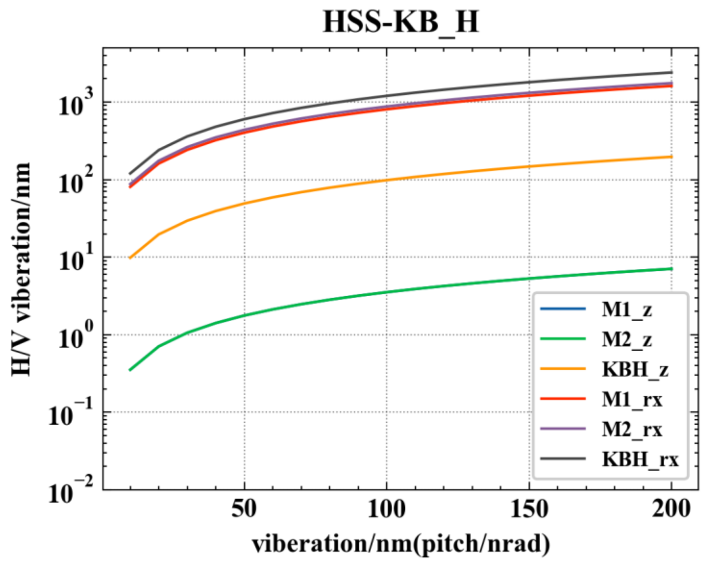

Figure 3.6-4 Comparison of the horizontal spot movement on the sample (HSS KB case)

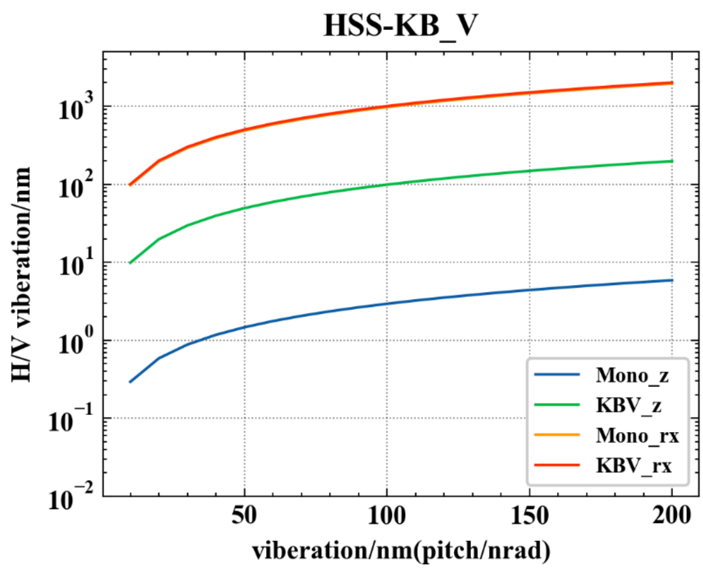

Figure 3.6-5 Comparison of the vertical spot movement on the sample (HSS KB case)

For the CDS endstation, the horizontal direction considers the offset mirrors and the horizontal focusing and deflection mirror, while the vertical direction considers the the vertical focusing and deflection mirror. Figures 3.6-6~11 gives the effects of CRL and KB in different directions. Figures 3.6-6~11 gives the effects of different cases in both directions.

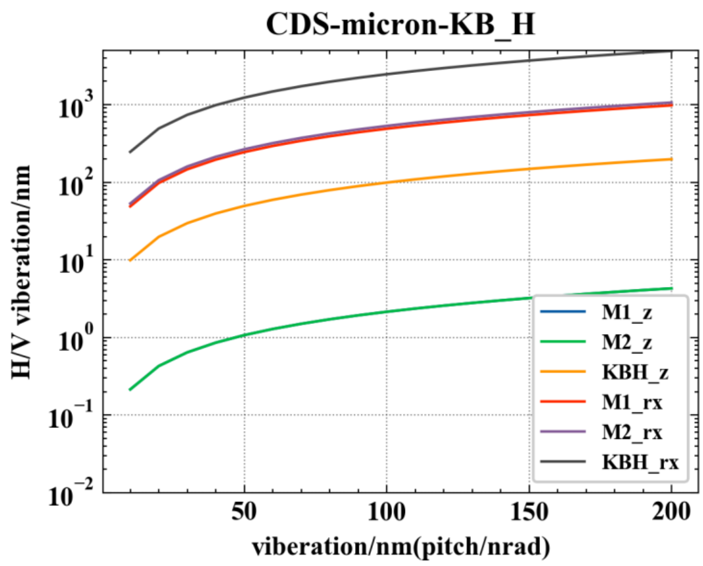

Figure 3.6-6 Comparison of the horizontal spot movement on the sample (CDS micron KB case)

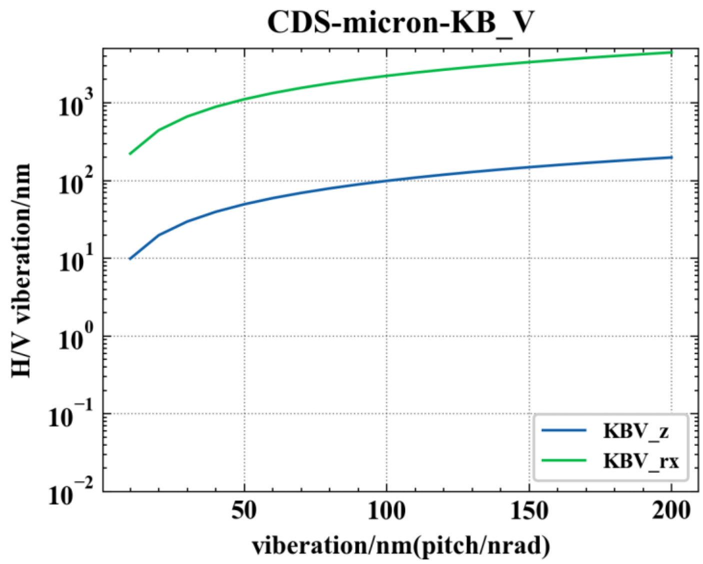

Figure 3.6-7 Comparison of the vertical spot movement on the sample (CDS micron KB case)

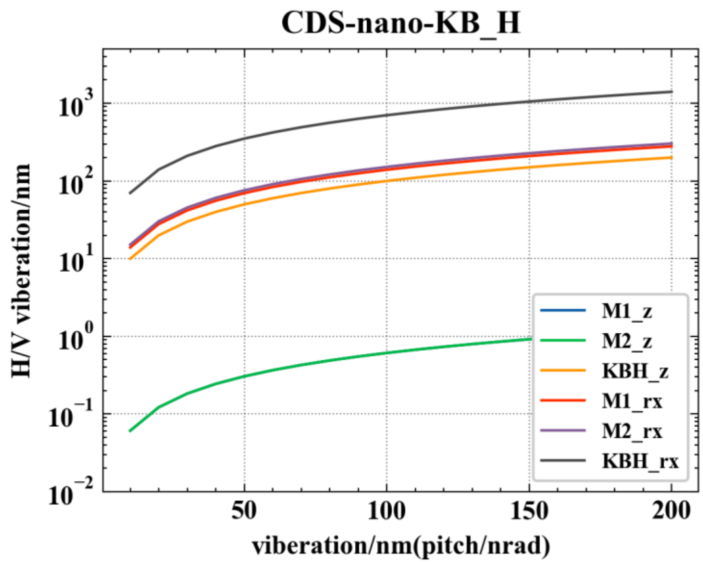

Figure 3.6-8 Comparison of the horizontal spot movement on the sample (CDS nano KB case)

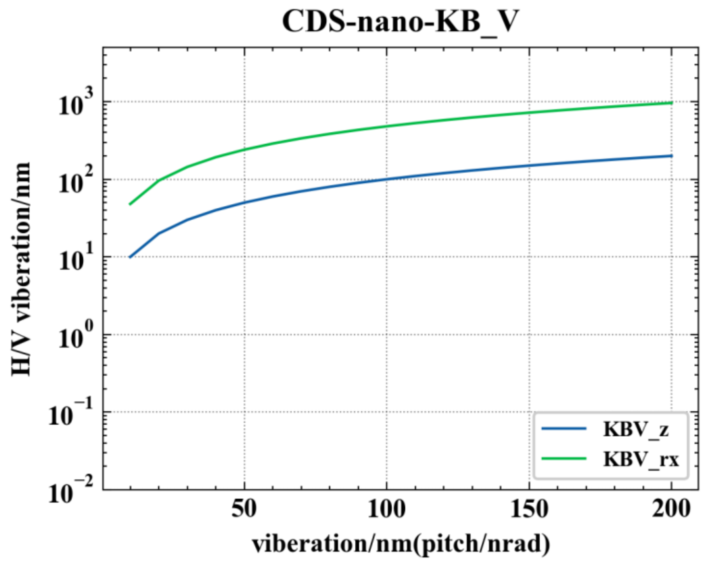

Figure 3.6-9 Comparison of the vertical spot movement on the sample (CDS second nano KB case)

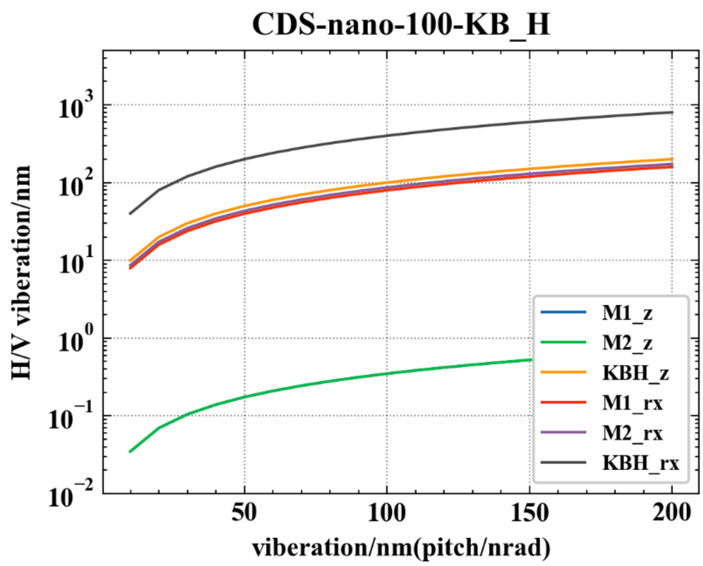

Figure 3.6-10 Comparison of the horizontal spot movement on the sample (CDS second nano KB case)

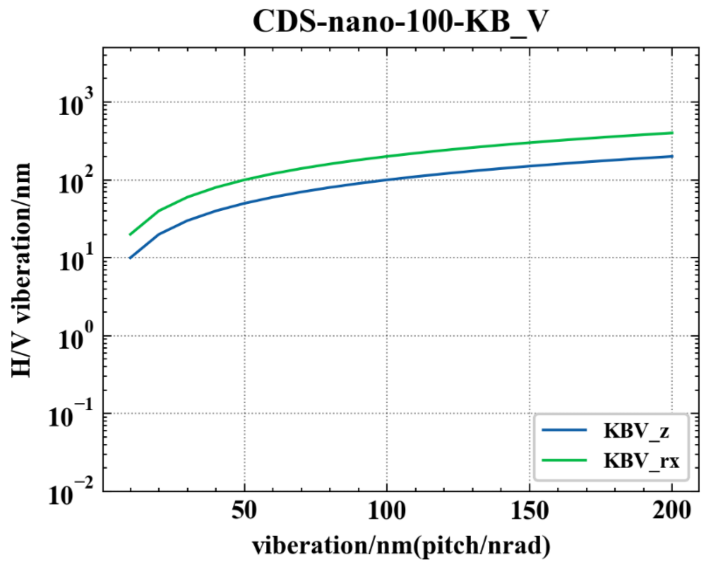

Figure 3.6-11 Comparison of the vertical spot movement on the sample (CDS second nano KB case)

3.7 Optical component list

Table 3.7-1 Technical specification of the M1 and M2a/M2b mirrors

	M1 mirror	M2a mirror	M2b mirror
Operating energy range	3 keV~15 keV	3 keV~7 keV	6 keV~15 keV
FWHM Footprint （L×W）	314×1.25 mm^2	327×1.31 mm^2	353×0.67 mm^2
Optical active length （L×W）	950 mm×40 mm	950 mm×40 mm	950 mm×40 mm
Mirror surface direction	horizontal reflection	horizontal reflection	horizontal reflection
Coating material	B_4C	B_4C	B_4C
Coating density	≥ 95% bulk		
Coating thickness	>500 Å	>500 Å	>500 Å

Mirror substrate	Single Crystal Silicon	Single Crystal Silicon	Single Crystal Silicon
Shape (before bending)[c]	Plane	Plane (bendable)	Plane (bendable)
Shape (after bending)	NA	Cylinder	Cylinder
Grazing incidence angle	1.9 mrad & 4 mrad	4 mrad	1.9 mrad
Tangential slope error before bending (RMS)	<0.05 μrad	<0.05 μrad	<0.05 μrad
Height error before bending (RMS/PV)	0.5 nm/2 nm	0.5 nm/2 nm	0.5 nm/2 nm
Sagittal slope error (RMS)	<1 μrad	<1 μrad	<1 μrad
Roughness (RMS, with coating)	≤0.2 nm	≤0.2 nm	≤0.2 nm
Vacuum	$<1\times10^{-9}$Torr, particle free		

Table 3.7-2 Crystal monochromator

Parameter	Value
Crystal	Si(111)，Si(311)
Energy range	3 - 15keV@ Si(111) 5.6 - 15keV@ Si(311)
Energy resolution	2×10^{-4}@ Si(111) 5×10^{-5}@ Si(311)
Location from source	332m
Incident Beam height	1300m
Beam vertical offset (full energy range)	15 mm
Bragg angle	-5° - 45°

	Si(111):7.58~41.3° Si(311):14.62~42.5°
Crystal dimention	1st: 30×30×30mm^3@ Si(111) (footprint 11mm @Si(111)) 30×30×30mm^3@ Si(311) (footprint 7mm @Si(311)) 2nd: 100×30×30mm^3@ Si(111) (footprint 54.5mm@Si(111)) 100×30×30mm^3@ Si(311) (footprint 25mm@Si(311))
Slope error	1μrad@ Si(111) 1μrad@ Si(311)
Defects thickness	<60nm
Roughness	<1 nm
Maximum Beam cross section at 1st crystal	4.8mm×4.8mm (H×V)
Maximum heat load	18W @7keV&10kHz
RoC	Center of the first crystal
Beam stability	50nrad
cooling	Cryo-cooling
Vacuum pressure in operation 运行时真空度	1×10^{-9}Torr, particle free

Table 3.7-3 Technical specification of KB system

	EM1	EM2	M3/M4	EM3	EM4	EM5	EM6	EM7	EM8
Operating energy range	3~15 keV								
FWHM footprint（L×W）	467×1.9 mm^2	467×1.9 mm^2	1567×6.3 mm^2	1567×6.3 mm^2	1567×6.3 mm^2	1815×6.4 mm^2	1815×6.4 mm^2	1848×6.5 mm^2	1848×6.5 mm^2
Optical effective length（L×W）	950×40 mm^2	950×40 mm^2	950×40 mm^2	950×40 mm^2	950×40 mm^2	950×40 mm^2	950×40 mm^2	950×40 mm^2	950×40 mm^2
Mirror surface direction	horizontal reflection	Vertical reflection	Horizontal/Vertical reflection	horizontal reflection	Vertical reflection	horizontal reflection	Vertical reflection	horizontal reflection	Vertical reflection
Coating material	Two stripes B_4C/Ru	Two stripes B_4C/Ru	Two stripes B_4C/Ru	Two stripes B_4C/Ru	Two stripes B_4C/Ru	Two stripes B_4C/Ru	Two stripes B_4C/Ru	Two stripes B_4C/Ru	Two stripes B_4C/Ru
Coating width Strip1/blank/strip2	19mm/2mm /19mm	19mm/2mm /19mm	19mm/2mm /19mm	19mm/2mm /19mm	19mm/2mm /19mm	19mm/2mm /19mm	19mm/2mm /19mm	19mm/2mm /19mm	19mm/2mm /19mm
Coating density	≥ 95% bulk	≥ 95% bulk	≥ 95% bulk	≥ 95% bulk	≥ 95% bulk	≥ 95% bulk	≥ 95% bulk	≥ 95% bulk	≥ 95% bulk
Coating thickness	>500 Å	>500 Å	>500 Å	>500 Å	>500 Å	>500 Å	>500 Å	>500 Å	>500 Å
Mirror substrate	Single Crystal Silicon	Single Crystal Silicon	Single Crystal Silicon	Single Crystal Silicon	Single Crystal Silicon	Single Crystal Silicon	Single Crystal Silicon	Single Crystal Silicon	Single Crystal Silicon
Shape (before bending)[c]	Elliptical (bendable)	Elliptical (bendable)	Plane	Elliptical	Elliptical	Elliptical	Elliptical	Elliptical	Elliptical
Shape (after bending)	Elliptical cylinder (bendable)	Elliptical cylinder (bendable)							

p/q	340m/6m	341.2/4.8m		1145.7m/12.3m	1146.9m/11.1m	1154.5m/3.5m	1155.6m/2.4m	1175.9m/2.1m	1177m/1m
radius	2947.99m	2366.71m		6084.69m	5496.81m	1174.72m	1197.52m	1048.131m	499.58m
Grazing angle	4 mrad	4 mrad	4 mrad	4 mrad	4 mrad	3.5 mrad	3.5 mrad	3.5 mrad	3.5 mrad
tangential slope error before bending	<0.05 μrad	<0.05 μrad	<0.05 μrad	<0.05 μrad	<0.05 μrad	<0.05 μrad	<0.05 μrad	<0.05 μrad	<0.05 μrad
Height error before bending (RMS/PV)	0.5 nm/2nm	0.5 nm/2nm	0.5 nm/2nm	0.5 nm/2nm	0.5 nm/2nm	0.5 nm/2nm	0.5 nm/2nm	0.5 nm/2nm	0.5 nm/2nm
Sagittal slope error (RMS)	<1 μrad	<1 μrad	<1 μrad	<1 μrad	<1 μrad	<1 μrad	<1 μrad	<1 μrad	<1 μrad
Roughness (RMS, with coating)	≤0.2 nm	≤0.2 nm	≤0.2 nm	≤0.2 nm	≤0.2 nm	≤0.2 nm	≤0.2 nm	≤0.2 nm	≤0.2 nm

Table 3.7-4 CRL1 lenses

Actuator	1	2	3	4	5	6	7	8
Lenses N×R (mm)	1×7.0	1×5.8	1×5.0	1×4.0	1×3.0	1×2.5	2×4.0	2×3.0
N/R (mm-1)	0.14	0.17	0.2	0.25	0.33	0.4	0.5	0.67

Table 3.7-5 CRL2/CRL3 lenses

Actuator	1	2	3	4	5	6	7	8	9	10
Lenses N×R (mm)	1×5.0	1×4.0	1×2.5	1×2.0	2×2.5	2×2.0	4×2.0	4×1.0	4×0.5	5×0.3
N/R (mm-1)	0.20	0.25	0.40	0.50	0.80	1.00	2.00	4.00	8.00	16.67

Table 3.7-6 CRL2-1D lenses

Actuator	1	2	3	4	5	6
Lenses N×R (mm)	6×1.0	5×1.0	4×1.0	3×1.0	2×1.0	1×1.0
N/R (mm-1)	6.00	5.00	4.00	3.00	2.00	1.00

Table 3.7-7 Solid attenuator configuration

Arm NO.		1	2	3	4	5	6	7	8
1	Material	CVD	CVD	CVD	CVD	CVD	CVD	CVD	CVD
	Thickness (μm)	40	80	160	320	640	1280	2560	5000
2	Material	Graphite	Graphite	Si	Si	Si	Si	Si	Si
	Thickness (μm)	10000	20000	80	160	320	640	1280	2560
3		空	空	空	空	空	空	空	空

4. Beamline components

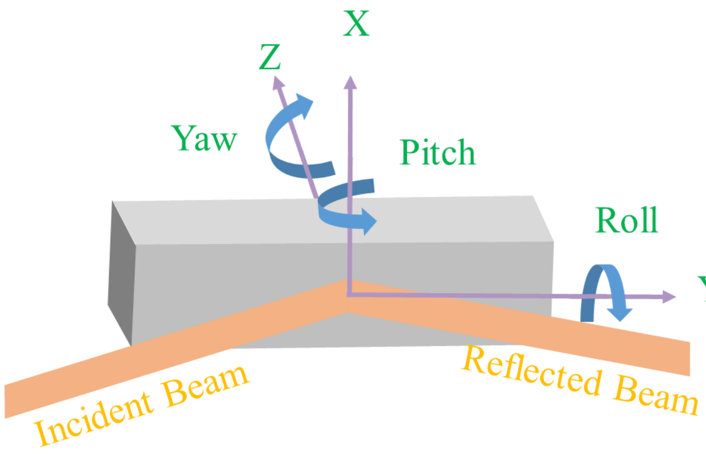

Figure 4-1 Axes definition for mirror system

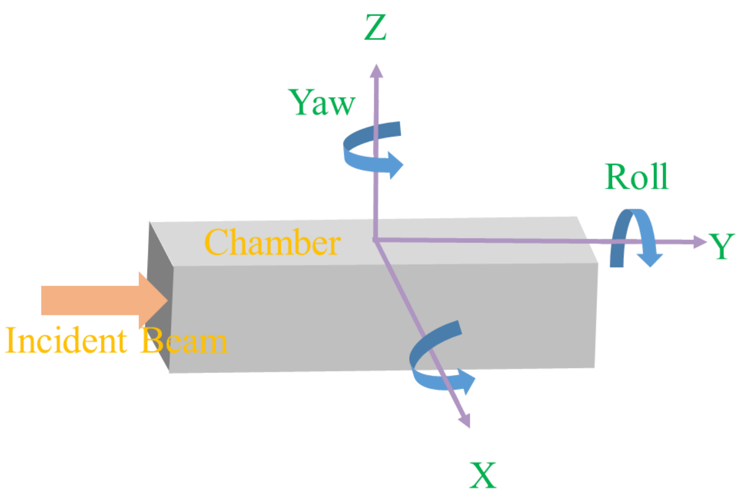

Figure 4-2 Axes definition for the chamber support system

4.1 Offset mirror

Table 4.1-1 Requirements of the offset mirror

	M1 mirror	M2a mirror	M2b mirror
Operating energy range	3 keV~15 keV	3 keV~15 keV	3 keV~15 keV

FWHM Footprint （L×W）	314×1.25 mm^2	327×1.31 mm^2	353×0.67 mm^2
Optical active length （L×W）	950 mm×40 mm	950 mm×40 mm	950 mm×40 mm
Mirror surface direction	horizontal reflection	horizontal reflection	horizontal reflection
Coating material	B_4C	B_4C	B_4C
Coating density	≥ 95% bulk		
Coating thickness	>500 Å	>500 Å	>500 Å
Mirror substrate	Single Crystal Silicon	Single Crystal Silicon	Single Crystal Silicon
Shape (before bending)[c]	Plane	Plane (bendable)	Plane (bendable)
Shape (after bending)	NA	Cylinder	Cylinder
Grazing incidence angle	1.9 mrad & 4 mrad	4 mrad	1.9 mrad
Tangential slope error before bending (RMS)	<0.05 μrad	<0.05 μrad	<0.05 μrad
Height error before bending (RMS/PV)	0.5 nm/2 nm	0.5 nm/2 nm	0.5 nm/2 nm
Tangential slope error after bending at full bending range(RMS)	NA	<0.1 μrad (R=30 km~1200 km)	<0.1 μrad (R=30 km~2500 km)
Height error after bending (RMS/PV)	NA	3 nm/12nm@ full range 1.5 nm /6nm@ 550mm central part	3 nm /12nm@ full range 1.5 nm /6nm@ 550mm central part

		0.7 nm /3nm@ 250mm central part	0.7 nm /3nm@ 250mm central part
Final requirements	2 nm /8nm@ full range 1nm /4nm@ 550mm central part 0.5 nm/2nm @ 250mm central part		
Sagittal slope error (RMS)	<1 μrad	<1 μrad	<1 μrad
Roughness (RMS, with coating)	≤0.2 nm	≤0.2 nm	≤0.2 nm
Bending resolution	NA	1/(1200 km) (R=30 km~1200 km)	1/(2500 km) (R=30 km~2500 km)
Bending repetitive accuracy	NA	1/(240 km) (R=30 km~1200 km)	1/(500 km) (R=30 km~2500 km)
Bending stability	NA	1/(1200 km) (R=30 km~1200 km) / 10min 1/(400 km) (R=30 km~1200 km) /24 h	1/(2500 km) (R=30 km~2500 km) / 10min 1/(800 km) (R=30 km~2500 km) /24 h
Cooling	vibration-free cooling		
Vacuum	$<1\times10^{-9}$Torr, particle free		

The mirror system should be supported by a manually adjustable mechanism. To ensure the installation precision, the adjustment requirements are listed in Table 4.1-1. All the translations require the locking mechanism.

Table 4.1-2 Requirements of the offset mirror chamber support

Motion	Range	Resolution	Note
Pitch (Rx)	±0.5°	0.01°	Manual
Roll (Ry)	±0.5°	0.01°	Manual
Yaw (Rz)	±0.5°	0.01°	Manual
X (horizontal)	±50 mm	0.05 mm	Manual
Y (along beam)	±10 mm	0.05 mm	Manual
Z (perpendicular)	±50 mm	0.05 mm	Manual

The adjustments of the mirror positions are listed in Table 4.1-2. The mirror support should be isolated from the chamber.

Table 4.1-3 Technical specifications for the adjustment system of the M1 and M2a/M2b mirrors

Axis		M1 mirror	M2a mirror	M2b mirror
X Vertical scan Change coating area	Range	±20mm	±20 mm	±20mm
	Resolution	≤10 μm	≤10 μm	≤10 μm
	repeatability	≤50 μm	≤50 μm	≤50 μm
	Pitch and roll repeatability	Pitch <50nrad,roll <50urad		
Z In/out of the beam	Range	±10 mm	±10 mm	±10 mm
	Resolution	≤1 μm	≤1 μm	≤1 μm
	repeatability	≤5 μm	≤5 μm	≤5 μm
Pitch	Range	±0.3°	±0.3°	±0.3°
	Resolution	≤20 nrad	≤20 nrad	≤20 nrad
	repeatability	≤60 nrad	≤60 nrad	≤60 nrad
Roll	Range	±1.5°	±1.5°	±1.5°
	Resolution	≤10 μrad	≤10 μrad	≤10 μrad
	repeatability	≤50 μrad	≤50 μrad	≤50 μrad

Yaw	Installation accuracy	200 μrad	200 μrad	200 μrad
Encoder	All the axes with Encoder			
Vacuum	1×10^{-9}Torr, particle free			
	The effect of X and Z on the pitch must be less than 1.0 μrad			

The mirror stability requirements are listed in Table 4.1-4.

Table 4.1-4 Stability requirements of the offset mirrors

stability(RMS)	offset mirrors
Pitch （RMS, < 100Hz）	<50 nrad / 10min (The manufacturer needs to guarantee the vibration parameter is able to meet this requirement based on the condition of SHINE hall.)
roll （RMS, <100 Hz）	<0.5 μrad/30min

4.2 Monochromator

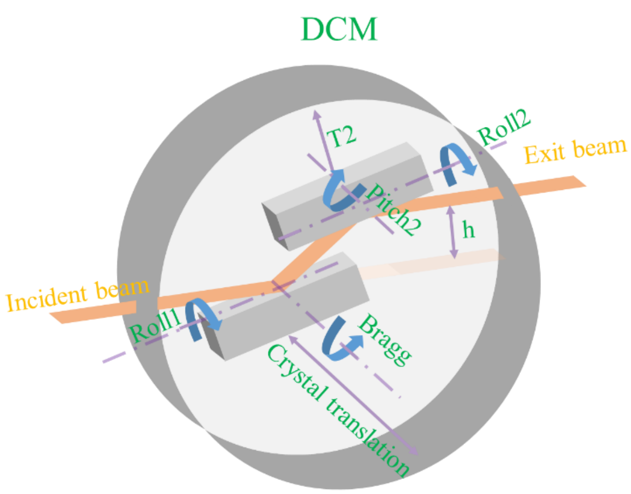

Figure 4.2-1 Diagram of Double crystal monochromator

The diagram of double crystal monochrator is shown in Figure 4.2-1, and axis of crystal and chamber is the same as Figures 4-1 and 4-2

Table 4.2-1 Crystal monochromator

Parameter	Value
Crystal	Si(111)，Si(311)
Energy range	3 - 15keV@ Si(111) 5.6 - 15keV@ Si(311)
Energy resolution	2×10^{-4}@ Si(111) 5×10^{-5}@ Si(311)
Location from source	332m
Incident Beam height	1300m
Beam horizontal offset (full energy range)	15 mm
Bragg angle Bragg	-5° - 45° Si(111):7.58~41.3° Si(311):14.62~42.5°
Crystal dimention	1st: $30\times30\times30mm^3$@ Si(111) (11mm @Si(111)) $30\times30\times30mm^3$@ Si(311) (7mm @Si(311)) 2nd: $100\times30\times30mm^3$@ Si(111) (54.5mm@Si(111)) $100\times30\times30mm^3$@ Si(311) (25mm@Si(311))
Slope error	1μrad@ Si(111) 1μrad@ Si(311)
Defects thickness	<60nm
Roughness	<1nm
Maximum Beam cross section at 1st crystal (6σ)	4.8mm×4.8mm (H×V)
Maximum heat load	180W @7keV&100kHz
RoC	Center of the first crystal
Beam stability	50nrad
Cooling	Cryo-cooling
Vacuum pressure in operation 运行时真空度	1×10^{-9}Torr, particle free

Table 4.2-2 Chamber support requirements

Motion	Range	Resolution	Note
Pitch (Rx)	±0.5°	0.01°	Manual
Roll (Ry)	±0.5°	0.01°	Manual
Yaw (Rz)	±0.5°	0.01°	Manual
X (horizontal)	±50 mm	0.05 mm	Manual

Y (along beam)	±10 mm	0.05 mm	Manual
Z (perpendicular)	±50 mm	0.05 mm	Manual

Table 4.2-3 Technical specifications of the crystal adjustments

Axis	parameter	DCM	
		First crystal	Second crystal
X Change Crystals and let the pink peak pass	Range	±80 mm(TBD)	±80 mm(TBD)
	Resolution	≤10 μm	≤10 μm
	repeatability	≤50 μm	≤50 μm
	Pitch and roll repeatability When change crystal	Pitch<1urad roll<2urad	Pitch<1urad roll<2urad
T2	Range		±5mm
	Resolution		≤1 μm
	repeatability		≤5 μm
	Pitch and roll repeatability		Pitch<1urad roll<2urad
Bragg	Range	0-45°	
	Resolution	≤0.4 μrad	
	accuracy	≤1 μrad	
	speed	0.5°/s	
Pitch	Range		±0.3°
	Resolution		≤20 nrad
	repeatability		≤100 nrad
Roll	Range	±1°	±1°
	Resolution	≤100 nrad	≤100 nrad
	repeatability	≤500 nrad	≤500 nrad
Encoder	All the axis with Encoder		
Cooling	Cryo cooling		
Vacuum	1×10^{-9}Torr, particle free		

a) KB mirrors

4.3.1 KB KB optical requirements

Table 4.3-1 Technical specification of KB system

	EM1	EM2	M3/M4	EM3	EM4	EM5	EM6	EM7	EM8
Operating energy range	3~15 keV								
Substrate material	Silicon crystal	Silicon crystal	Silicon crystal	Silicon crystal	Silicon crystal	Silicon crystal	Silicon crystal	Silicon crystal	Silicon crystal
Optical effective length（L×W）	950×40 mm^2	950×40 mm^2	950×40 mm^2	950×40 mm^2	950×40 mm^2	950×40 mm^2	950×40 mm^2	950×20 mm^2	950×20 mm^2
Mirror surface direction	horizontal reflection	Vertical reflection	Horizontal/Vertical reflection	horizontal reflection	Vertical reflection	horizontal reflection	Vertical reflection	horizontal reflection	Vertical reflection
Coating material	B_4C/Ru	B_4C/Ru	B_4C/Ru	B_4C/Ru	B_4C/Ru	B_4C/Ru	B_4C/Ru	Pt	Pt
Coating width	19mm/2mm /19mm	19mm/2mm /19mm	19mm/2mm /19mm	19mm/2mm /19mm	19mm/2mm /19mm	19mm/2mm /19mm	19mm/2mm /19mm	20mm	20mm
Coating density	≥ 95% bulk	≥ 95% bulk	≥ 95% bulk	≥ 95% bulk	≥ 95% bulk	≥ 95% bulk	≥ 95% bulk	≥ 95% bulk	≥ 95% bulk
Coating thickness	>500 Å	>500 Å	>500 Å	>500 Å	>500 Å	>500 Å	>500 Å	>500 Å	>500 Å
Mirror substrate	Single Crystal Silicon	Single Crystal Silicon	Single Crystal Silicon	Single Crystal Silicon	Single Crystal Silicon	Single Crystal Silicon	Single Crystal Silicon	Single Crystal Silicon	Single Crystal Silicon
Shape (before bending)[c]	Elliptical (bendable)	Elliptical (bendable)	Plane	Elliptical	Elliptical	Elliptical	Elliptical	Elliptical	Elliptical
Shape (after bending)	Elliptical cylinder (bendable)	Elliptical cylinder (bendable)							

p/q	340m/6m	341.2/4.8m		1145.6m/12.4m	1147m/11m	1154.5m/3.5m	1155.6m/2.4m	1172.8m/3.1m	1173.9m/2m
radius	2947.99m	2366.71m		6084.68m	5496.80m	1993.95m	1368.59m	951.34m	614.34m
Grazing angle	4 mrad	4 mrad	4 mrad	4 mrad	4 mrad	3.5 mrad	3.5 mrad	7 mrad	7 mrad
tangential slope error before bending	<0.05 μrad	<0.05 μrad	<0.05 μrad	<0.05 μrad	<0.05 μrad	<0.05 μrad	<0.05 μrad	<0.05 μrad	<0.05 μrad
Height error before bending (RMS/PV)	0.5 nm/2nm	0.5 nm/2nm	0.5 nm/2nm	0.5 nm/2nm	0.5 nm/2nm	0.5 nm/2nm	0.5 nm/2nm	0.5 nm/2nm	0.5 nm/2nm
Tangential slope error after bending or clamping (RMS)	<0.1 μrad	<0.1 μrad	<0.1 μrad	<0.1 μrad	<0.1 μrad	<0.1 μrad	<0.1 μrad	<0.1 μrad	<0.1 μrad
Height error after bending (RMS/PV)	3 nm/12nm@full range 1.5nm /6nm@400mm central part	3 nm/12nm@full range 1.5nm /6nm@400mm central part	1 nm/4nm	1 nm/4nm	1 nm/4nm	1.2 nm/5nm	1.2nm/5nm	1 nm/4nm	1 nm/4nm
Sagittal slope error (RMS)	<1 μrad	<1 μrad	<1 μrad	<1 μrad	<1 μrad	<1 μrad	<1 μrad	<1 μrad	<1 μrad
Roughness (RMS, with coating)	≤0.2 nm	≤0.2 nm	≤0.2 nm	≤0.2 nm	≤0.2 nm	≤0.2 nm	≤0.2 nm	≤0.2 nm	≤0.2 nm
Bending resolution	1/(4000 km)	1/(4000 km)							
Bending repetitive accuracy	1/(1000 km)	1/(1000 km)							

Bending stability	1/(4000 km) /10min 1/(1300 km) /24 h	1/(4000 km) /10min 1/(1300 km) /24 h							

4.3.2 HSS KB

The mirror chamber should be supported by a manually adjustable mechanism to ensure installation precision. The adjustment requirements are listed in Table 4.3-2. All the translations require the locking mechanism. The whole mirror system should move along Z axis to change the height and work at pink and mono beam mode. The heigh different is 15mm.

Table 4.3-2 Mirror chamber support requirements

Motion	Range	Resolution	Note
Pitch (Rx)	±0.5°	0.01°	Manual
Roll (Ry)	±0.5°	0.01°	Manual
Yaw (Rz)	±0.5°	0.01°	Manual
X (horizontal)	±50 mm	0.05 mm	Manual
Y (along beam)	±10 mm	0.05 mm	Manual
Z (perpendicular) Pink and mono beam	±50 mm	0.005 mm	Motor

The adjustment of the mirror position is listed in Table 4.3-3. The mirror support should be isolated from the chamber.

Table 4.3-3 Technical specification for the adjustment system of the EM1/EM2 mirrors

Axis		EM1	EM2
X Vertical scan	Range	±20 mm	±20 mm
	Resolution	≤10 μm	≤10 μm
	repeatability	≤50 μm	≤50 μm
Z In/out of the beam	Range	-10~+2 mm	-10~+18 mm
	Resolution	≤1 μm	≤1 μm
	repeatability	≤5 μm	≤5 μm
Pitch	Range	±0.3°	±0.3°
	Resolution	≤0.05μrad	≤0.05 μrad
	repeatability	≤0.2 μrad	≤0.2 μrad
Roll	Range		±0.3°
	Resolution		≤10 μrad
	repeatability		≤50 μrad
Yaw	Range	±0.3°	±0.3°
	Resolution	≤10 μrad	≤10 μrad
	repeatability	≤50 μrad	≤50 μrad
Encoder	All the axes with Encoder		
Vacuum	1×10^{-9}Torr, particle free		

The mirror stability requirements are listed in Table 4.3-4.

Table 4.3-4 Stability requirements of HSS KB

Stability (RMS)	

Pitch （RMS, <100 Hz）	<50 nrad / 10min (The manufacturer needs to guarantee the vibration parameter is able to meet this requirement based on the condition of SHINE hall.)

4.3.3 CDS micron-KB

The mirror system should be supported by a manually adjustable mechanism to ensure installation precision. The adjustment requirements are listed in Table 4.3-5. All the translations require the locking mechanism.

Table 4.3-5 Requirements of the mirror chamber support

Motion	Range	resolution	Note
Pitch (Rx)	±0.5°	0.01°	Manual
Roll (Ry)	±0.5°	0.01°	Manual
Yaw (Rz)	±0.5°	0.01°	Manual
X (horizontal)	±50 mm	0.05 mm	Manual
Y (along beam)	±10 mm	0.05 mm	Manual
Z (perpendicular)	±50 mm	0.05 mm	Manual

The adjustment of the mirror position is listed in Table 4.3-6. The mirror support should be isolated from the chamber.

Table 4.3-6 Technical specification for the adjustment system of the M3, M4, EM3 and EM4

Axis		M3	EM3	EM4	M4
X Vertical scan	Range	±20 mm	±20 mm	±20 mm	±20 mm
	Resolution	≤10 μm	≤10 μm	≤10 μm	≤10 μm
	repeatability	≤50 μm	≤50 μm	≤50 μm	≤50 μm
Z In/out of the beam	Range	-2~+10 mm	-2~+2 mm	-2~+10 mm	-2~+2 mm
	Resolution	≤1 μm	≤1 μm	≤1 μm	≤1 μm
	repeatability	≤5 μm	≤5 μm	≤5 μm	≤5 μm
Pitch	Range	±0.3°	±0.3°	±0.3°	±0.3°
	Resolution	≤20 nrad	≤20 nrad	≤20 nrad	≤20 nrad
	repeatability	≤100 nrad	≤100 nrad	≤100 nrad	≤100 nrad
Roll	Range			±0.3°	±0.3°
	Resolution			≤10 μrad	≤10 μrad
	repeatability			≤50 μrad	≤50 μrad
Yaw	Range		±0.3°	±0.3°	
	Resolution		≤10 μrad	≤10 μrad	
	repeatability		≤50 μrad	≤50 μrad	
Encoder	All the axes with Encoder				
Vacuum	1×10^{-9}Torr, particle free				

The mirror stability requirements are listed in Table 4.3-7.

Table 4.3-7 Stability requirements of the micron-KB

Stability (RMS)	

Pitch （RMS, <100 Hz）	<50 nrad / 10min (The manufacturer needs to guarantee the vibration parameter is able to meet this requirement based on the condition of SHINE hall.)

4.3.4 CDS nano-KB

The mirror bender system should be supported by a manually adjustable mechanism to ensure the installation precision. The adjustment requirements are listed in Table 4.3-8. All the translations require the locking mechanism.

Table 4.3-8 Requirements of mirror chamber support

Motion	Range	resolution	Note
Pitch (Rx)	±0.5°	0.01°	Manual
Roll (Ry)	±0.5°	0.01°	Manual
Yaw (Rz)	±0.5°	0.01°	Manual
X (horizontal)	±50 mm	0.05 mm	Manual
Y (along beam)	±10 mm	0.05 mm	Manual
Z (perpendicular)	±50 mm	0.05 mm	Manual

The adjustments of the mirror positions are listed in Table 4.3-9. The mirror support should be isolated from the chamber. The local temperature stability should be lower than 0.05° RMS.

Table 4.3-9 Technical specifications for the adjustment system of the EM5, EM6, EM7 and EM8

Axis		EM5/EM7	EM6/EM8
X Vertical scan	Range	±20 mm	±20 mm
	Resolution	≤10 μm	≤10 μm
	repeatability	≤50 μm	≤50 μm
Z In/out of the beam	Range	-2~＋10 mm	-2~＋10 mm
	Resolution	≤1 μm	≤1 μm
	repeatability	≤5 μm	≤5 μm
Pitch	Range	±0.3°	±0.3°
	Resolution	≤20 nrad	≤20 nrad
	repeatability	≤100 nrad	≤100 nrad
Roll	Range		±0.3°
	Resolution		≤1 μrad
	repeatability		≤5 μrad
Yaw	Range	±0.3°	±0.3°
	Resolution	≤1 μrad	≤1 μrad
	repeatability	≤5 μrad	≤5 μrad
Encoder	All the axes with Encoder		
Vacuum	1×10^{-9}Torr, particle free		

The mirror stability requirements are listed in Table 4.3-10.

Table 4.3-10 Stability requirements of the nano-KB

Stability (RMS)	
Pitch （RMS, <100 Hz）	<50 nrad / 10min (The manufacturer needs to guarantee the vibration parameter is able to meet this requirement based on the condition of SHINE hall.)

4.4 Compound refractive lenses

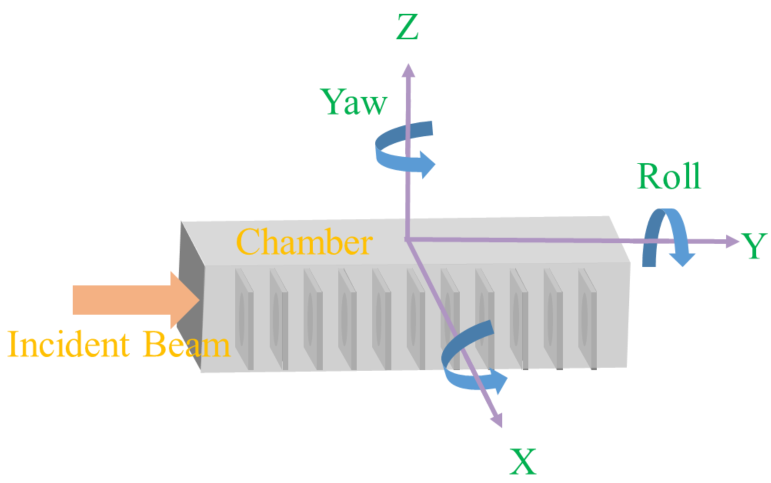

Figure 4.4-1 Axes definition of lens

Table 4.4-1 Technical specifications for the CRL adjustment system

Clear aperture	>5 mm			
	Axes	Range	Resolution	Repeatability
Alignment of lens	X	5 mm	0.5 μm	1 μm
	Z	40 mm	0.5 μm	1 μm
Support adjustment	X	±20 mm	1 μm	5 μm
	Y	±150 mm(CRL 2 and CRL 3)	1 μm	5 μm
	Z(pink and mono beam)	±20 mm	1 μm	5 μm
	Pitch(r-X)	±2°	0.5″	2″
	Yaw(r-Z)	±2°	0.5″	2″
Vacuum	1×10^{-9}Torr, particle free			
Cooling	water			

4.5 Solid attenuator

Table 4.5-1 Technical specification for the adjustment system of the solid attenuator

Energy range	3~15 keV			
Filter size	20 mm×20 mm			
Mask aperture	Φ10 mm			
Number of arms	8			
	Axes	Range	Resolution	Repeatability
Arm translation	X	130 mm	5μm	25μm
Support adjustment	X	±30 mm	5μm	25μm
	Z	±30 mm	5μm	25μm
Cooling	water			
Vacuum	~10^{-9}Torr			

4.6 Power slit

Table 4.6-1 Technical specification of power slit

Surface roughness of Blade(μm)		≤ 1（WC） ≤ 1（B4C）
Aperture(mm)	Horizontal	-20~20
	Vertical	-20~20
Resolution (μm)	Horizontal	5
	Vertical	5
Repeatability (μm)	Horizontal	±5(bi-directional)
	Vertical	±5(bi-directional)
	Horizontal	≤ 10

<table>
<tr><td>Straightness of blade edge(μm)</td><td>Vertical</td><td>≤ 10</td></tr>
<tr><td rowspan="2">Parallelism of blades (mrad)</td><td>Horizontal</td><td>≤ 1</td></tr>
<tr><td>Vertical</td><td>≤ 1</td></tr>
<tr><td colspan="2">Blade material</td><td>Combination blade of B4C&&WC</td></tr>
<tr><td colspan="2">Angle of knife edge(°)</td><td>TBD</td></tr>
<tr><td colspan="2">Blade movement with Linear Encoder</td><td>Yes</td></tr>
<tr><td colspan="2">Vacuum (Torr)</td><td>$<1\times10^{-9}$</td></tr>
<tr><td colspan="2">Support Adjustment</td><td>X, Z direction :±20mm;
Mounted on adjustable support structure</td></tr>
<tr><td colspan="2">Remark</td><td>Each Blade Independent Motions;
Weak Current Extraction;
Fiducial Holes;</td></tr>
</table>

5. Performance simulation

5.1 Focus

Figure 5.1-1 shows the focusing spot of CRL at 8.9 keV. Theoretical CRL focusing can reach 2.4 μm×2.6 μm, but since CRLs have thickness errors, radius errors, voids, etc., the final focusing spot will be larger. As shown in Figures 5.1-2~6, the beam size can be changed by the bending mirrors. The height error in use for the simulation is 0.5 nm RMS. The final height error may be worse, and the enlarged beam will be nonuniform.

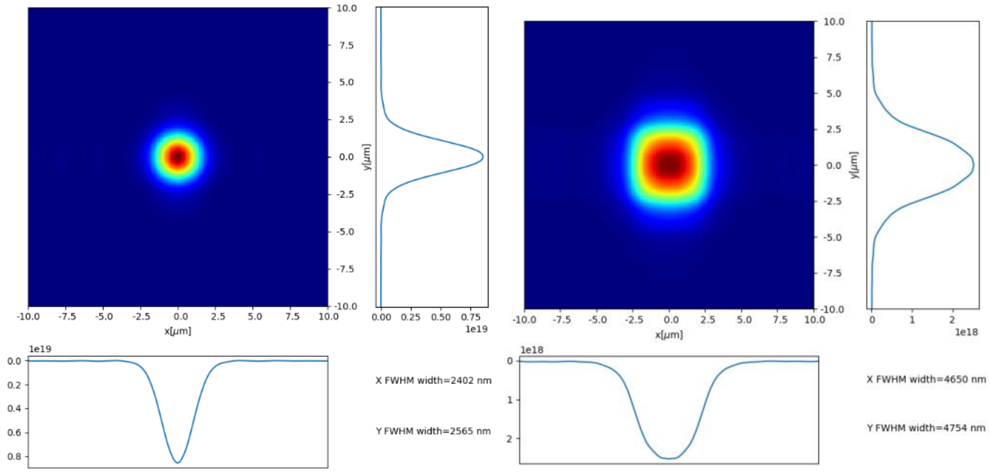

Figure 5.1-1 Focusing spot of HSS CRL at 8.9 keV (a: focus, b: 0.1 m defocus)

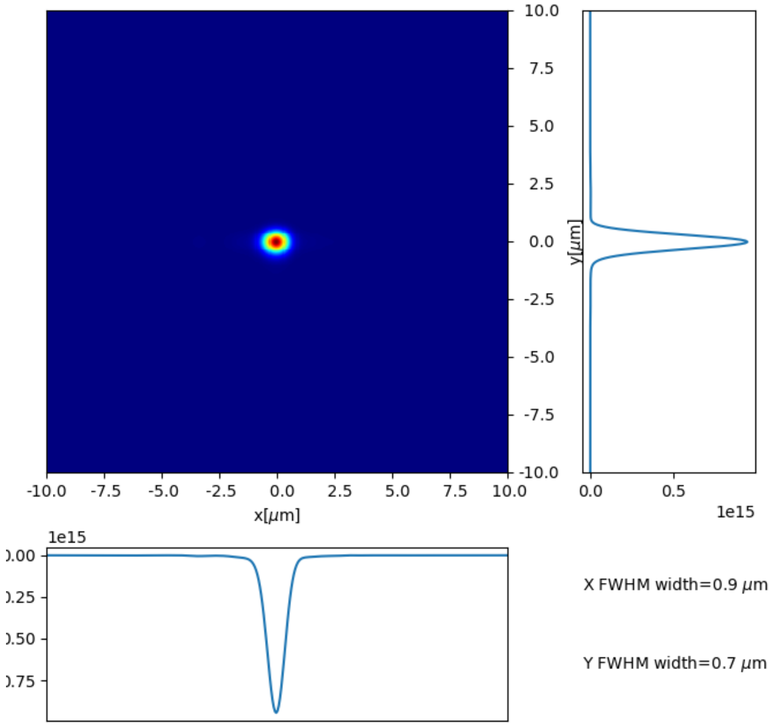

Figure 5.1-2 Focusing spot of HSS KB in focus at 7 keV

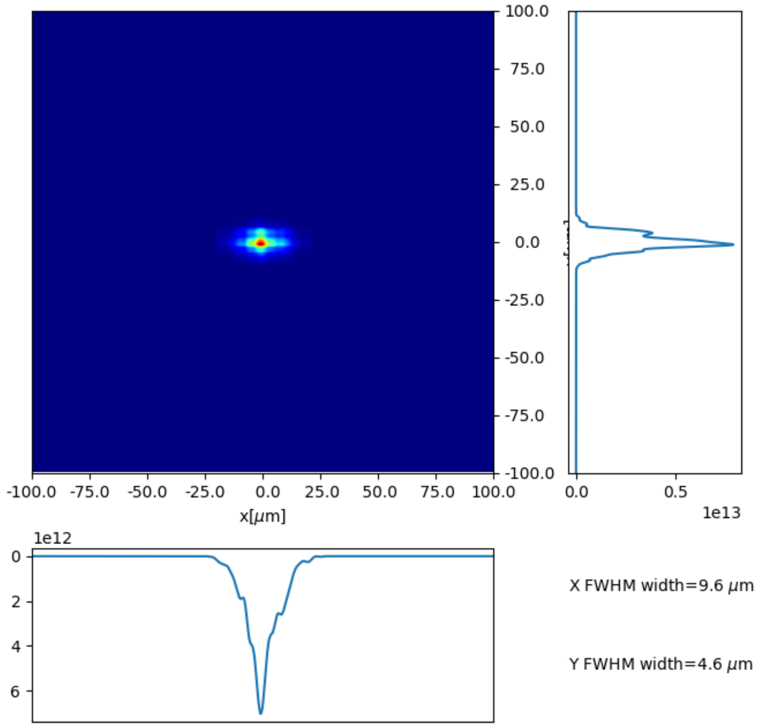

Figure 5.1-3 Focusing spot of HSS KB out of focus at 7 keV (0.2 m defocus)

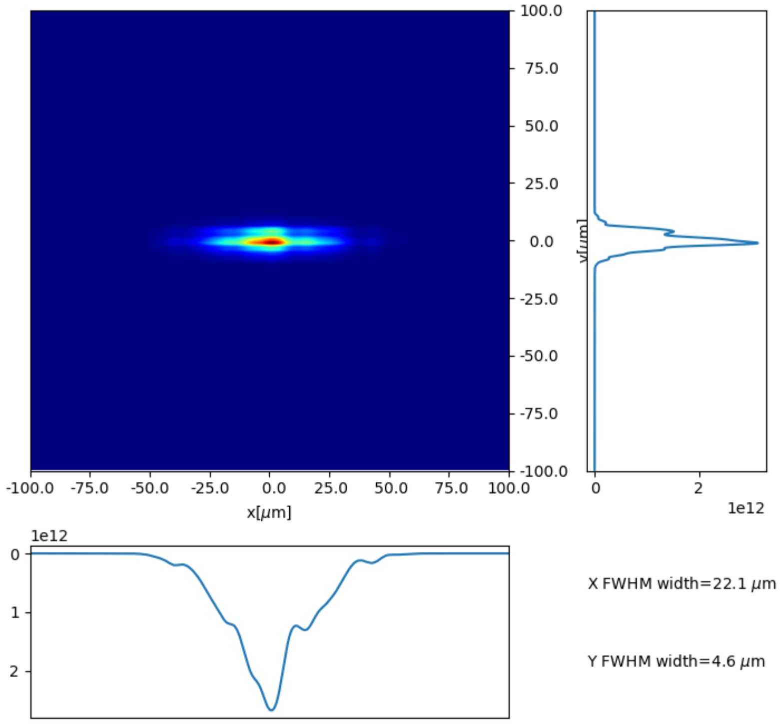

Figure 5.1-4 Focusing spot of HSS KB out of focus at 7 keV (defocus 0.5 m)

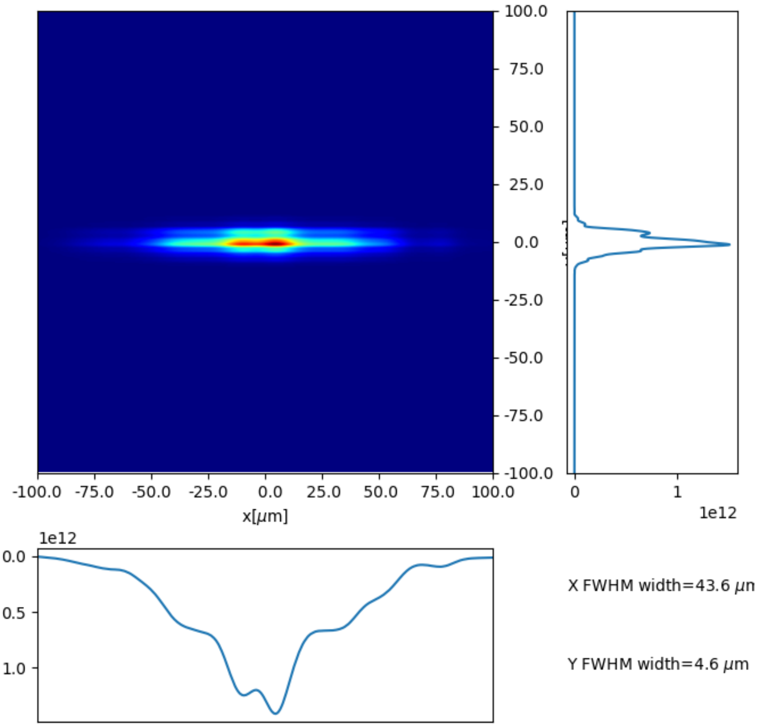

Figure 5.1-5 Focusing spot of HSS KB out of focus at 7 keV (defocus 1 m)

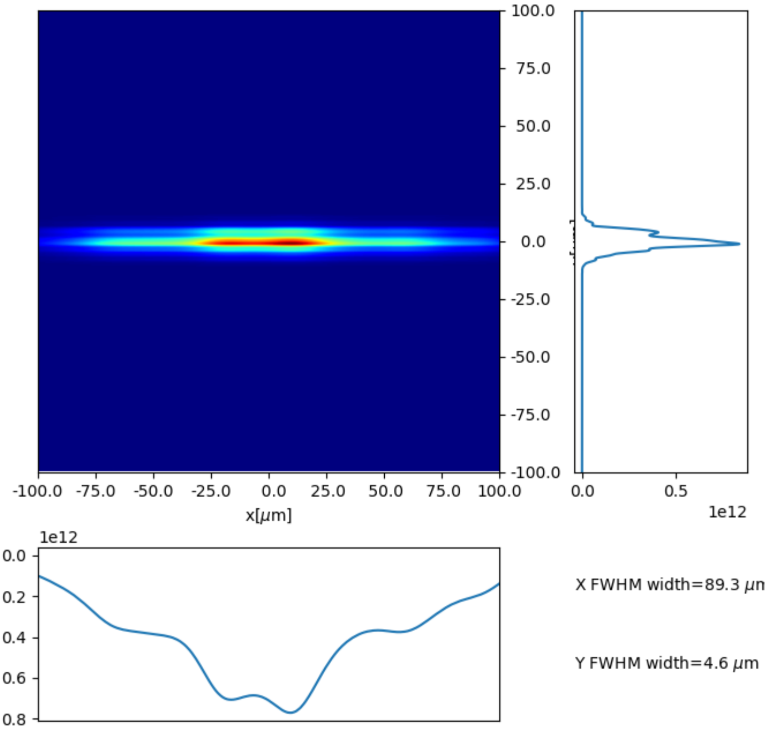

Figure 5.1-6 Focusing spot of HSS KB out of focus at 7 keV (defocus 2 m)

The focusing spot at CDS is shown in Figures 5.1-7, 5.1-8, and 5.1-9, which are the results of micron-focus and nano-focus using data from Genesis at 7 keV. The simulation results are the same as the theoretical analysis results above.

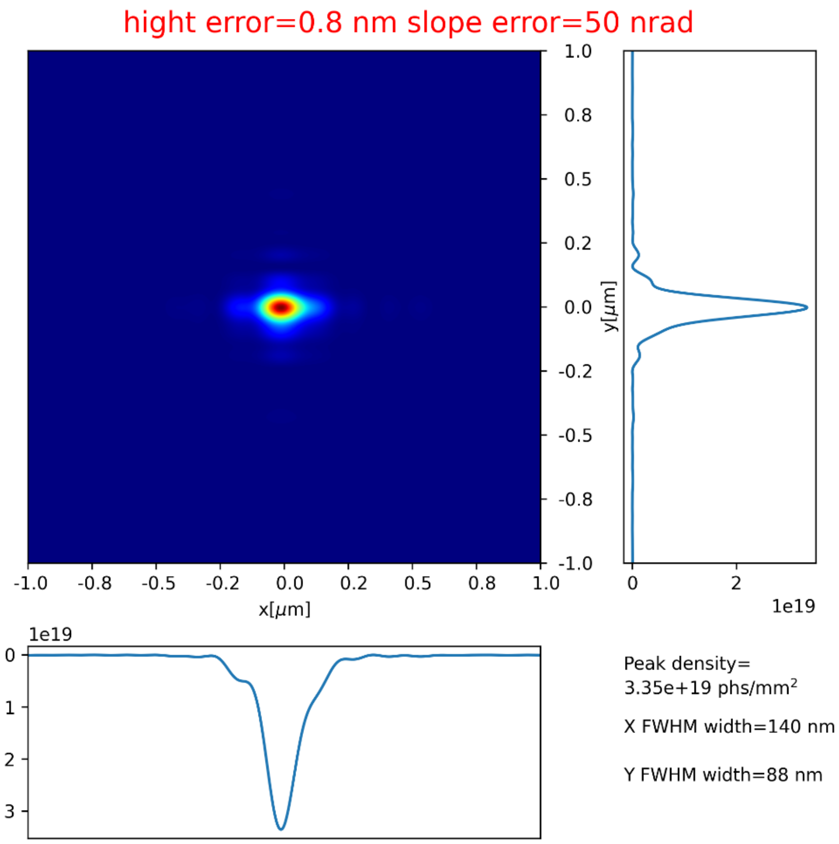

Figure 5.1-7 Nano-focus spot of CDS KB with Genesis data f=2 m

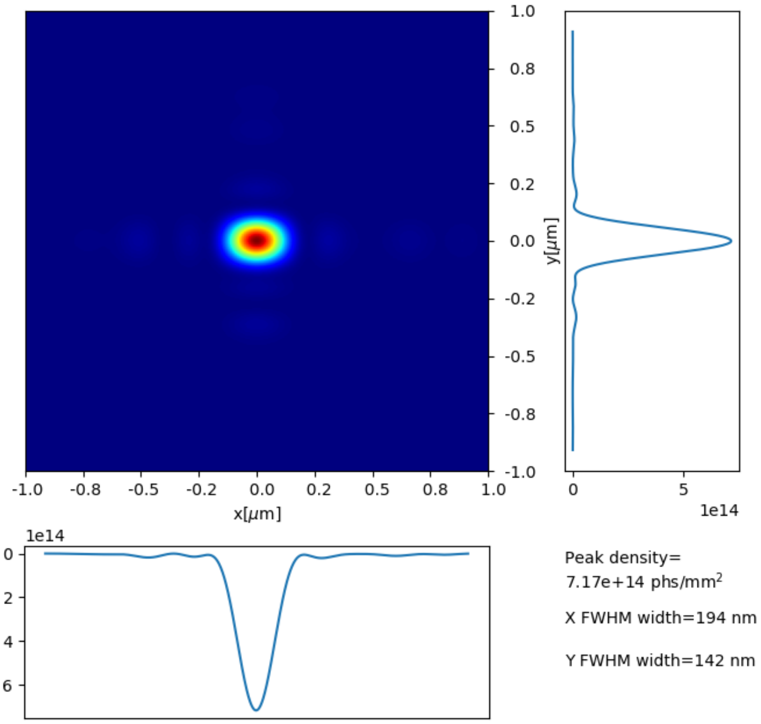

Figure 5.1-8 Nano-focus spot of CDS KB with Genesis data f=2.5 m

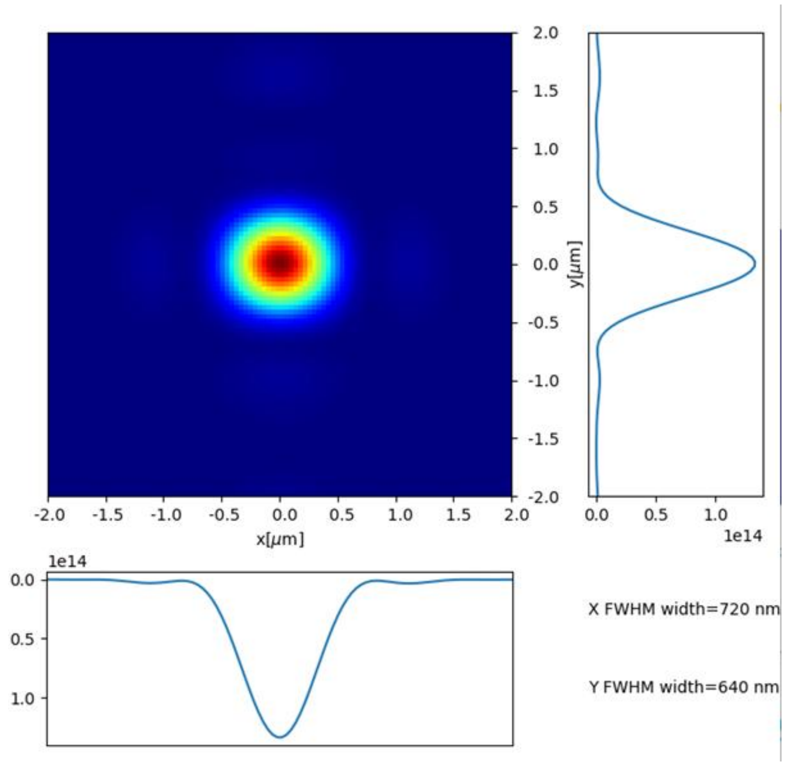

Figure 5.1-9 Micron-focus spot of CDS KB with Genesis data

5.2 Transmission efficiency

In the HSS, the reflectivity of the offset mirrors, CRL absorption, KB mirror reflectivity, and diffraction loss are mainly considered. The transmission efficiency is shown in Figures 5.2-1 and 5.2-2. In the CDS endstation, the offset mirrors, KB mirror reflectivity, and diffraction loss are considered. The transmission efficiency of CDS KB is shown in Figure 5.2-3.

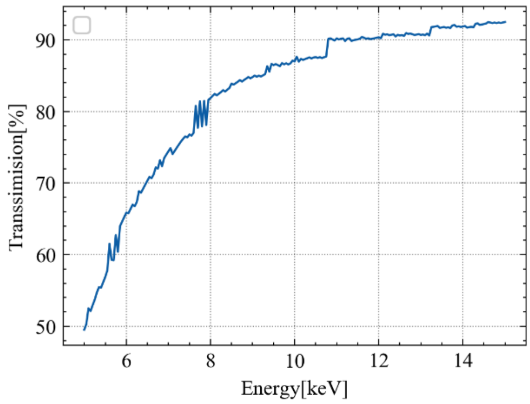

Figure 5.2-1 The efficiency at the HSS when the CRL is used

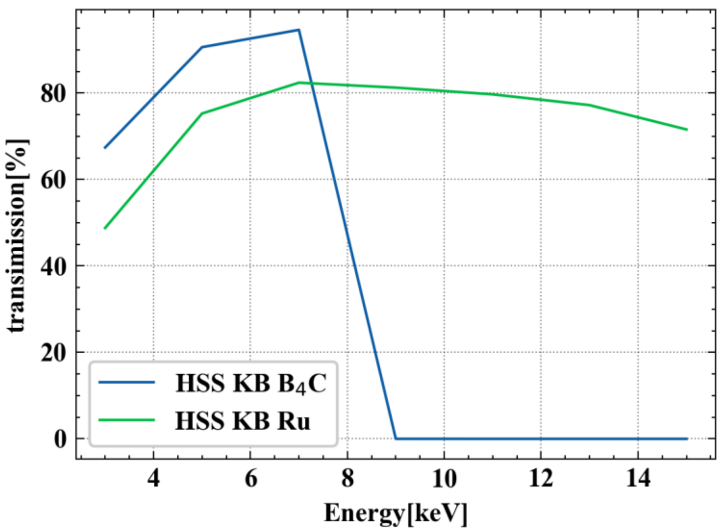

Figure 5.2-2 The efficiency at the HSS when the KB is used

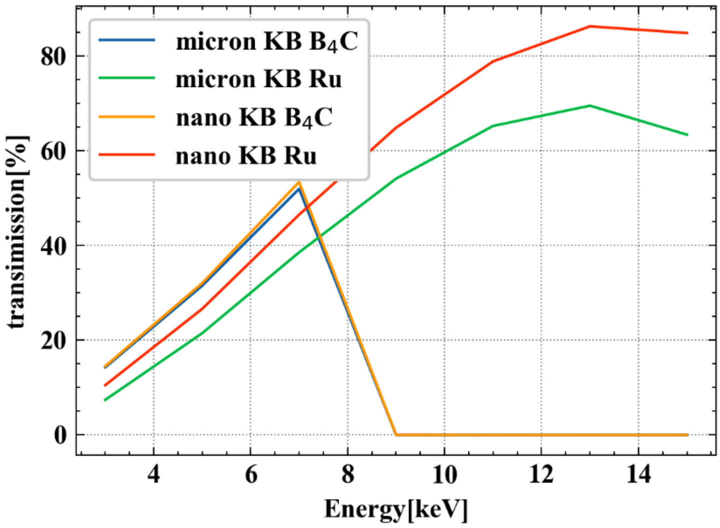

Figure 5.2-3 The efficiency at the CDS

In the energy range of 3-15 keV, the use of CRL and KB focusing in the HSS can have transmission efficiencies higher than 50%, and most energy ranges are higher than 80%. Affected by the aperture of KB and the diffraction loss at the CDS, the low-energy range has low efficiency, and the high-energy range can reach more than 50% at 7 keV. The final efficiency can be improved, especially the loss from the KB aperture, which can be eliminated by weakly focusing the beam with the CRL or M2a/M2b.

6. Thermal FEA on the optical elements

6.1 Thermal analysis of the offset mirrors

6.1.1 Thermal analysis model and parameters

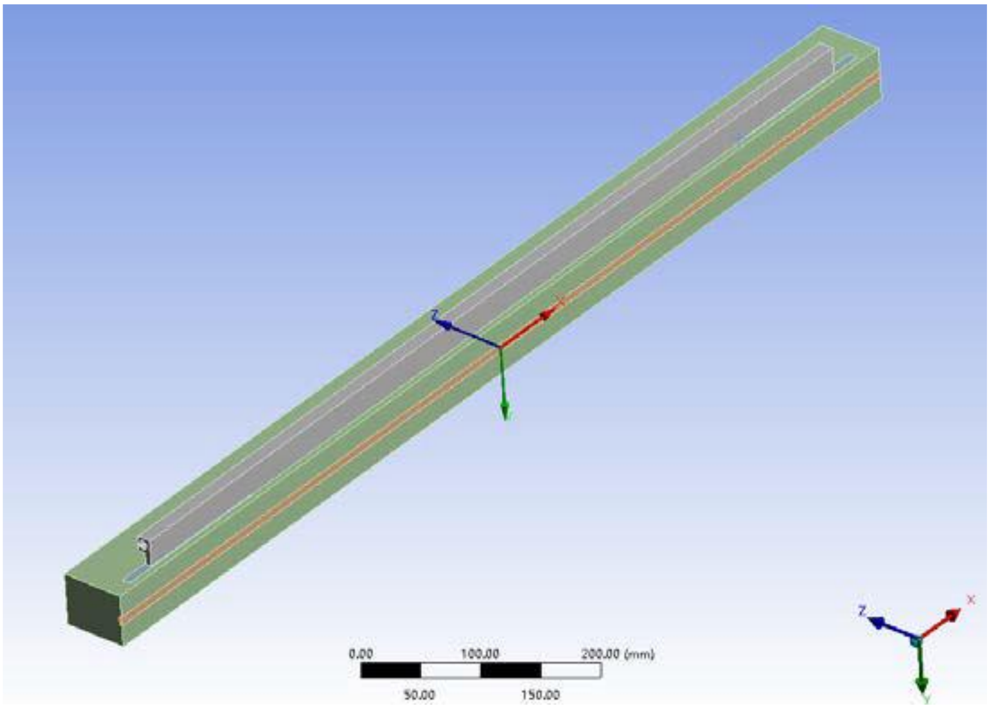

Figure 6.1-1 Thermal analysis model of the offset mirrors

Table 6.1-1. Material parameters

Material	Density /kg·m-3	Elastic modulus /GPa	Poisson's ratio	Yield stress /MPa	Thermal conductivity /W·m^{-1}·°C^{-1}	Thermal expansion coefficient /°C^{-1}, 25°C
Silicon	2329	112.40	0.28	120.00	148.00	2.50×10^{-6}
Copper	8900	110.00	0.34	220.00	391.00	1.75×10^{-5}
In-Ga	6350	--	--	--	28	--

Figure 6.1-1 shows the model used in the FEA. The side of the optical element is

slotted, and indium gallium alloy is used in the slot. A water-cooled copper block is immersed in the indium gallium alloy. On one hand, it has a good heat transfer effect, while on the other hand, it can well isolate the vibration caused by the cooling water from the mirror. During the simulation process, the distance between the cooling slot and the optical surface, as well as the size of the cooling slot were optimized and compared.

6.1.2 Analysis of the FEA results

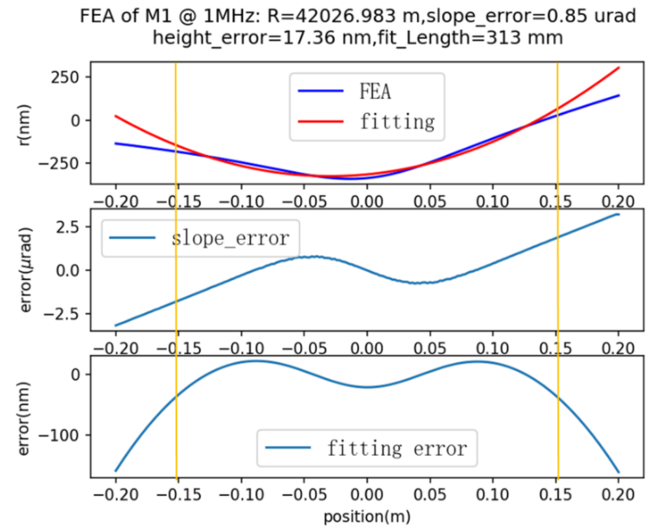

Figure 6.1-2 Analysis of the results under M1, 7 keV and 1.9 mrad conditions

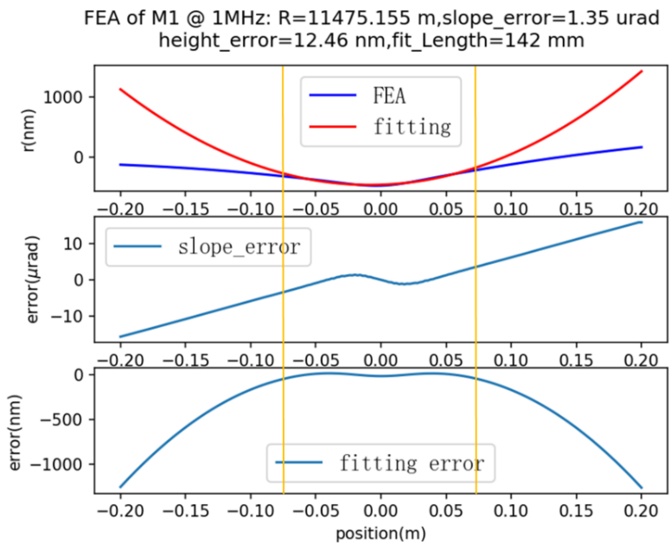

Figure 6.1-3 Analysis of results under M1, 7 keV 4 mrad conditions

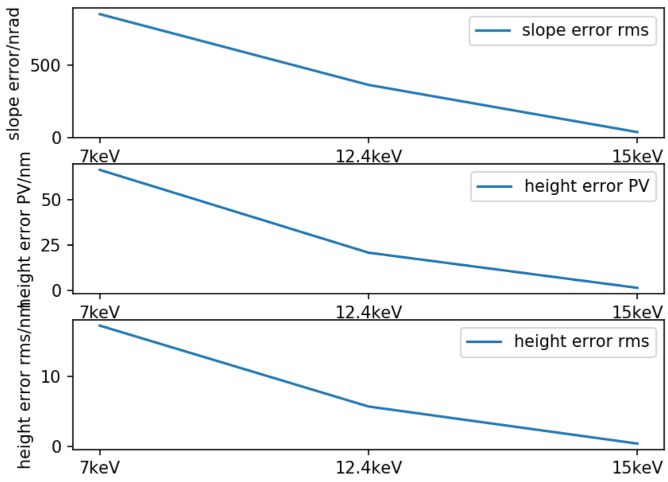

Figure 6.1-4 The statistical results of the height error and slope error of different energies under the condition of M1, 1.9 mrad

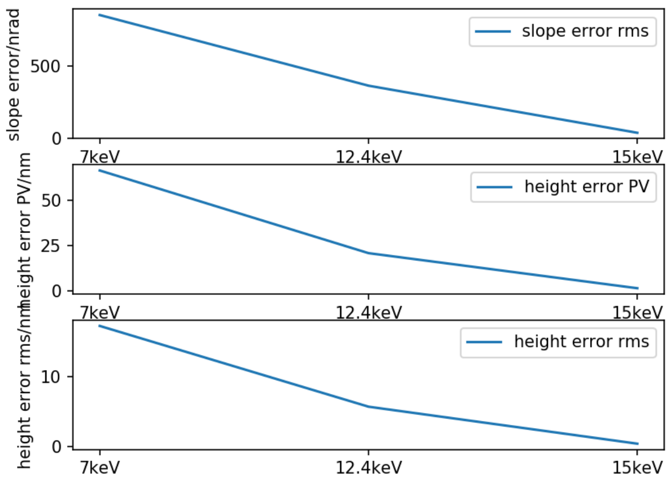

Figure 6.1-5 The statistical results of the height error and slope error of different energies under the condition of M1, 4 mrad

Table 6.1-2 Calculation results of M1 under different conditions

Energy（keV）	Grazing angle（mrad）	Repetition rate（MHz）	radius（m）	Residual height error（nm）	Working repetition rate（MHz）	Residual radius（m）
3	4	1	81840	8.66	0.2	409200
5	4	1	34662	10.72	0.1	346620
7	4	1	11475	12.46	0.05	229500
7	1.9	1	42026	17.36	0.1	420260
12.4	1.9	1	84368	5.7	0.1	843680
15	1.9	1	374919	0.36	1	374919

Table 6.1-3 Calculation results of M2a and M2b under different conditions

	Energy（keV）	Grazing angle（mrad）	Repetition rate（MHz）	radius（m）	Residual height error（nm）	Working repetition rate（MHz）	Residual radius（m）
M2a	3	4	1	361236	0.46	1	361236
	5	4	1	147525	0.58	1	147525
	7	4	1	47551	0.61	1	47551
M2b	7	1.9	1	183035	0.78	1	183035
	12.4	1.9	1	248972	0.14	1	248972
	15	1.9	1	1785261	0.14	1	1785261

Figures 6.1-2 and 6.1-3 show the results of 7 keV at different grazing incidence angles. It can be seen that under the conditions of the adopted model, within the FWHM length of the footprint, the residual height error is 10 nanometers. The expansion coefficient of the silicon material is linear at this temperature, so as to meet the Strehl ratio requirement, the heat load needs to be reduced by more than 10 times. Table 6.1-2 and Table 6.1-3 give the working conditions of each component and the radius to be corrected, respectively.

The above calculations are performed in the 1 MHz taper mode. In the nontapered mode, the tolerable repetition rate can be increased by 3-5 times.

6.2 Thermal analysis of the KB mirrors

6.2.1 Thermal analysis model and parameters

The model of the KB mirror horizontal focusing mirror is the same as that of the offset mirror group, and the cooling of the vertical focusing mirror adopts slot cooling on one side of the mirror. Other parameters are consistent with the offset lens group

6.2.2 Analysis of the FEA results

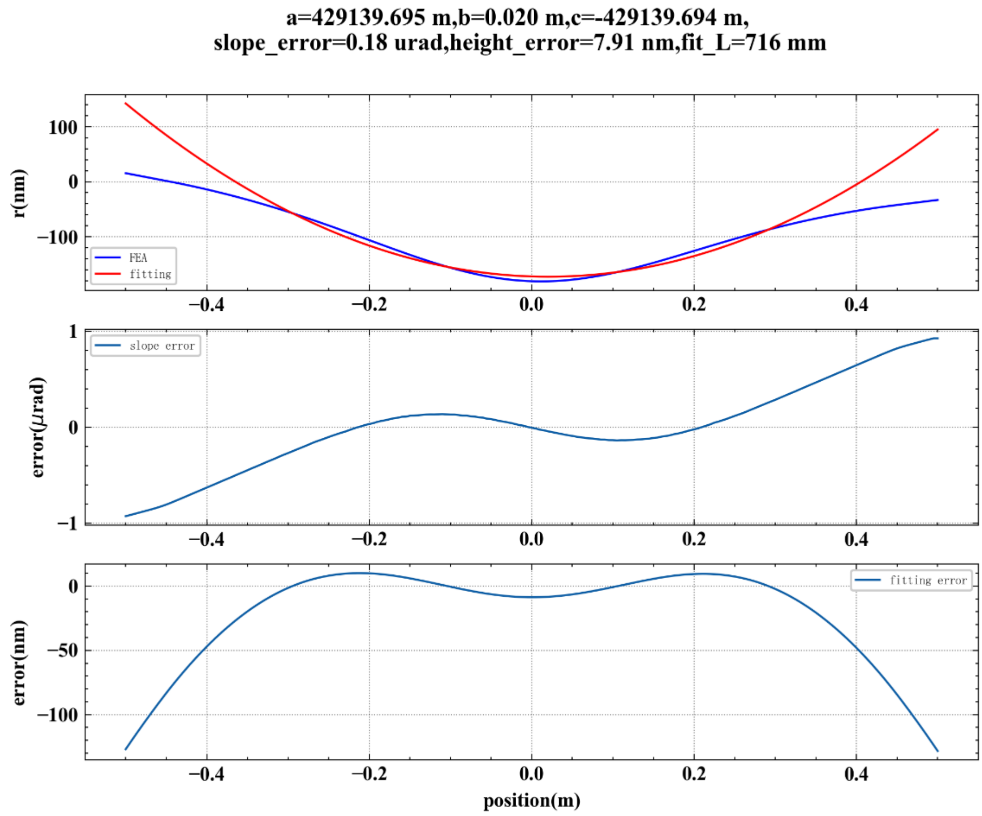

Figure 6.2-1 The results of the CDS KB mirror with B4C coating at 7 keV

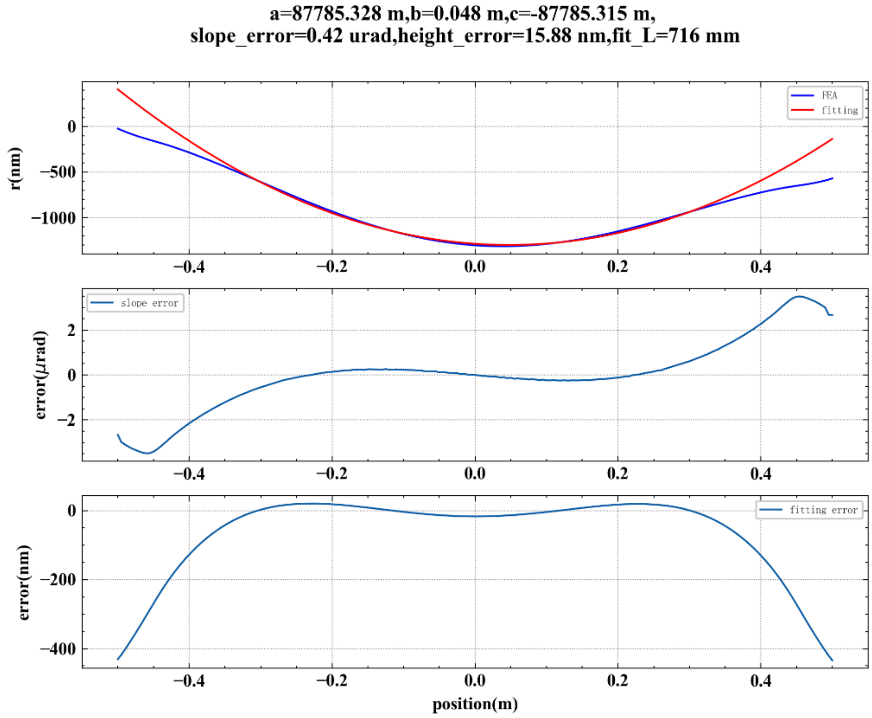

Figure 6.2-2 The results of the CDS KB mirror with Ru coating at 7 keV

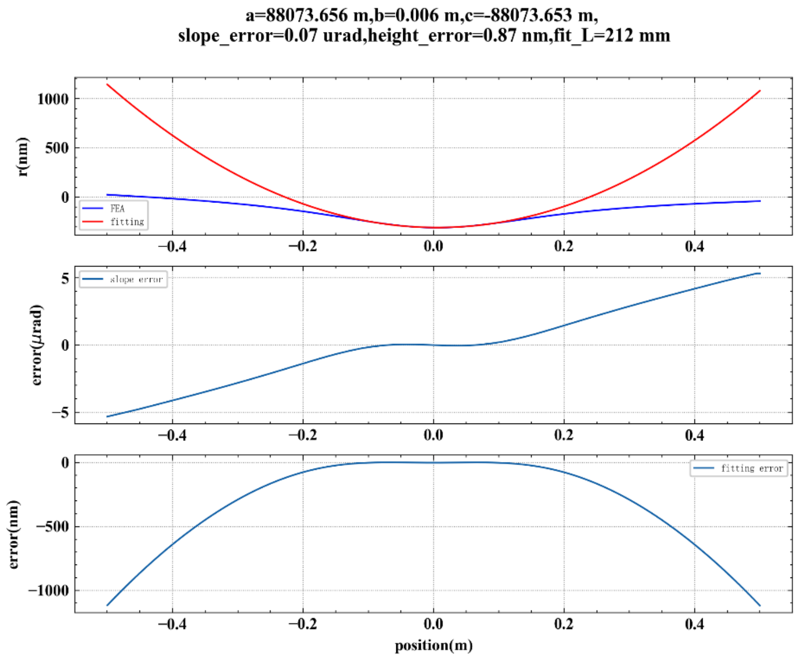

Figure 6.2-3 The results of the HSS KB mirror with Ru coating at 7 keV

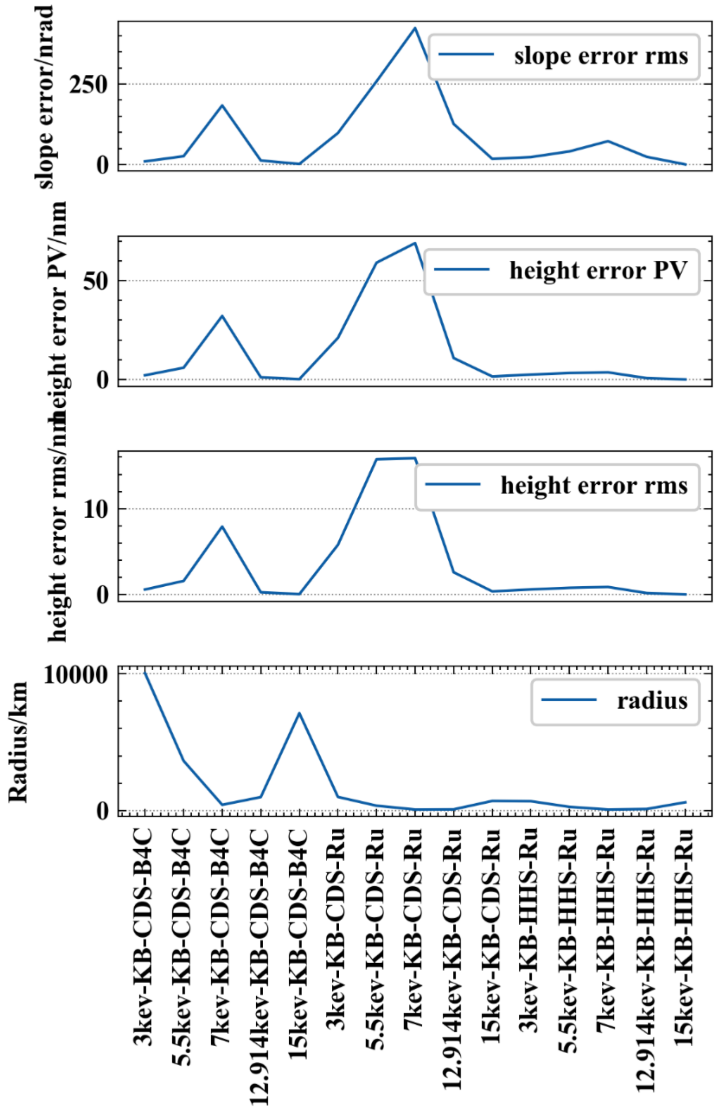

Figure 6.2-4 The statistics of the FEA result

Figures 6.2-1~4 show the analysis results of the KB mirrors of the CDS and HSS. Due to the large footprint on the KB of CDS, the residual height error after fitting has also reached 10 nm, so the KB also needs to further optimize the cooling methods and limit the repetition rate.

6.3 Monochromator thermal analysis

6.3.1 Thermal analysis model and parameters

The crystal size is 60 mm×28 mm×20 mm. The size of the copper block is 60 mm×10 mm×20 mm, and the inner diameter of the cooling water channel is 6 mm. Liquid nitrogen was used for cooling; the reference temperature was 80 K, and the flow rate was 3 L/min. The FEL repetition frequency is 10 kHz.

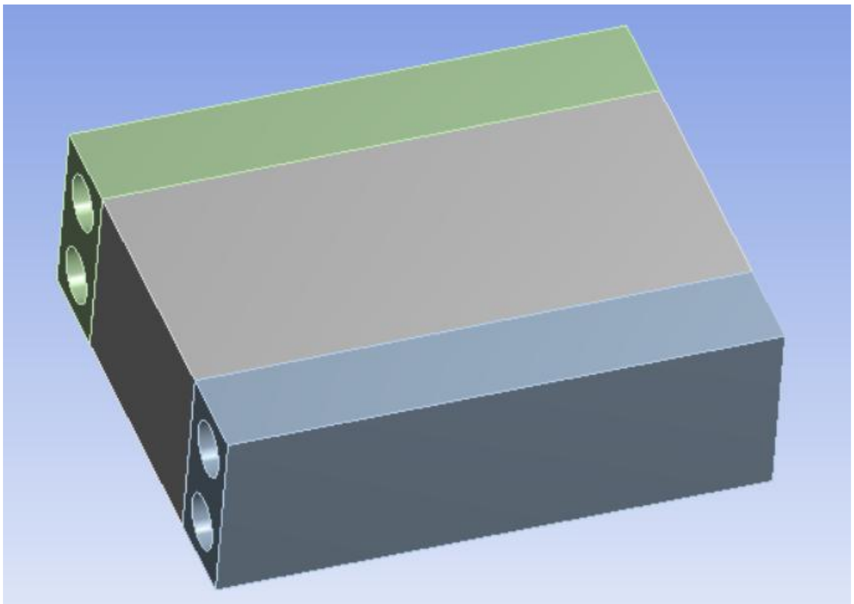

Figure 6.3-1 Crystal and cooling block model

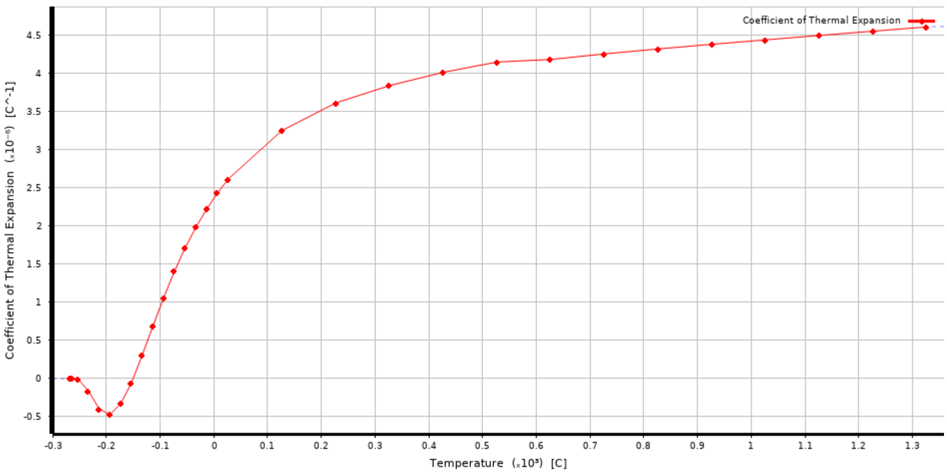

Figure 6.3-2 Si thermal expansion coefficient curve

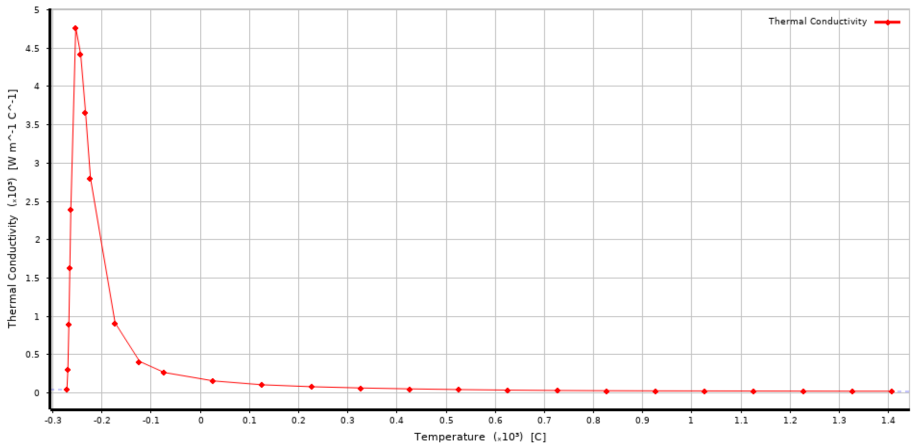

Figure 6.3-3 Si thermal conductivity curve

Table 6.3-1 Cu material property parameters

Density (kg/m^3)	8900
Modulus (GPa)	110
Poisson’s ratio	0.34
Thermal conductivity (W/(m*k))	391
Thermal expansion coefficient (10^{-5}/k)	1.75

6.3.2 Analysis of the FEA results

The figure shows the results of the finite element analysis. From the results, we can see the residual height error at 10 kHz. If the Strehl ratio is used, the crystal needs to reach a residual height error of 0.01 nm. It can be seen from the calculation results that this requirement can be met. Regarding the influence of the radius, from the previous analysis results, as long as the radius R is greater than 2000 m at 8.9 keV, the flux and resolution requirements can be met. The residual errors are slightly larger than the requirements.

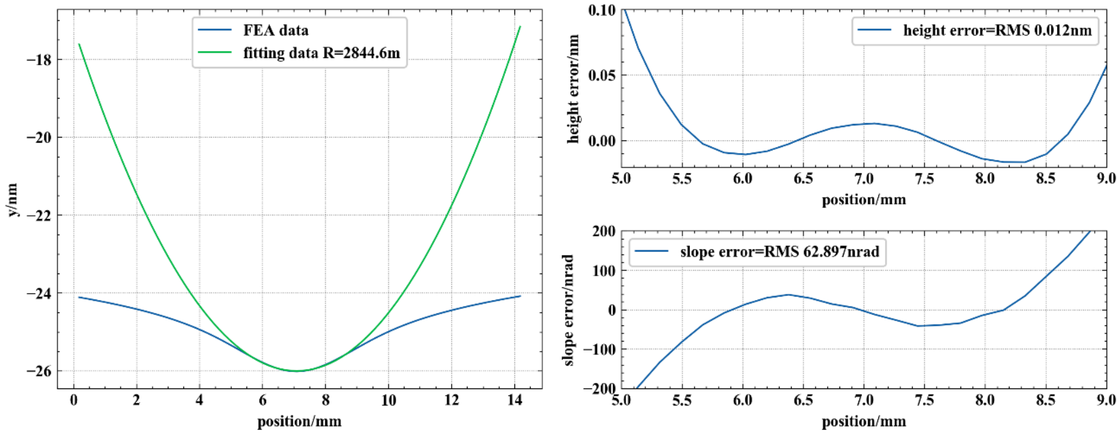

Figure 6.3-4 The results of the Si(111) crystal at 7 keV and 10 kHz

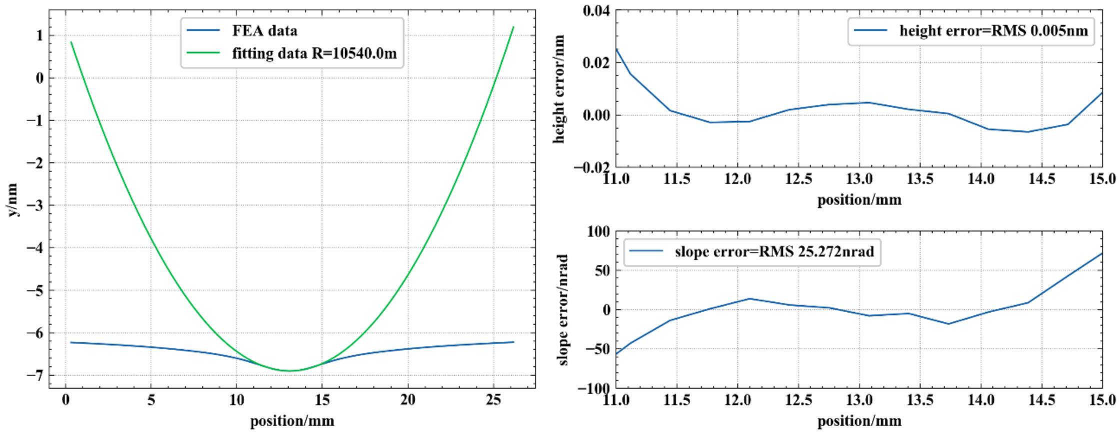

Figure 6.3-5 The results of the Si(111) crystal at 12.4 keV and 10 kHz

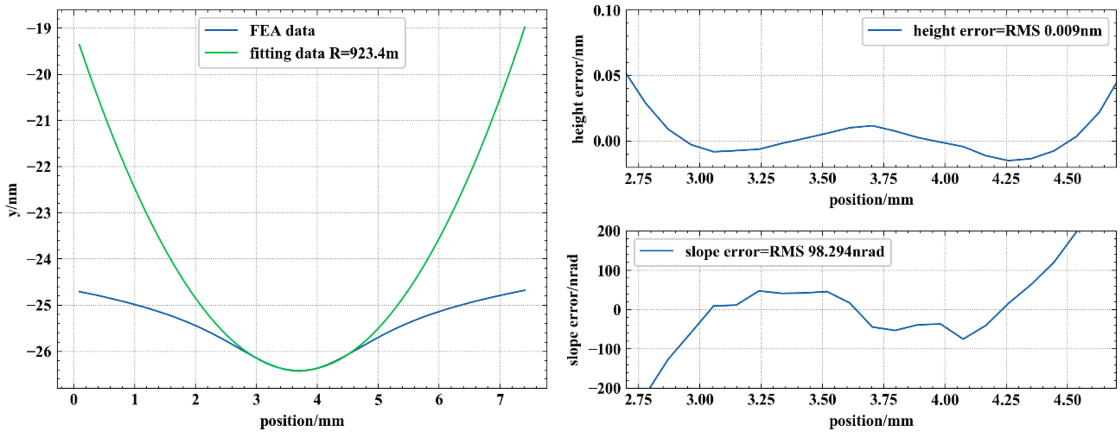

Figure 6.3-6 The results of the Si(311) crystal at 7 keV and 10 kHz

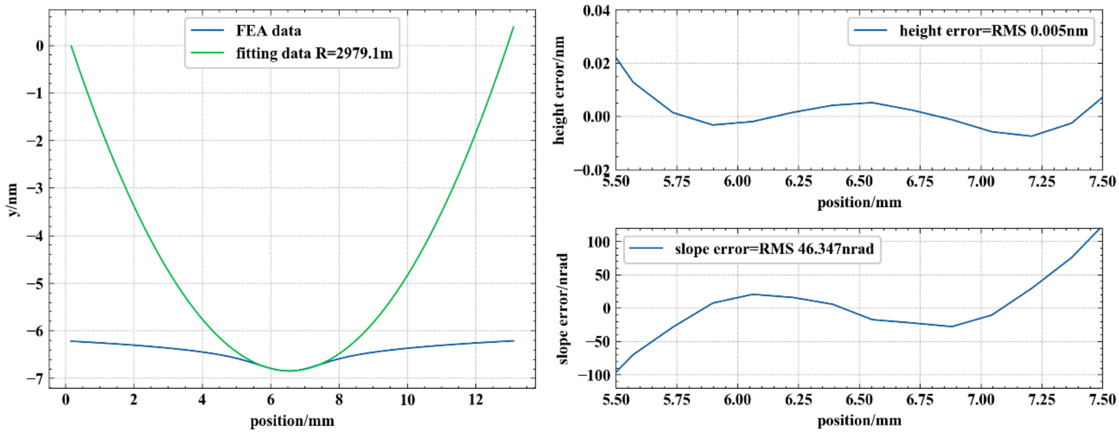

Figure 6.3-7 The results of the Si(311) crystal at 12.4 keV and 10 kHz

7. Summary

Based on the analysis and simulations above, the physical scheme of the FEL-I beamline meets the design specifications regarding energy range, spot size, energy resolution, and transmission efficiency. However, when aiming for higher beamline performance, there are still international challenges to be addressed in areas such as the manufacturing of optical components, cooling, precision clamping and bending, and multi-pulse damage.

Table 7-1 Design result

Parameter	Objective	Nominal	design result
Energy range	3.0 – 15.0 keV	5.0 – 13.0 keV	3.0 – 15.0 keV
Energy resolution (△E/E)	2.0×10^{-4}@8.9 keV	2.0×10^{-4}@8.9 keV	5.0×10^{-5}@8.9 keV

Transmission efficiency	30%@7keV(no monochromator)	15%@7keV(no monochromator)	50%@7keV(no monochromator)
spot size	10 µm @HSS 0.1 µm&1 µm @CDS	15 µm @HSS	2.56 µm @HSS CRL 0.064µm&0.72 µm @CDS

Table 7-2 CDS instrument design result

	Parameter	CDS	design result
1	Energy range	3~15 keV	3~15 keV
2	Energy resolution	/	/
3	Efficiency of beamline	≥50%@7keV	≥60%@7keV(1)
4	Percent of harmonics	≤0.05%	≤0.01%
5	Spot size (FWHM)(H×V)	objective：300 nm×100nm@7keV nominal：600 nm×300nm@7keV	120 nm×90nm@7keV(2) 200 nm×150nm@7keV(2) 720 nm×640nm@7keV(2)
6	Working distance	>0.2m	√
7	Beam stability（RMS）	/	/
8	focusing	/	/
9	attenuator	6 orders	6 orders

Table 7-3 HSS instrument design result

	Parameter	HSS	design result
1	Energy range	3~15 keV	3~15 keV
2	Energy resolution	Si(111): 2×10^{-4}@3~15keV Si(311): 5×10^{-5}@5.6~15keV	Si(111): 2×10^{-4}@3~15keV Si(311): 5×10^{-5}@5.6~15keV
3	Efficiency of beamline	≥60%@7keV	≥70%@7keV(1)
4	Percent of harmonics	≤0.01%	≤0.01%
5	Spot size	objective：(5μm~200μm)×(5μm~200μm)	(5μm~200μm)×(5μm~200μm)

	(FWHM)(H×V)	nominal：10μm×10μm	
6	Working distance		
7	Beam stability（RMS）	≤3um	≤3um[3]
8	focusing	K-B	K-B
9	attenuator	4 order	6 order

[1] no monochromator

[2] only one direction

[3] calculated with 50nrad

8. List of beamline devices

No	Devices	Position(m)
1	Fixed Aperture	103.1
2	shutter 1	103.8
3	gamma absorber	105.1
4	safety shutter	105.7
5	BLM1	132.2
6	fast value	132.5
7	slit1	135.5
8	Imager1	136.2
9	GMD-V	138.8
10	HAMP-V	139.5
11	HAMP-H	140.3
12	GMD-H	141
13	Imager2	145
14	GAT	160
15	Imager3	197
16	SAT	198.3
17	CRL1	200
18	Imager4	224.7
19	BPIM1	225.3
20	collimator 1	226
21	M1	230
22	Imager5	231.8
23	BLM2	232.3
24	slit2	233
25	M2a	234.75
26	M2b	240
27	Imager6	243.56
28	collimator 2	244
29	Single pulse pectrometer	249~259
30	shutter 2	320.95

31	BLM3	321.6
32	slit3	322.4
33	Imager7	323
34	DCM	332
35	slit4	335.3
36	CRL2	336.5
37	Imager8	337.6
38	shutter 3	338.2
39	EM1	340.45
40	EM2	341.7
41	diamond window	344
42	PAM1(HSS)	344.5
43	BPIM2	345
44	focusing imager	346.5
45	PLM(HSS)	350.5
46	shutter 4	352.2
47	Imager9	400
48	Imager10	750
49	Imager11	1050
50	Imager12	1105
51	GMD/HAMP	1110
52	BLM4	1130.5
53	shutter 4	1131
54	slit 4	1141
55	M3	1144.5
56	EM3	1145.6
57	EM4	1147
58	M4	1148.1
59	shutter 5	1149.5
60	BLM5	1151
61	slit 5	1151.5
62	EM5	1154.5
63	EM6	1155.6

64	PAM2(CDS)	1156.8
65	focusing imager	1158
66	Wavefront sensor	1158
67	BPIM3(1160.1)	1164.5
68	shutter 6	1165
69	CRL3	1165.9
70	EM7	1172.8
71	EM8	1173.9
72	Wavefront sensor	1175.9
73	shutter 7	1180

9. Acknowledgments

Besides those in the author list, other colleagues contributed to this design report. Thanks to Huaidong Jiang, Zhibin Sun, Qing Xie, Yang Du, Menglu Hu, Yonggan Nie for the discussion about CDS; Thanks to Tsu-Cien Weng, Jianwei Meng for the discussion about HSS; Thanks to Liangliang Ji, Jiancai Xu for the discussion about SEL; Wanqian Zhu, Jiahua Chen, Nan Wang, Yan Zhao, Yongjun Li, Yichen Fan, Hongxin Luo, Ming Chen, Huayan Huang, Yifei Zhang for the discussion about Engineering;

Thanks to colleagues from the machine side: Dong Wang, Bo Liu, Haixiao Deng, Tao Liu etc.

Thanks to Bart Faatz for the discussion of beamline layout.

Thanks to people from European XFEL for the discussion on beamline design, diagnostics design: Harald Sinn, Jan Gruenert, Jia Liu, Maurizio Vannoni, Daniele la Civita, Fan Yang, Wei Lu.

10.References

[1] "LCLS-II ConceptualDesign Report,LCLSII-1.1-DR-0001-R0, 11-10 (2014)."

[2] K. Tono *et al.*, "Beamline, experimental stations and photon beam diagnostics for the hard x-ray free electron laser of SACLA," *New Journal of Physics,* vol. 15, no. 8, p. 083035, 2013.

[3] A. A. A.P. Mancuso, G. Borchers, and K. Giewekemeyer,, "TR-2013-004_TDR_SPB," 2013.

[4] R. J. Bean, A. Aquila, L. Samoylova, and A. P. Mancuso, "Design of the mirror optical systems for coherent diffractive imaging at the SPB/SFX instrument of the European XFEL," *Journal of Optics,* vol. 18, no. 7, p. 074011, 2016.

[5] B. Lengeler *et al.*, "Imaging by parabolic refractive lenses in the hard X-ray range," *Journal of Synchrotron Radiation,* vol. 6, no. 6, pp. 1153-1167, 1999.

[6] J. H. A. Madsen, T. Roth, and G. Ansaldi, "TECHNICAL DESIGN REPORT Scientific Instrument Materials Imaging and Dynamics (MID)," 2013.

[7] K. A. M. Nakatsutsumi, G. Priebe, I. Thorpe, A. Pelka, B. Muller, and Th. Tschentscher, "TECHNICAL DESIGN REPORT Scientific Instrument High Energy Density Physics (HED)," 2014.

[8] R. Celestre, S. Berujon, T. Roth, M. S. del Rio, and R. Barrett, "Modelling phase imperfections in compound refractive lenses," (in English), *Journal of Synchrotron Radiation,* vol. 27, pp. 305-318, Mar 2020.

[9] M. D. H. Sinn, X. Dong, D. La Civita, L. Samoylova, R. Villanueva, and F. Yang, "CONCEPTUAL DESIGN REPORT X-Ray Optics and Beam Transport," 2012.

[10] LCLS-II, "LCLS-II Final Design Report," 2014.

[11] T. Koyama *et al.*, "Damage threshold of coating materials on x-ray mirror for x-ray free electron laser," *Rev Sci Instrum,* vol. 87, no. 5, p. 051801, May 2016.

[12] S. P. Hau-Riege *et al.*, "Multiple pulse thermal damage thresholds of materials for x-ray free electron laser optics investigated with an ultraviolet laser," *Applied Physics Letters,* vol. 93, no. 20, 2008.